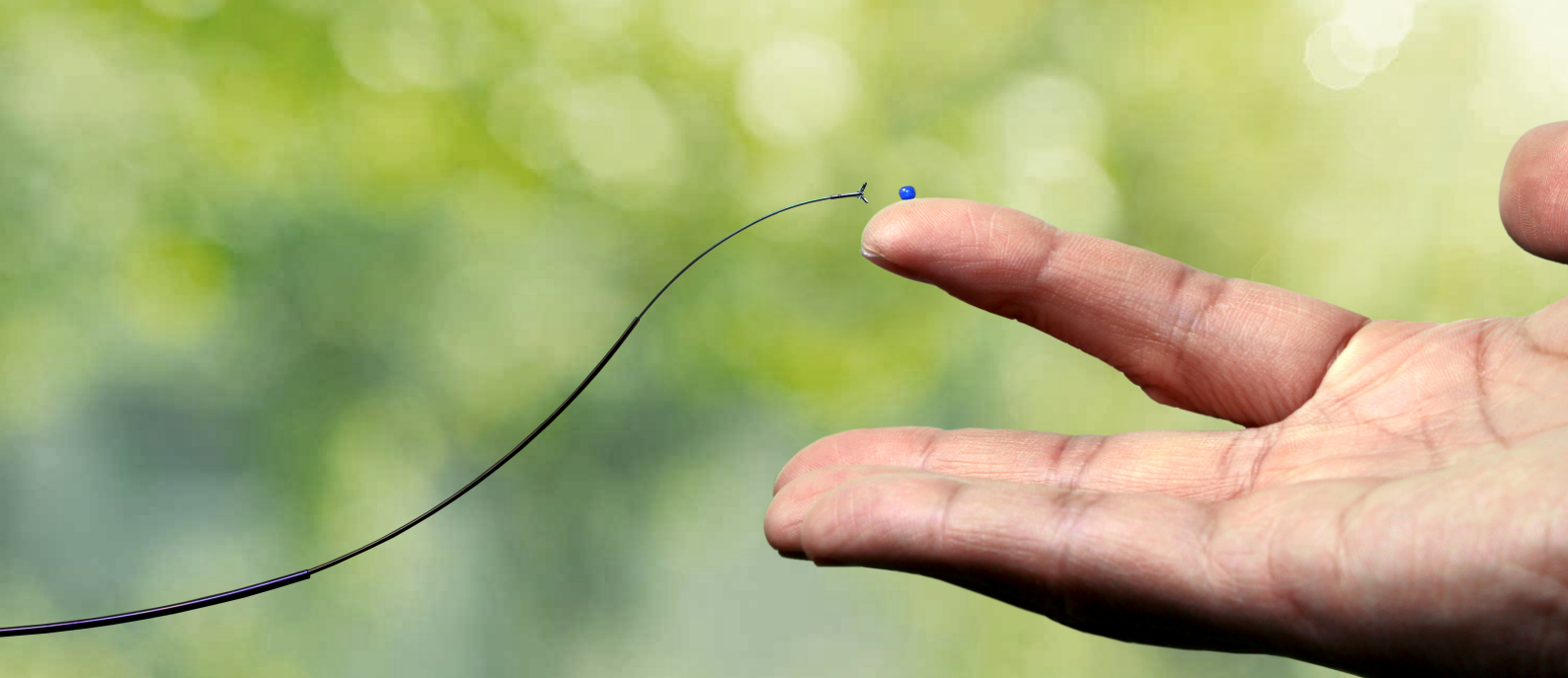




Laboratory for  
Continuum Robotics



Leibniz  
Universität  
Hannover



# Continuum Robotics

## Kinematic Modeling

**Prof. Dr.-Ing. Jessica Burgner-Kahrs**

Co-Authors: Josephine Granna, Sven Lilge, Malte Bormann, Ph.D. M. Taha Chikhaoui

**Leibniz Universität Hannover**  
Laboratory for Continuum Robotics  
Prof. Dr.-Ing. Jessica Burgner-Kahrs  
Appelstr. 11  
30167 Hannover  
Germany

# Preface

This script provides supporting material for the course *Continuum Robotics* from Prof. Dr.-Ing. Jessica Burgner-Kahrs at Leibniz Universität Hannover. The course has been established in the winter term 2016-2017 and is taught for the second time in the winter term 2017-2018. As there exists no textbook on continuum robotics nor does other course material exist worldwide, it is our mission to publish the first textbook on continuum robotics in the next years. This script marks the first milestone towards a textbook.

In this first edition of the script, we will primarily be concerned with developing and analyzing kinematic models for continuum robots. In particular, we will develop methods to represent the basic geometric aspects of continuum robots which are based on Lie algebra, screw theory, and differential geometry.

*Jessica Burgner-Kahrs*  
Hannover, December 2017

## Note to Readers

This is the first edition of the script. The nature of first editions implies that it is likely that the authors did not identify all flaws in the text yet.

If you note any errors, typos, inconsistencies while reading and working through the script, please be so kind and email us:

**continuumrobotics@lkr.uni-hannover.de**

# Notation and Kinematics Nomenclature

## Mathematical Fundamentals

$Ad$	-	Adjoint transformation.
$\mathcal{C}$	-	Curve.
$e$	-	Canonical vector.
$W$	-	Wrench.
$f$	-	Force.
$g$	-	Transformation.
$h$	-	Pitch of a screw.
$I$	-	Identity matrix.
$l$	-	Axis of a screw.
$M$	-	Magnitude of a screw.
$O$	-	Global coordinate frame.
$r$	-	Position vector.
$R$	-	Rotation matrix.
$r$	-	Translational vector.
$s$	-	Arc length.
$V$	-	Velocity of a rigid body.
$V^b$	-	Body velocity.
$V^s$	-	Spatial velocity.
$V^h$	-	Hybrid velocity.
$v$	-	Twist coordinates.
$w$	-	Rotational components the twist.
$\xi$	-	Moment of wrench.
$\theta$	-	Rotational angle.
$\kappa$	-	Curvature.
$\xi$	-	Twist.

## Cosserat rod theory

$A^*$	- Reference value if the motion of a rod is regarded.
$d_1$ and $d_2$	- Directors of the cross section of a rod.
$d_3$	- Tangent vector of a rod.
$f$	- Resultant force acting on an element of a rod.
$l$	- Resultant moment acting on an element of a rod.
$m$	- Contact moment acting on an element of a rod.
$m_1$ and $m_2$	- Bending moments.
$m_3$	- Twisting moment.
$n$	- Contact force acting on an element of a rod.
$n_1$ and $n_2$	- Shear forces.
$n_3$	- Axial force.
$\{m, n\}$	- Moment and force components of a rod within triples.
$r$	- Smooth curve describing the configuration of a rod.
$u_1$ and $u_2$	- Flexural strains.
$u_3$	- Torsional strain.
$\{u, v\}$	- Strain variables of a rod within triples.
$\{u, v\}$	- Strain vectors of a rod.
$W$	- Strain energy density function.
$v_1$ and $v_2$	- Shear strains.
$v_3$	- Dilatation.

## Constant Curvature Kinematic Framework

- $j$  - Link index.
- $\ell_j$  - Total length of the  $j^{\text{th}}$  link.
- $N$  - Number of links.
- $\mathbf{q}$  - Configuration space.
- $s_j$  - Arc-length of the  $j^{\text{th}}$  link.
- $\mathbf{x}$  - Task space.
- $\kappa_j$  - Curvature of the  $j^{\text{th}}$  link of the robot's shape.
- $\phi_j$  - Bending plane angle of the  $j^{\text{th}}$  link.
- $\theta_j$  - Angle through which the arc of the  $j^{\text{th}}$  link bends.

## Tubular Continuum Robot

$E_i$	-	Young's modulus of tube $i$ .
$\mathbf{f}$	-	External forces.
$G_i$	-	Shear modulus of tube $i$ .
$i$	-	Tube index.
$I_i$	-	Second moment of area of tube $i$ .
$J_i$	-	Polar moment of inertia of tube $i$ .
$L_i$	-	Length of tube $i$ .
$L_i^s$	-	Straight length of tube $i$ .
$L_i^c$	-	Curved length of tube $i$ .
$\ell$	-	Link length.
$\mathbf{l}$	-	External loads.
$M$	-	Moment applied to differential element.
$\mathbf{m}_i$	-	Internal moments of tube $i$ .
$n$	-	Number of component tubes.
$\mathbf{n}_i$	-	Internal forces of tube $i$ .
$\mathbf{q}$	-	Joint parameters ( $\mathbf{q} = [\alpha_1, \dots, \alpha_n, \beta_1, \dots, \beta_n]$ ).
$R_{i_i}$	-	Inner radius of tube.
$R_{o_i}$	-	Outer radius of tube.
$\alpha_i$	-	Relative z-axis rotation angle of tube $i$ .
$\beta_i$	-	Translation of tube $i$ .
$\kappa_i$	-	Curvature of the $i^{\text{th}}$ tube precurved section.
$\nu$	-	Poisson's ratio.
$\phi_i$	-	Orientation of the combined tubes in a fixed global frame.
$\psi_i$	-	Tube's absolute material orientation away from a fixed material frame along the length of the robot.
$\theta_i$	-	Rotational difference of the $i^{\text{th}}$ tube to a reference frame about the z-axis.
$\xi$	-	Twist vector.

## Tendon Actuated Continuum Robot

$\mathbf{B}_j$	- Base disk coordinate frame.
$d_j$	- Pitch circle diameter of segment $j$ .
$\mathbf{E}_j$	- End disk coordinate system.
$\mathbf{F}$	- Point force on the robot's backbone.
$\mathbf{f}_e$	- External force on the robot's backbone.
$\mathbf{f}_i$	- Distributed force on the $i^{\text{th}}$ tendon.
$\mathbf{f}_t$	- Collective distributed force on the robot's backbone applied by the tendons.
$i$	- Index of the tendons (secondary backbone).
$j$	- Number of segments.
$\mathbf{L}$	- Point moment on the robot's backbone.
$\ell_j$	- Segment length.
$\ell_{ji}$	- Length of the $i^{\text{th}}$ secondary backbone of segment $j$ .
$\mathbf{l}_t$	- Collective distributed moment on the robot's backbone applied by the tendons.
$\mathbf{l}_e$	- External moment on the robot's backbone.
$n_j$	- Index of the disks of the $j^{\text{th}}$ segment.
$\mathbf{P}_j$	- Bending plane coordinate system.
$\mathbf{q}$	- Joint variables.
$q_{ji}$	- Joint variables of the $i^{\text{th}}$ secondary backbone of segment $j$ .
$r_j$	- Radius of curvature of each segment $j$ .
$r_{ji}$	- Radius of curvature of the $i^{\text{th}}$ secondary backbone of segment $j$ .
$\mathbf{t}_i$	- Vector pointing from the origin of the backbone to the location of tendon $i$ on a cross section of the robot.
$s_j$	- Arc length of the $j^{\text{th}}$ link.
$\beta$	- Angle between wires/tendons.
$\Delta_{ji}$	- Offset between the projection of the $i^{\text{th}}$ secondary backbone on the segment bending plane and the primary backbone.
$\kappa_j$	- Curvature of segment $j$ .
$\phi_j$	- Rotation angle between the bending coordinate frame $\mathbf{P}_j$ and the base disk coordinate frame $\mathbf{B}_j$ .
$\sigma_{ji}$	- Angle of the $i^{\text{th}}$ secondary backbone about $\mathbf{z}_b$ .
$\tau_i$	- Tension of the $i^{\text{th}}$ tendon.
$\theta_j$	- Angle of the tangent to the $j^{\text{th}}$ primary backbone in the segment bending plane.

# Contents

<b>Preface</b>	<b>ii</b>
<b>Notation and Kinematics Nomenclature</b>	<b>iii</b>
<b>1 Introduction</b>	<b>1</b>
1 Robot Classification . . . . .	2
2 Continuum Robots . . . . .	4
References . . . . .	6
<b>2 Mathematical Fundamentals</b>	<b>7</b>
1 Lie Algebra . . . . .	8
1.1 Special Orthogonal Group . . . . .	9
1.2 Special Euclidean Group . . . . .	9
1.3 Lie Algebra of $SO(3)$ . . . . .	10
1.4 Lie Algebra of $SE(3)$ . . . . .	10
2 Screw Theory . . . . .	11
2.1 Exponential coordinates . . . . .	11
2.2 Definition of a Screw Motion . . . . .	11
2.3 Velocity of a Rigid Body . . . . .	13
2.4 Wrenches . . . . .	15
3 Curves in 3D Space . . . . .	15
3.1 Frenet Triad . . . . .	15
3.2 Bishop Frames . . . . .	19
3.3 Relating Bishop and Frenet Frames . . . . .	20
References . . . . .	20
<b>3 Cosserat Theory for Elastic Rods</b>	<b>21</b>
1 Special Cosserat Rod . . . . .	22
2 Kinematics of the Deformation . . . . .	23
3 Mechanics . . . . .	24
4 Constitutive Relations . . . . .	25
5 Governing Differential Equations . . . . .	27
References . . . . .	29
<b>4 Forward Kinematic Modeling</b>	<b>30</b>
1 General Idea . . . . .	32
1.1 Kinematics Frameworks . . . . .	32
1.2 Mechanics Frameworks . . . . .	34
2 Constant Curvature Kinematics Framework . . . . .	35
2.1 Robot Dependent Mapping . . . . .	36
2.2 Robot Independent Mapping . . . . .	44
2.3 Using Frenet-Serret Frames . . . . .	45
2.4 Accuracy . . . . .	48
3 Mechanics Framework using Elasticity Theory . . . . .	50
3.1 Tubular Continuum Robots . . . . .	50

3.2	Coupled Rod/Tendon Model for Tendon-actuated Continuum Robots	57
3.3	Solving the Explicit Model Equations	62
3.4	Accuracy	63
References		66

# 1 Introduction

1	Robot Classification	2
2	Continuum Robots	4
	References	6

Robots are impacting human life in many significant ways. Robotics is revolutionizing automation in the manufacturing sector and the number of industrial robot deployed worldwide is expected to increase from about 1,828,000 units at the end of 2016 to 3,053,000 units at the end of 2020 [1]. Robotics also found its way out of the factory into the service domain, where it has already had a significant impact in areas such as agriculture, surgery, logistics, or public relations and is growing in economic impact. There is a growing demand to monitor our everyday surroundings which results in increased and difficult-to-manage workloads and data flows. To meet this demand, robots will play an even greater role in the maintenance, security and rescue markets.

Robotics in personal and domestic applications has experienced strong global growth with a limited number of mass-market products: floor cleaning robots, robotic mowers and robots for education. The trend leads toward domestic robots of higher sophistication, capability and value, such as assistive robots for supporting the elderly, for helping with household chores, and for entertainment.

## 1 Robot Classification

Both in the manufacturing and service domain, the vast majority of robots are serial robot arms (see Figure 1.1 top). A considerably smaller portion are either parallel robots or mobile robots<sup>1</sup>. Serial and parallel robots are structurally composed of discrete rigid links and joints. These robots may be classified as **hard** robots as they are made from rigid and stiff materials. Usually, the number of joints equals the number of degrees of freedom (DOF) in task space and thus referred to as a **non-redundant** robot. Figure 1.2 shows the classification of robots based on materials and degrees of freedom.

Beside the general market trends in manufacturing and service, there exist applications which are characterized by hard-to-reach areas, tortuous paths, and highly unstructured environments, for instance intracorporal or intraluminal medical applications, or in maintenance, repair and operation (MRO). Those applications mostly require highly dexterous and miniaturized robots. Intuitively, one would increase the number of discrete joints and reduce the length of the rigid links in order to increase the DOF in task space. The robot is then referred to as **redundant** and in cases when the number of DoF is much higher than required (e.g. 10 DOF in configuration space, also known as joint space, vs. 6 required DOF in task space), a robot is referred to as **hyperredundant** (see Figure 1.1 middle). Typically, hyperredundant robots are snake-like robots [2]. However, the discrete structure of rigid links connected by joints cannot be miniaturized to any arbitrary size. In

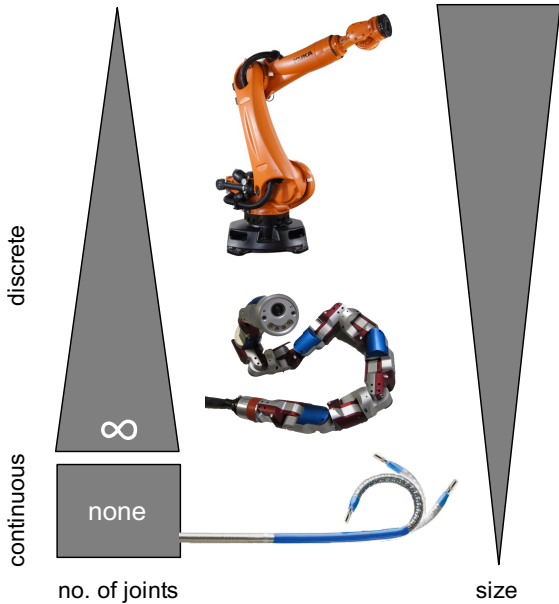


Figure 1.1: Conventional robots are characterized by discrete, rigid links, while continuum robots have an infinite degree of freedom, curvilinear structure. Miniaturization reaches a mechanical limit with discrete rigid link structures in terms of integration, whereas a continuous structure enables significantly smaller robots. (Images: top ©2015 Kuka Robotics Corp.; middle: ©2015 Carnegie Mellon University; bottom: ©2015 Hansen Medical Inc.)

<sup>1</sup>In this script, we neglect mobile robots which represent a special category of robots due to their ability of locomotion.

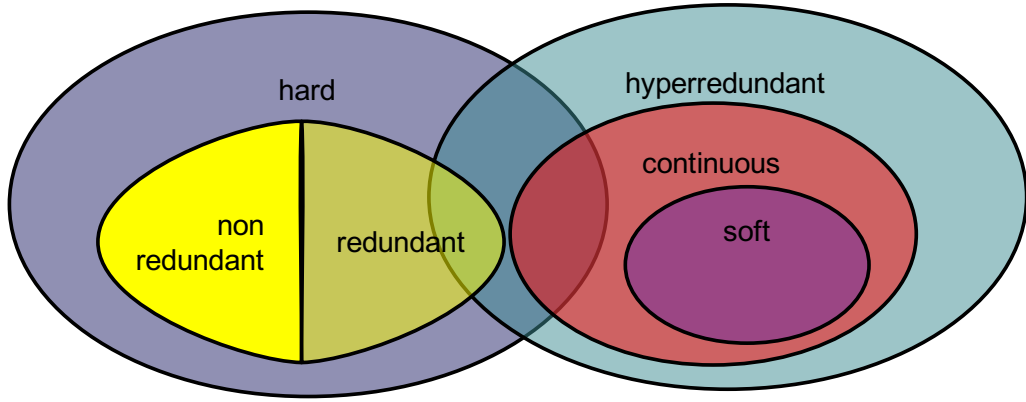


Figure 1.2: Robot classification based on materials and degrees of freedom. (Image adapted from [3])

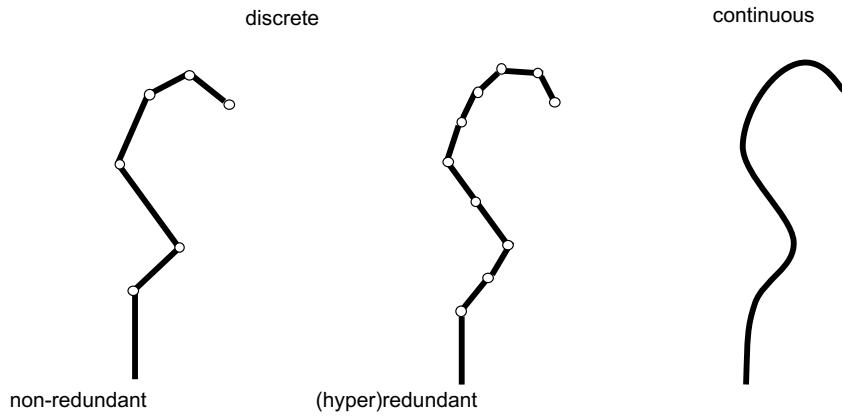


Figure 1.3: Appearance of non-redundant, (hyper)redundant, and continuum robots.

fact, the integration of all the mechatronic components reaches a physical miniaturization limit.

Theoretically, the number of joints could approach infinity and the link length could approach zero. The discrete structure then evolves to quasi-continuous and in the extreme case to **continuous**. Such a robot is classified as a continuum robot. Figure 1.3 illustrates the difference in appearance.

**Soft** robots<sup>2</sup> are continuum robots made of soft materials that undergo continuous elastic deformation and which are realized as compliant structures [4]. The Young's modulus of the materials is less than around 1 GPa for soft robots [5] and exhibit considerable compliance under normal loading conditions.

---

<sup>2</sup>Please note that the term soft robot is also used for robots with rigid links and mechanically (or passively) compliant joints with variable stiffness, and for robots with compliance and impedance control.

## 2 Continuum Robots

Continuum robots have a fundamentally different structure than conventional non- and (hyper)redundant robots. They have a joint-less structure which is continuous. This structure is inspired by biological trunks (e.g. elephant), tentacles, tongues, and worms. A continuous structure enables to traverse confined spaces, manipulate objects in complex environments, and to conform to curvilinear paths in task space.

As we have seen in the previous section, the transition from hyperredundant robots to continuum robots is somewhat smooth as the number of joints approaches infinity. In fact, some hyperredundant robots appear to be a continuum robot. For instance, the robot depicted in Figure 1.4(left) appears as a continuum robot, but as it is composed of joints and rigid links, it is a hyperredundant robot. One may refer as continuum-style or quasi-continuous robots to those cases. On the other hand, the robot in Figure 1.4(right) is a continuum robot but the appearance of the bellow structure may also suggest that the robot is composed of discrete elements.



Figure 1.4: Left: Snake-arm robot by OC Robotics. Right: Bionic handling assistant by FESTO.

In order to overcome the ambiguity of the term continuum robot, there exist several definitions. Researchers in the continuum robot community have not yet converged to a single definition, such that there exist four major definitions, which are stated in chronological order:

### Definition (Robinson & Davies, 1999)

Continuum robots do not contain rigid links and identifiable rotational joints. Instead the structures bend continuously along their length via elastic deformation and produce motion through the generation of smooth curves, similar to tentacles or tongues of the animal kingdom. [6]

### Definition (Webster III & Jones, 2010)

A continuum robot can be defined as a continuously bending, infinite-degree-of-freedom robot with an elastic structure. Continuum robots are thus related to, but distinct from, hyperredundant robots, which consist of (finitely) many short, rigid links. [7]

**Definition (Walker, 2013)**

Continuum robots can be viewed as being invertebrate robots, as compared with the vertebrate design of conventional rigid-link robots. Continuum robots can bend (and often extend/contract and sometimes twist) at any point along their structure. [8]

**Definition (Burgner-Kahrs, Rucker & Choset, 2015)**

A continuum robot is an actuatable structure, whose constitutive material forms curves with continuous tangent vectors. [9]

## References

- [1] International Federation of Robotics. *World Robotics Report*. 2017.
- [2] S. Hirose and Hiroya Yamada. “Snake-like robots [Tutorial]”. In: *IEEE Robotics & Automation Magazine* 16.1 (2009), pp. 88–98.
- [3] Deepak Trivedi et al. “Soft robotics: Biological inspiration, state of the art, and future research”. In: *Applied Bionics and Biomechanics* 5.3 (2008), pp. 99–117.
- [4] Cecilia Laschi, Barbara Mazzolai, and Matteo Cianchetti. “Soft robotics: Technologies and systems pushing the boundaries of robot abilities”. In: *Science Robotics* 1.1 (2016), eaah3690.
- [5] Daniela Rus and Michael T. Tolley. “Design, fabrication and control of soft robots”. In: *Nature* 521.7553 (2015), pp. 467–475. DOI: 10.1038/nature14543.
- [6] G. Robinson and J.B.C. Davies. “Continuum robots - a state of the art”. In: *IEEE International Conference on Robotics and Automation*. 1999, pp. 2849–2854.
- [7] Robert J. Webster and Bryan A. Jones. “Design and Kinematic Modeling of Constant Curvature Continuum Robots: A Review”. In: *The International Journal of Robotics Research* 29.13 (2010), pp. 1661–1683.
- [8] Ian D. Walker. “Continuous Backbone “Continuum” Robot Manipulators”. In: *ISRN Robotics* 2013 (2013), pp. 1–19.
- [9] Jessica Burgner-Kahrs, D. Caleb Rucker, and Howie Choset. “Continuum Robots for Medical Applications: A Survey”. In: *IEEE Transactions on Robotics* 31.6 (2015), pp. 1261–1280. ISSN: 1552-3098. DOI: 10.1109/TRO.2015.2489500.

## 2 Mathematical Fundamentals

<b>1</b>	<b>Lie Algebra</b>	<b>8</b>
1.1	Special Orthogonal Group	9
1.2	Special Euclidean Group	9
1.3	Lie Algebra of $SO(3)$	10
1.4	Lie Algebra of $SE(3)$	10
<b>2</b>	<b>Screw Theory</b>	<b>11</b>
2.1	Exponential coordinates	11
2.2	Definition of a Screw Motion	11
2.3	Velocity of a Rigid Body	13
2.4	Wrenches	15
<b>3</b>	<b>Curves in 3D Space</b>	<b>15</b>
3.1	Frenet Triad	15
3.1.1	Frenet-Serret Relations	17
3.1.2	Darboux Vector	19
3.2	Bishop Frames	19
3.3	Relating Bishop and Frenet Frames	20
	<b>References</b>	<b>20</b>

In this chapter the mathematical fundamentals necessary to develop kinematic models for continuum robots are introduced.

## 1 Lie Algebra

Lie groups represent the best-developed theory of continuous symmetry of mathematical objects and structures, which makes them indispensable tools for robotics. They provide a natural framework for analyzing the continuous symmetries of differential equations. The general concepts and relevant Lie groups and Lie algebras for continuum robotics are provided in the following. For a more in-depth review the book of Selig [1] is recommended.

Formally, a Lie Group is defined as a smooth manifold  $G$  with a distinguished element  $e$  and two continuous functions

$$\text{mult} : G \times G \longrightarrow G,$$

$$\text{inv} : G \longleftrightarrow G.$$

$\text{mult}$  is the group operation and the map  $\text{inv}$  is the inverse of an element. These functions are required to fulfill the axioms of a group, i.e.  $\text{mult}$  is associative,  $\text{inv}$  is bijective, and  $e$  is the identity element. Commonly, the functions are abbreviated as

$$\text{mult}(g_1, g_2) = g_1 g_2 \quad \text{and}$$

$$\text{inv}(g) = g^{-1}.$$

The group axioms can be written as

$$eg = ge = g \quad \text{idendity},$$

$$g^{-1}g = gg^{-1} = e \quad \text{inverse},$$

$$g_1(g_2g_3) = (g_1g_2)g_3 = g_1g_2g_3 \quad \text{associativity}.$$

For a Lie Group, it is further required that the functions  $\text{mult}$  and  $\text{inv}$  are differentiable mappings.

A Lie Algebra is a vector space  $\mathfrak{g}$  together with a non-associative, alternating bilinear map

$$\mathfrak{g} \times \mathfrak{g} \rightarrow \mathfrak{g}; (x, y) \mapsto [x, y]$$

called the Lie bracket, satisfying the Jacobi identity. Any Lie Group is corresponding to a Lie algebra. Conversely, to any finite-dimensional Lie algebra over real or complex numbers, there is a corresponding connected Lie group unique up to covering.

**Example**

The three-dimensional Euclidean space  $\mathbb{R}^3$  with the Lie bracket given by the cross product of vectors becomes a three-dimensional Lie algebra  $\mathfrak{g} = \mathbb{R}^3$ . The bracket is defined by  $[\mathbf{x}, \mathbf{y}] = \mathbf{x} \times \mathbf{y}$ . The bilinearity, skew-symmetry, and Jacobi identity are all known properties of the cross product. With the standard basis  $\{\mathbf{e}_1, \mathbf{e}_2, \mathbf{e}_3\}$ , the bracket operation is completely determined by the relations:

$$[\mathbf{e}_1, \mathbf{e}_2] = \mathbf{e}_3,$$

$$[\mathbf{e}_2, \mathbf{e}_3] = \mathbf{e}_1,$$

$$[\mathbf{e}_3, \mathbf{e}_1] = \mathbf{e}_2.$$

The relation  $[\mathbf{e}_2, \mathbf{e}_1] = -\mathbf{e}_3$  follows from the above by the skew-symmetry of the bracket. This Lie algebra is referred to as  $(\mathbb{R}^3, \times)$ .

## 1.1 Special Orthogonal Group

The set of rotations about the origin can be associated to a set of matrices which satisfy both

$$\mathbf{R}\mathbf{R}^T = \mathbf{I} \quad (2.1)$$

$$\det \mathbf{R} = 1 \quad (2.2)$$

where matrices satisfying  $\mathbf{R}\mathbf{R}^T = \mathbf{I}$  are denoted as orthogonal matrices and orthogonal matrices satisfying  $\det(\mathbf{R}) = 1$  are called special orthogonal, abbreviated to  $SO(n)$ , where  $n$  is the dimension of space, i.e.  $n \times n$  matrices. The space of rotation matrices can be defined as

$$SO(n) = \{\mathbf{R} \in \mathbb{R}^{n \times n} : \mathbf{R}\mathbf{R}^T = \mathbf{I}, \det \mathbf{R} = +1\} \quad (2.3)$$

For  $n = 3$ , the group  $SO(3)$  is also referred to as the *rotation group* on  $\mathbb{R}^3$ . For instance, coordinate frames corresponding to right-handed frames are represented by orthogonal matrices with determinant 1.  $SO(3)$  is a Lie group using the identity matrix  $\mathbf{I}$  as the identity element and matrix multiplication as the group operation.

Every configuration of a rigid body that is free to rotate relative to a fixed frame can be identified with a unique  $\mathbf{R} \in SO(3)$ . Under this identification, the rotation group  $SO(3)$  is referred to as the configuration space of the system and a trajectory of the system is a curve  $\mathbf{R}(t) \in SO(3)$  for  $t \in [0, T]$ .

## 1.2 Special Euclidean Group

The representation of general rigid body motion, involving both translation  $\mathbf{r}$  and rotation  $\mathbf{R}$  on  $\mathbb{R}^3$  is defined by the Special Euclidean Group and denoted  $SE(3)$ :

$$SE(3) = \{(\mathbf{r}, \mathbf{R}) : \mathbf{r} \in \mathbb{R}^3, \mathbf{R} \in SO(3)\} = \mathbb{R}^3 \times SO(3). \quad (2.4)$$

$SE(3)$  is of central importance to robotics and in particular for the modeling of continuum robots.

$SE(3)$  is a Lie group of dimension 6, defined by the set of mappings  $\mathbf{g} : \mathbb{R}^3 \rightarrow \mathbb{R}^3$  of the form  $\mathbf{g}(\mathbf{x}) = \mathbf{R}\mathbf{x} + \mathbf{r}$ , where  $\mathbf{R} \in SO(3)$  and  $\mathbf{x} \in \mathbb{R}^3$ . The representation is also referred to as homogeneous representation. The group can be identified with the space of

$4 \times 4$  transformation matrices of the form

$$\mathbf{g} = \begin{bmatrix} \mathbf{R} & \mathbf{r} \\ \mathbf{0} & 1 \end{bmatrix} \quad (2.5)$$

with  $\mathbf{R} \in SO(3)$  and  $\mathbf{r} \in \mathbb{R}^3$ . The inverse of such a matrix is given by

$$\mathbf{g}^{-1} = \begin{bmatrix} \mathbf{R} & \mathbf{r} \\ \mathbf{0} & 1 \end{bmatrix}^{-1} = \begin{bmatrix} \mathbf{R}^T & -\mathbf{R}^T \mathbf{r} \\ \mathbf{0} & 1 \end{bmatrix} \quad (2.6)$$

### 1.3 Lie Algebra of $SO(3)$

The Lie algebra of  $SO(3)$ , denoted as  $so(3)$ , can be identified with  $3 \times 3$  skew-symmetric matrices of the form

$$\hat{\mathbf{w}} = \begin{bmatrix} 0 & -w_3 & w_2 \\ w_3 & 0 & -w_1 \\ -w_2 & w_1 & 0 \end{bmatrix} \quad (2.7)$$

with the bracket structure

$$[\hat{\mathbf{w}}_1, \hat{\mathbf{w}}_2] = \hat{\mathbf{w}}_1 \hat{\mathbf{w}}_2 - \hat{\mathbf{w}}_2 \hat{\mathbf{w}}_1,$$

with  $\mathbf{w}_1, \mathbf{w}_2 \in \mathbb{R}^3$ .  $so(3)$  can be identified with  $\mathbb{R}^3$  using the mapping in equation (2.7), which maps a vector  $\mathbf{w} \in \mathbb{R}^3$  to a matrix  $\hat{\mathbf{w}} \in so(3)$ . It can be shown that

$$[\hat{\mathbf{w}}_1, \hat{\mathbf{w}}_2] = (\mathbf{w}_1 \times \mathbf{w}_2)^\wedge.$$

Thus,  $\mathbf{w} \mapsto \hat{\mathbf{w}}$  is a Lie algebra isomorphism between the Lie algebra  $(\mathbb{R}^3, \times)$  and the Lie algebra  $(so(3), [\cdot, \cdot])$ . Please note, that the notation  $\hat{\mathbf{a}}$  is used synonymous for  $(\mathbf{a})^\wedge$ .

### 1.4 Lie Algebra of $SE(3)$

The Lie algebra of  $SE(3)$ , denoted  $se(3)$ , can be identified with  $4 \times 4$  matrices of the form

$$\hat{\boldsymbol{\xi}} = \begin{bmatrix} \hat{\mathbf{w}} & \mathbf{v} \\ 0 & 0 \end{bmatrix}, \quad \mathbf{w}, \mathbf{v} \in \mathbb{R}^3. \quad (2.8)$$

The bracket structure is given as  $[\hat{\boldsymbol{\xi}}_1, \hat{\boldsymbol{\xi}}_2] = \hat{\boldsymbol{\xi}}_1 \hat{\boldsymbol{\xi}}_2 - \hat{\boldsymbol{\xi}}_2 \hat{\boldsymbol{\xi}}_1$ , such that for

$$\begin{aligned} \hat{\boldsymbol{\xi}}_1 &= \begin{bmatrix} \hat{\mathbf{w}}_1 & \mathbf{v}_1 \\ 0 & 0 \end{bmatrix} \quad \text{and} \quad \hat{\boldsymbol{\xi}}_2 = \begin{bmatrix} \hat{\mathbf{w}}_2 & \mathbf{v}_2 \\ 0 & 0 \end{bmatrix} \\ [\hat{\boldsymbol{\xi}}_1, \hat{\boldsymbol{\xi}}_2] &= \begin{bmatrix} (\mathbf{w}_1 \times \mathbf{w}_2)^\wedge & \mathbf{w}_1 \times \mathbf{v}_2 - \mathbf{w}_2 \times \mathbf{v}_1 \\ 0 & 0 \end{bmatrix}. \end{aligned}$$

The vector space  $se(3)$  is isomorphic to  $\mathbb{R}^6$  via the mapping  $\hat{\boldsymbol{\xi}} \mapsto \boldsymbol{\xi} = (\mathbf{v}, \mathbf{w}) \in \mathbb{R}^6$ . In robotics, twists are commonly denoted  $\boldsymbol{\xi}$  and used to parameterize rigid body motions.

## 2 Screw Theory

### 2.1 Exponential coordinates

For convenience, one can represent a skew-symmetric matrix as the product of a unit skew-symmetric matrix  $\hat{\omega} \in so(3)$ ,  $\|\omega\| = 1$  (representing the axis of rotation) and a real number  $\theta \in \mathbb{R}$  (representing the angle of rotation). The exponential of  $\hat{\omega}\theta$  is a rotation matrix written as

$$\exp(\hat{\omega}\theta) = e^{\hat{\omega}\theta} = \mathbf{I} + \theta\hat{\omega} + \frac{\theta^2}{2!}\hat{\omega}^2 + \frac{\theta^3}{3!}\hat{\omega}^3 + \dots \quad (2.9)$$

$$= \mathbf{I} + \hat{\omega} \sin \theta + \hat{\omega}^2(1 - \cos \theta) \quad (2.10)$$

with the relations

$$\hat{\mathbf{a}}^2 = \hat{\mathbf{a}}\hat{\mathbf{a}}^T - \|\hat{\mathbf{a}}\|^2 \mathbf{I}$$

and

$$\hat{\mathbf{a}}^3 = -\|\hat{\mathbf{a}}\|^2 \hat{\mathbf{a}}$$

for  $\hat{\mathbf{a}} \in so(3)$ . Eq. (2.10) is commonly referred to as *Rodrigues' formula* and is an effective method to compute  $\exp(\hat{\omega}\theta)$ .

It is also useful to mention that exponentials of skew matrices are orthogonal  $e^{\hat{\omega}\theta} \in SO(3)$  and that the exponential map is surjective onto  $SO(3)$ :

*Given  $\mathbf{R} \in SO(3)$ , there exists  $\mathbf{w} \in \mathbb{R}^3$ ,  $\|\omega\| = 1$  and  $\theta \in \mathbb{R}$  such that  $\mathbf{R} = \exp(\hat{\omega}\theta)$ .*

Thus, exponential coordinates (also called *canonical coordinates* of the rotation group) are defined by the components of the vector  $\mathbf{w}\theta \in \mathbb{R}^3$ . The assumptions above lead to the following theorem:

#### Euler's Theorem

Any orientation  $\mathbf{R} \in SO(3)$  is equivalent to a rotation about a fixed axis  $\omega \in \mathbb{R}^3$  through an angle  $\theta \in [0, 2\pi]$ .

The previous theorem allows to introduce the *axis-angle representation*. However, this representation is not unique due to the surjectivity of the exponential mapping. For instance, the pair  $(\omega' = -\omega, \theta' = 2\pi - \theta)$  produces the same rotation as  $(\omega, \theta)$ .

### 2.2 Definition of a Screw Motion

A screw axis is defined as the line representing the rotation axis as well as the translation axis of a body that is subject to Euclidean displacement in three-dimensional space.

The infinitesimal version of a screw motion is called a twist and it provides a description of the instantaneous velocity of a rigid body in terms of its linear and angular components. Screw theory is based on Chasles' theorem, which says that the most general rigid body displacement can be produced by a translation along a line (called its screw axis) followed by a rotation about that line. Screws and twists play a central role in the formulation of the kinematics of continuum robots.

#### Chasles' Theorem

Every rigid body motion can be realized by a rotation about an axis combined with a translation parallel to that axis.

The second major result upon which screw theory is founded on, is the representation of forces acting on a rigid body. Poinsot discovered that any system of forces acting on a rigid body can be replaced by a single force applied along a line, combined with a torque about the same line. Such a force is referred to as a wrench. Wrenches are dual to twists, i.e. theorems which apply to twists can be extended to wrenches.

The following summary of screw theory is based on Chapter 2 of Murray, Li, and Sastry, which gives a more comprehensive overview of screw theory and its application to rigid link serial robots [2].

Fig. 2.1 sketches the motion of a rigid body consisting of a rotation about an axis in space through an angle  $\theta$ , followed by a translation along the same axis by an amount  $d$ . The point  $p$  is on the rigid body and the point  $q$  is on the unit vector  $w$  specifying the direction. In the case of nonzero rotation ( $\theta \neq 0$ ), this motion describes a screw motion that has a pitch defining the ratio of translation to rotation  $h := d/\theta$  and a net translation after rotation by  $h\theta$ .

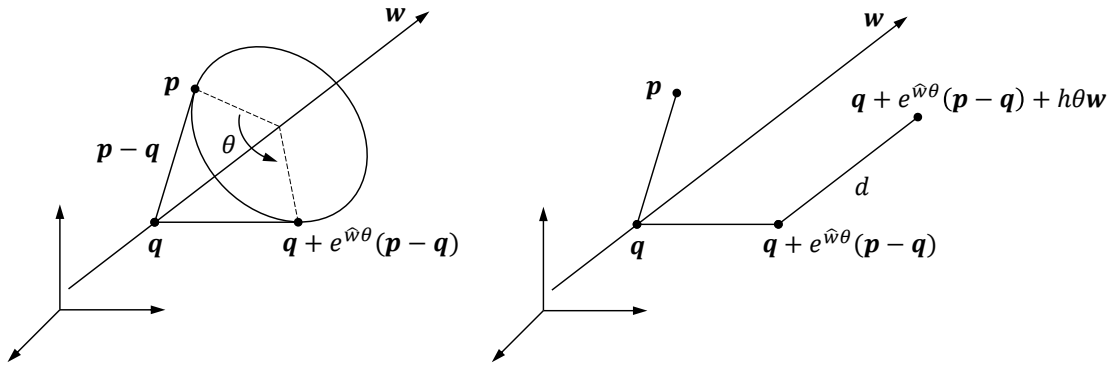


Figure 2.1: A general screw motion for nonzero rotation, adapted from [2]. (Left) Rotation of point  $p$  around the axis  $w$  through an angle  $\theta$  followed by (Right) a translation with an amount  $d$  along the same axis.

In the case of pure translation (Fig. 2.2), the axis is supposed to be the line through the origin in the direction  $v$ . Thus, the pitch of the screw motion  $h = \infty$  and this case represents the action of a prismatic joint. When  $h = 0$ , the motion corresponds to a pure rotation, which represents the action of a revolute joint.

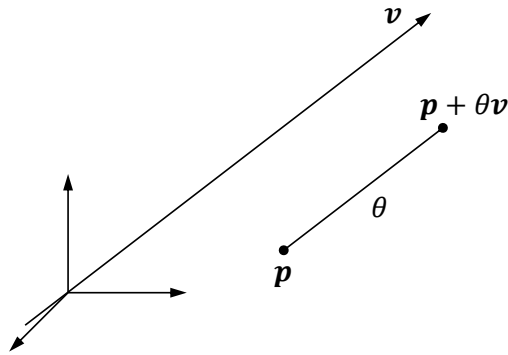


Figure 2.2: A screw motion for pure translation, adapted from [2].

In summary, a screw motion is naturally associated with a twist. It consists of a rotation by an amount  $\theta = M$  called *magnitude* about the *axis l* followed by a translation by an amount  $h\theta$  parallel the same axis *l*, where *h* is the *pitch*. Thus, the rigid body

transformation given by a screw is

$$\mathbf{g} = \begin{bmatrix} e^{\hat{\mathbf{w}}\theta} & (\mathbf{I} - e^{\hat{\mathbf{w}}\theta})\mathbf{x} + h\theta\mathbf{w} \\ \mathbf{0} & 1 \end{bmatrix} \quad (2.11)$$

Let us assume a twist  $\hat{\boldsymbol{\xi}} \in se(3)$ . The twist is defined by:

$$\boldsymbol{\xi} = \begin{bmatrix} \mathbf{v} \\ \mathbf{w} \end{bmatrix} \in \mathbb{R}^6.$$

The screw coordinates related to this twist are defined by the pitch

$$h = \frac{\mathbf{w}^T \mathbf{v}}{\|\mathbf{w}\|^2},$$

the axis

$$\mathbf{l} = \begin{cases} \left\{ \frac{\mathbf{w} \times \mathbf{v}}{\|\mathbf{w}\|^2} + \lambda \mathbf{w} : \lambda \in \mathbb{R} \right\}, & \text{if } \mathbf{w} \neq 0 \\ \{0 + \lambda \mathbf{v} : \lambda \in \mathbb{R}\}, & \text{if } \mathbf{w} = 0 \end{cases}$$

and the magnitude

$$M = \begin{cases} \|\mathbf{w}\|, & \text{if } \mathbf{w} \neq 0 \\ \|\mathbf{v}\|, & \text{if } \mathbf{w} = 0 \end{cases}.$$

### 2.3 Velocity of a Rigid Body

Based on the definition of the rigid body transformation introduced in Eq. (2.5), assume  ${}^a\mathbf{g}_b(t)$  is time dependent and representing the motion of a frame  $b$  attached to the body with respect to a fixed frame  $a$ . The twist-like expression is

$${}^a\dot{\mathbf{g}}_b(t) {}^a\mathbf{g}_b(t)^{-1} = \begin{bmatrix} {}^a\dot{\mathbf{R}}_b & {}^a\dot{\mathbf{p}}_b \\ \mathbf{0} & 0 \end{bmatrix} \begin{bmatrix} {}^a\mathbf{R}_b^T & -{}^a\mathbf{R}_b^T {}^a\mathbf{p}_b \\ \mathbf{0} & 1 \end{bmatrix} = \begin{bmatrix} {}^a\dot{\mathbf{R}}_b {}^a\mathbf{R}_b^T & -{}^a\dot{\mathbf{R}}_b {}^a\mathbf{R}_b^T {}^a\mathbf{p}_b + {}^a\dot{\mathbf{p}}_b \\ \mathbf{0} & 0 \end{bmatrix}$$

This yields the definition of the *spatial velocity*  ${}^a\widehat{\mathbf{V}}_b^s = {}^a\dot{\mathbf{g}}_b {}^a\mathbf{g}_b^{-1}$  (omitting the use of the time variable  $t$ ) such that

$${}^a\mathbf{V}_b^s = \begin{bmatrix} {}^a\mathbf{v}_b^s \\ {}^a\mathbf{w}_b^s \end{bmatrix} = \begin{bmatrix} -{}^a\dot{\mathbf{R}}_b {}^a\mathbf{R}_b^T {}^a\mathbf{p}_b + {}^a\dot{\mathbf{p}}_b \\ ({}^a\dot{\mathbf{R}}_b {}^a\mathbf{R}_b^T)^\vee \end{bmatrix}, \quad (2.12)$$

where the Lie algebra isomorphism  $^\vee$  is the reciprocal of  $^\wedge$ .

It is also possible to define the *body velocity*  ${}^a\widehat{\mathbf{V}}_b^b = {}^a\mathbf{g}_b^{-1} {}^a\dot{\mathbf{g}}_b$  of the same frames by

$${}^a\mathbf{V}_b^b = \begin{bmatrix} {}^a\mathbf{v}_b^b \\ {}^a\mathbf{w}_b^b \end{bmatrix} = \begin{bmatrix} {}^a\mathbf{R}_b^T {}^a\dot{\mathbf{p}}_b \\ ({}^a\mathbf{R}_b^T {}^a\dot{\mathbf{R}}_b)^\vee \end{bmatrix}. \quad (2.13)$$

In robotics, these quantities describe the end-effector velocity of a manipulator, given that  $\mathbf{g} \in SE(3)$  maps from the coordinate system related to the base to that of the end-effector. Hence, the *body velocity*  ${}^a\widehat{\mathbf{V}}_b^b$  represents the velocity of the end-effector while  ${}^a\widehat{\mathbf{V}}_b^s$  is that of the base frame. These two velocities are related by a similarity transformation written as

$$\mathbf{V}^b = \begin{bmatrix} \mathbf{R} & \hat{\mathbf{p}}\mathbf{R} \\ \mathbf{0} & \mathbf{R} \end{bmatrix} \mathbf{V}^s = Ad_g \mathbf{V}^s. \quad (2.14)$$

where  $Ad_g \in \mathbb{R}^{6 \times 6}$  is the *adjoint transformation* associated with the homogeneous representation  $\mathbf{g} \in SE(3)$ .

Using the same approach, one can express the spatial velocity of a first coordinate frame  $a$  relative to a third one  $c$  given the relative velocities with respect to a second coordinate frame  $b$  such that

$${}^a\mathbf{V}_c^s = {}^a\mathbf{V}_b^s + Ad_{a g_b} {}^b\mathbf{V}_c^s. \quad (2.15)$$

*Proof.* The composition of rigid body transformations is defined by

$${}^a\mathbf{g}_c = {}^a\mathbf{g}_b {}^b\mathbf{g}_c$$

The spatial velocity is given by

$$\begin{aligned} {}^a\widehat{\mathbf{V}}_c^s &= {}^a\dot{\mathbf{g}}_c {}^a\mathbf{g}_c^{-1} \\ &= \left( {}^a\dot{\mathbf{g}}_b {}^b\mathbf{g}_c + {}^a\mathbf{g}_b {}^b\dot{\mathbf{g}}_c \right) \left( {}^b\mathbf{g}_c^{-1} {}^a\mathbf{g}_b^{-1} \right) \\ &= {}^a\dot{\mathbf{g}}_b {}^a\mathbf{g}_b^{-1} + {}^a\mathbf{g}_b \left( {}^b\dot{\mathbf{g}}_c {}^b\mathbf{g}_c^{-1} \right) {}^a\mathbf{g}_b^{-1} \\ &= {}^a\widehat{\mathbf{V}}_b^s + {}^a\mathbf{g}_b {}^b\widehat{\mathbf{V}}_c^s {}^a\mathbf{g}_b^{-1}, \end{aligned}$$

which can be written in twist coordinates using the statement:

If  $\hat{\boldsymbol{\xi}} \in se(3)$  is a twist with twist coordinates  $\boldsymbol{\xi} \in \mathbb{R}^6$ , then for any  $\mathbf{g} \in SE(3)$ ,  $\mathbf{g}\hat{\boldsymbol{\xi}}\mathbf{g}^{-1}$  is a twist with twist coordinates  $Ad_g \boldsymbol{\xi} \in \mathbb{R}^6$ .  $\square$

Please note that the same proof applies to define the relative body velocities

$${}^a\mathbf{V}_c^b = Ad_{b g_c^{-1}} {}^a\mathbf{V}_b^b + {}^b\mathbf{V}_c^b. \quad (2.16)$$

In general, the following identities hold for two coordinate systems

$$\begin{aligned} {}^a\widehat{\mathbf{V}}_b^b &= -{}^b\widehat{\mathbf{V}}_a^s \\ {}^a\widehat{\mathbf{V}}_b^b &= -Ad_{b g_a} {}^b\widehat{\mathbf{V}}_a^b. \end{aligned}$$

In the case of the velocity of a rigid body relative to a frame attached to its origin, but whose orientation remains fixed relative to the inertial frame, one can define the *hybrid velocity*. It is defined with respect to the body velocity by the relationship

$$\mathbf{V}^h = \begin{bmatrix} \mathbf{R} & \mathbf{0} \\ \mathbf{0} & \mathbf{R} \end{bmatrix} \mathbf{V}^b \quad (2.17)$$

Similar to the relative body (Eq. (2.16)) and spatial (Eq. (2.15)) velocities, the relative hybrid velocity can also be defined as follows

$${}^a\mathbf{V}_c^h = Ad_{(-{}^a R_b {}^b p_c)} {}^a\mathbf{V}_b^h + Ad_{a R_b} {}^b\mathbf{V}_c^h \quad (2.18)$$

where  $Ad_p$  and  $Ad_R$  are the adjoint transformations of a pure translation by  $\mathbf{p}$  and a pure rotation by  $\mathbf{R}$ , respectively.

Based on the definitions above, the hybrid velocity of a rigid body:

- is independent of the position of the spatial frame
- is independent of the orientation of the body frame.

## 2.4 Wrenches

Analogous to the representation of twists, wrenches  $\mathbf{W}$  can be described by a pair constituted of a force and a moment such that

$$\mathbf{W} = \begin{bmatrix} \mathbf{f} \\ \boldsymbol{\chi} \end{bmatrix} \in \mathbb{R}^6.$$

For the assumed coordinate frames defined at  $a$  and  $b$  mapped by the transformation  ${}^a\mathbf{g}_b$ , one can express the equivalent wrench by

$$\mathbf{W}_b = Ad_{\mathbf{g}_b}^T \mathbf{W}_a \quad (2.19)$$

Similar to velocities,  $\mathbf{W}^s := \mathbf{W}_a$  is the *spatial wrench* and  $\mathbf{W}^b := \mathbf{W}_b$  is the *body wrench*.

It is also convenient to associate a screw to a given wrench  $\mathbf{W} = (\mathbf{f}, \boldsymbol{\tau})$ , with the same attributes, namely pitch  $h$ , axis  $\mathbf{l}$ , and magnitude  $M$  defined respectively by

$$\begin{aligned} h &= \frac{\mathbf{f}^T \boldsymbol{\tau}}{\|\mathbf{f}\|^2}, \\ \mathbf{l} &= \begin{cases} \left\{ \frac{\mathbf{f} \times \boldsymbol{\tau}}{\|\mathbf{f}\|^2} + \lambda \mathbf{f} : \lambda \in \mathbb{R} \right\}, & \text{if } \mathbf{f} \neq 0 \\ \{0 + \lambda \boldsymbol{\tau} : \lambda \in \mathbb{R}\}, & \text{if } \mathbf{f} = 0 \end{cases}, \\ M &= \begin{cases} \|\mathbf{f}\|, & \text{if } \mathbf{f} \neq 0 \\ \|\boldsymbol{\chi}\|, & \text{if } \mathbf{f} = 0 \end{cases}. \end{aligned}$$

## 3 Curves in 3D Space

The geometric features of space curves or curves in three-dimensional space are a classic topic in differential geometry. In general, a moving frame for a curve is a coordinate system with one axis aligned with the tangent of the curve. The other axes of the moving frame must be normal to the curve, but are otherwise allowed to rotate freely about the curve.

### 3.1 Frenet Triad

In the 19th century, the notion of curvature of a plane curve was extended to a space curve by Serret (1851) and Frenet (1852). Their work is the basis for most treatments of space curves. The remainder of this section is based on the book of O'Reilly [3].

A curve  $\mathcal{C}$  in Euclidean three-dimensional space  $\mathbb{R}^3$  (see Fig. 2.3) can be represented in terms of points on the curve in respect to some global coordinate frame  $\mathbf{O}$  and an associated frame. The curve is parameterized in respect to arc length  $s$ . A common way is to formulate the frames at each point on the curve as a Frenet triad – a set of three orthonormal vectors –  $\{\mathbf{e}_t, \mathbf{e}_n, \mathbf{e}_b\}$  (see Fig. 2.4), which also relates the curve's curvature  $\kappa$  and torsion  $\tau$ .

#### Note

The radius of curvature is the inverse of the curvature  $\kappa$ .

The torsion  $\tau$  describes the deviation of the curve out of the plane.

Classical differential geometry typically treats moving frames using the Frenet frame formalism because of its close association with a curve's curvature and torsion, which are coordinate-system independent.

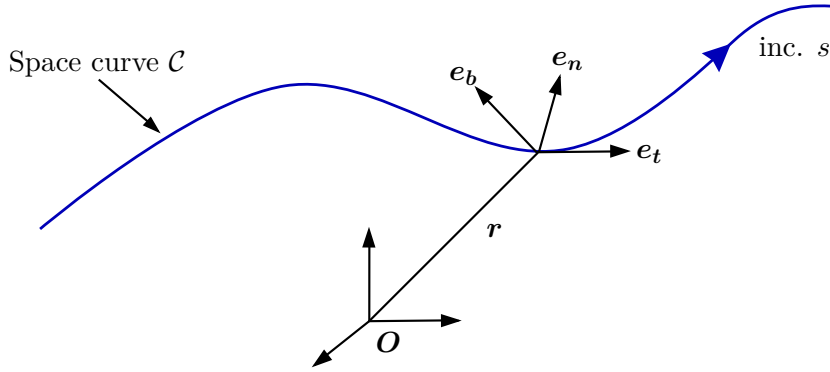


Figure 2.3: A curve in three-dimensional space presented in terms of points on the curve  $r$  in respect to an arc length parameter  $s$  (increasing towards the right-hand side) and associated frames (Frenet triad and global coordinate frame  $\mathbf{O}$ ).

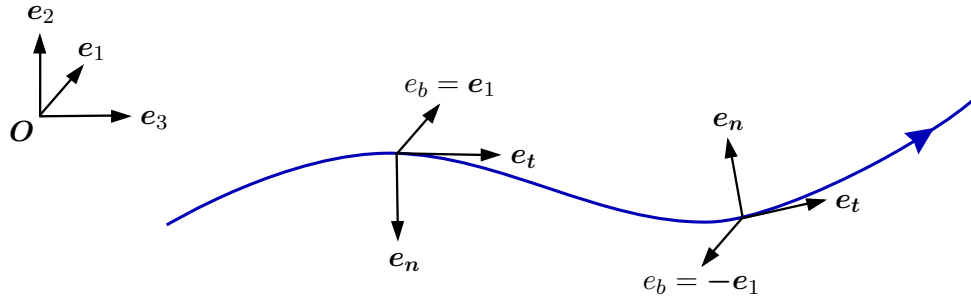


Figure 2.4: A space curve with the evolution of the Frenet triad in respect to arc length  $s$  in a global frame  $\mathbf{O}$ .

The position vector  $\mathbf{r}$  of any point on the curve can be defined by specifying the value of  $s$  at the point of interest:

$$\mathbf{r} = \mathbf{r}(s) = x_1(s)\mathbf{e}_1 + x_2(s)\mathbf{e}_2 + x_3(s)\mathbf{e}_3.$$

The unit tangent vector  $\mathbf{e}_t$  of the curve is defined as

$$\mathbf{e}_t = \frac{\frac{\partial \mathbf{r}}{\partial s}}{\left\| \frac{\partial \mathbf{r}}{\partial s} \right\|}. \quad (2.20)$$

The derivative of this vector defines the curvature  $\kappa$  and the unit normal vector  $\mathbf{e}_n$ :

$$\frac{\partial \mathbf{e}_t}{\partial s} = \kappa \mathbf{e}_n. \quad (2.21)$$

That is,

$$\kappa = \left\| \frac{\partial \mathbf{e}_t}{\partial s} \right\|, \quad \mathbf{e}_n = \frac{1}{\kappa} \frac{\partial \mathbf{e}_t}{\partial s}. \quad (2.22)$$

The Frenet triad is then defined by the tangent and normal unit vectors as an orthonormal, right-handed frame:

$$\{\mathbf{e}_t, \mathbf{e}_n, \mathbf{e}_b = \mathbf{e}_t \times \mathbf{e}_n\}, \quad (2.23)$$

where  $\mathbf{e}_b$  is referred to as the unit binormal vector.

As the Frenet triad is orthonormal, the torsion  $\tau$  of the space curve is defined by the relation

$$\frac{\partial \mathbf{e}_b}{\partial s} = -\tau \mathbf{e}_n. \quad (2.24)$$

The curvature  $\kappa$  and torsion  $\tau$  are two important measures for a space curve and can also be defined without referring explicitly to the Frenet triad:

$$\kappa = \left\| \frac{\partial^2 \mathbf{r}}{\partial s^2} \right\|, \quad \tau = \left[ \frac{\partial \mathbf{r}}{\partial s}, \frac{\partial^2 \mathbf{r}}{\partial s^2}, \frac{\partial^3 \mathbf{r}}{\partial s^3} \right], \quad (2.25)$$

where  $[\mathbf{a}, \mathbf{b}, \mathbf{c}]$  denotes the scalar triple product  $\mathbf{a} \cdot (\mathbf{b} \times \mathbf{c}) = \mathbf{b} \cdot (\mathbf{c} \times \mathbf{a}) = \mathbf{c} \cdot (\mathbf{a} \times \mathbf{b})$ . A curve  $\mathcal{C}$  is referred to as right-handed, if  $\tau > 0$ , and as left-handed if  $\tau < 0$ . For a curve where  $\mathbf{r} = \mathbf{r}(s, t)$  the Frenet triad needs to be calculated at each instant  $t$ .

### Note

The Frenet frame of a curve does not exist at points where the speed or the curvature vanishes, i.e. equal to zero. In this case,  $\mathbf{n}$  is not uniquely defined. As the parameter  $s$  passes through such a point,  $\mathbf{n}$  suffers a discontinuous change. This means, Frenet frames are only applicable to regular curves.

### 3.1.1 Frenet–Serret Relations

The Frenet–Serret relations are compact expressions of the rate of change of the Frenet triad basis vectors expressed with respect to the basis  $\{\mathbf{e}_t, \mathbf{e}_n, \mathbf{e}_b\}$ . These relations are obtained by using the definitions Eq. (2.20) and Eq. (2.24) and by differentiating the relation  $\mathbf{e}_n = \mathbf{e}_b \times \mathbf{e}_t$ :

$$\frac{\partial \mathbf{e}_t}{\partial s} = \kappa \mathbf{e}_n, \quad \frac{\partial \mathbf{e}_n}{\partial s} = -\kappa \mathbf{e}_t + \tau \mathbf{e}_b, \quad \frac{\partial \mathbf{e}_b}{\partial s} = -\tau \mathbf{e}_n. \quad (2.26)$$

Note that the matrix is skew-symmetric.

The Frenet–Serret relations are also known as Frenet–Serret theorem, and can be stated more concisely using matrix notation

$$\begin{bmatrix} \mathbf{e}'_t \\ \mathbf{e}'_n \\ \mathbf{e}'_b \end{bmatrix} = \begin{bmatrix} 0 & \kappa & 0 \\ -\kappa & 0 & \tau \\ 0 & -\tau & 0 \end{bmatrix} \begin{bmatrix} \mathbf{e}_t \\ \mathbf{e}_n \\ \mathbf{e}_b \end{bmatrix} \quad (2.27)$$

**Example: A circular helix**

Beginning the calculation of  $\mathbf{e}_t$ ,  $\mathbf{e}_n$  and  $\mathbf{e}_b$  with the definition for a circular helix as the one illustrated in Fig. 2.28, which can be expressed as

$$\mathbf{r} = R\mathbf{e}_r + R\alpha\theta\mathbf{e}_3, \quad (2.28)$$

where  $R$  represents the radius of the helix,  $\theta$  represents a cylindrical polar coordinate and furthermore the following applies for  $\mathbf{e}_r$  and  $\mathbf{e}_\theta$ :

$$\mathbf{e}_r = \cos(\theta)\mathbf{e}_1 + \sin(\theta)\mathbf{e}_2, \quad \mathbf{e}_\theta = \cos(\theta)\mathbf{e}_2 - \sin(\theta)\mathbf{e}_1. \quad (2.29)$$

In the illustrated example the circular helix is right handed. To define the alignment of the helix it is common to introduce a pitch parameter  $\gamma$ :

$$\gamma = \arctan(\alpha). \quad (2.30)$$

In the right handed case  $\gamma > 0$  or equivalent  $\alpha > 0$ . If  $\gamma < 0$  or equivalent  $\alpha < 0$  the helix is left handed and if  $\gamma = \alpha = 0$  the helix corresponds to a circle.

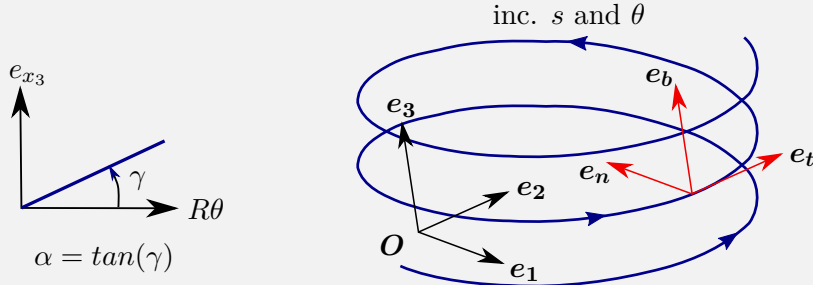


Figure 2.5: Example of a right handed circular helix.

Due to these definitions, the determination of the Frenet Triad of a circular helix starts following Eq. (2.20) by differentiating  $\mathbf{r}$  with respect to  $s$  and using the chain rule:

$$\mathbf{e}_t = \frac{\partial \mathbf{r}}{\partial s} = \frac{\partial \theta}{\partial s} (R\mathbf{e}_\theta + R\alpha\theta\mathbf{e}_3). \quad (2.31)$$

Knowing that  $\mathbf{e}_t$  is a unit vector, the term  $\frac{d\theta}{ds} = \pm \frac{1}{R\sqrt{1+\alpha^2}}$  can be inferred and the Frenet Triad  $\mathbf{e}_t, \mathbf{e}_n, \mathbf{e}_b$  results. In the case of  $\frac{d\theta}{ds} > 0$ , the Frenet Triad arises as follows:

$$\mathbf{e}_t = \frac{1}{\sqrt{1+\alpha^2}} (\mathbf{e}_\theta + \alpha\mathbf{e}_3), \quad \mathbf{e}_n = -\mathbf{e}_r, \quad \mathbf{e}_b = \frac{1}{\sqrt{1+\alpha^2}} (\mathbf{e}_3 - \alpha\mathbf{e}_\theta), \quad (2.32)$$

and alternatively, when  $\frac{d\theta}{ds} < 0$ :

$$\mathbf{e}_t = \frac{-1}{\sqrt{1+\alpha^2}} (\mathbf{e}_\theta + \alpha\mathbf{e}_3), \quad \mathbf{e}_n = -\mathbf{e}_r, \quad \mathbf{e}_b = \frac{-1}{\sqrt{1+\alpha^2}} (\mathbf{e}_3 - \alpha\mathbf{e}_\theta). \quad (2.33)$$

Applying the pitch angle  $\gamma$ , Eq. (2.32) and Eq. (2.33) simplify to the single prescription:

$$\mathbf{e}_t = \cos(\gamma)\mathbf{e}_\theta + \sin(\gamma)\mathbf{e}_3, \quad \mathbf{e}_n = -\mathbf{e}_r, \quad \mathbf{e}_b = \sin(\gamma)\mathbf{e}_\theta + \cos(\gamma)\mathbf{e}_3. \quad (2.34)$$

### 3.1.2 Darboux Vector

The Darboux vector  $\omega_F$  is the angular velocity vector of the Frenet frame of a space curve (named after the mathematician Darboux):

$$\omega_F = \tau e_t + \kappa e_b \quad (2.35)$$

and has the symmetrical properties

$$\omega_F \times e_t = e'_t \quad \omega_F \times e_n = e'_n \quad \omega_F \times e_b = e'_b. \quad (2.36)$$

The Darboux vector provides a concise way of interpreting curvature the  $\kappa$  and the torsion  $\tau$  geometrically: the curvature is the measure of the rotation of the Frenet frame about the binormal unit vector, whereas the torsion is the measure of the rotation of the Frenet frame about the tangent unit vector.

## 3.2 Bishop Frames

Bishop explored different ways to frame curves and defined an alternative to the standard Frenet frame. A Bishop's frame for a curve is also called the natural frame or the rotation-minimizing frame and often referred to as *parallel transport frame*.

$$\frac{\partial e_t}{\partial s} = \kappa_1 e_{n_1} + \kappa_2 e_{n_2}, \quad \frac{\partial e_{n_1}}{\partial s} = -\kappa_1 e_t, \quad \frac{\partial e_{n_2}}{\partial s} = -\kappa_2 e_n, \quad (2.37)$$

where

$$\kappa = \sqrt{\kappa_1^2 + \kappa_2^2} \quad \tau = \frac{\kappa_1 \kappa'_2 + \kappa_2 \kappa'_1}{\kappa_1^2 + \kappa_2^2}.$$

While the Frenet frame is uniquely defined for any regular curve with nonzero curvature, by contrast, the Bishop's frame is not unique and is well defined even at points where the curvature vanishes. The freedom lies in choosing a starting frame. For instance, by selecting the unit vector  $e_{n_1}$  lying in the plane normal at a chosen location  $s = s_0$  on the curve. This choice then determines the second unit vector  $e_{n_2}$ .

The Bishop relations can be stated concisely in matrix notation as:

$$\begin{bmatrix} e'_t \\ e'_{n_1} \\ e'_{n_2} \end{bmatrix} = \begin{bmatrix} 0 & \kappa_1 & \kappa_2 \\ -\kappa_1 & 0 & 0 \\ -\kappa_2 & 0 & 0 \end{bmatrix} \begin{bmatrix} e_t \\ e_{n_1} \\ e_{n_2} \end{bmatrix}. \quad (2.38)$$

For a Bishop frame, one can define a vector

$$\omega_B = \kappa_1 e_{n_2} - \kappa_2 e_{n_1}, \quad (2.39)$$

where

$$\omega_B \times e_t = e'_t, \quad \omega_B \times e_{n_1} = e'_{n_1}, \quad \text{and} \quad \omega_B \times e_{n_2} = e'_{n_2}. \quad (2.40)$$

### Example: Bishop Motion

Let the motion of a rigid body with a non-zero translational velocity be given by a  $\mathbf{g} \in SE(3)$  as

$$\mathbf{g}(t) = \begin{bmatrix} \mathbf{R}(t) & \mathbf{r}(t) \\ \mathbf{0} & 1 \end{bmatrix}.$$

The rotation matrix is given as a Bishop frame, i.e.  $\mathbf{R}(t) = [\mathbf{e}_t \mid \mathbf{e}_{n_1} \mid \mathbf{e}_{n_2}]$ . The body fixed velocity of such a motion is given by the twist vector

$$\boldsymbol{\xi} = \begin{bmatrix} 0 \\ \kappa_1 \\ \kappa_2 \\ 1 \\ 0 \\ 0 \end{bmatrix}$$

### 3.3 Relating Bishop and Frenet Frames

A Bishop frame can be related to the Frenet triad by defining an angle  $\theta_B$  (see Fig. 2.6):

$$\begin{aligned} \mathbf{e}_n &= \cos(\theta_B)\mathbf{e}_{n_1} + \sin(\theta_B)\mathbf{e}_{n_2} \\ \mathbf{e}_b &= -\sin(\theta_B)\mathbf{e}_{n_1} + \cos(\theta_B)\mathbf{e}_{n_2}. \end{aligned}$$

With the Frenet-Serret relations in Eq. (2.26) and assuming that  $\kappa \neq 0$ , the curvature  $\kappa_1$  and  $\kappa_2$  can be computed from  $\kappa$  and  $\tau$ :

$$\begin{aligned} \kappa_1 &= \kappa \cos(\theta_B) \\ \kappa_2 &= \kappa \sin(\theta_B). \end{aligned}$$

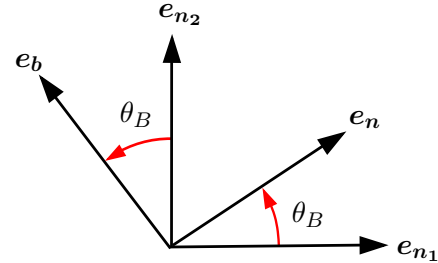


Figure 2.6: The angle  $\theta_B$  relating the normal vectors of Frenet and Bishop frames.

The angle  $\theta_B$  is found by integrating the relation

$$\tau = \frac{\partial \theta_B}{\partial s}. \quad (2.41)$$

Furthermore, the Darboux vector and the vector  $\omega_B$  are related by

$$\begin{aligned} \omega_B &= \kappa_1 \mathbf{e}_{n_2} - \kappa_2 \mathbf{e}_{n_1} = \kappa \mathbf{e}_b \\ \omega_F &= \tau \mathbf{e}_t + \omega_B. \end{aligned}$$

## References

- [1] J M Selig. *Geometric Fundamentals of Robotics*. Springer, 2005.
- [2] Richard M Murray, Zexiang Li, and S Shankar Sastry. *A Mathematical Introduction to Robotic Manipulation*. CRC Press, 1994.
- [3] Oliver M O'Reilly. *Modeling Nonlinear Problems in the Mechanics of Strings and Rods*. Springer International Publishing, 2017.

### **3 Cosserat Theory for Elastic Rods**

<b>1</b>	<b>Special Cosserat Rod . . . . .</b>	<b>22</b>
<b>2</b>	<b>Kinematics of the Deformation . . . . .</b>	<b>23</b>
<b>3</b>	<b>Mechanics . . . . .</b>	<b>24</b>
<b>4</b>	<b>Constitutive Relations . . . . .</b>	<b>25</b>
<b>5</b>	<b>Governing Differential Equations . . . . .</b>	<b>27</b>
	<b>References . . . . .</b>	<b>29</b>

Continuum robots can mechanically be seen as slender structures, i.e. structures that are much longer in one direction than the other two directions. Slender structures may be described by elastic rod theory, if one is interested in the phenomena on length scales much larger than the lateral dimensions. Classical beam theory is a simplified version of elastic rod theory, which is only applicable if small deformations are considered. Beam theory usually holds for structural engineering applications where only small deformations occur by design, such as in bridges or buildings. But in those applications where large deformations need to be described, elastic rod theory is the theory of choice in order to account for nonlinear geometric effects.

Cosserat theory for elastic rods represents a general tool for describing the deformation of continuum robots. For tendon-actuated robots, this approach allows to model distributed wrenches that a tendon exerts on the backbone structure. Thus, not only straight tendons can be accounted for, but also general routing paths. Further, using Cosserat rod theory, it is possible to account for independent torsion of each individual tube, hence for multiple elastica. In the following, we outline the mathematical model for the spatial deformation of a rod, namely the special theory of Cosserat rods. It was developed by the Cosserat brothers (Eugène and Françoise) in the beginning of the 20th century. The section is based on Antman's extensive book on nonlinear problems of elasticity [1] (in particular Chapter 8) and Goss' thesis [2].

The general idea of Cosserat theory is to describe a rod as a set of material points which form a curve in Cartesian space, which corresponds to the centerline or line of centroids. The points lying on the curve posses their own local coordinate system with a triad of basis vectors, which are referred to as directors. If the rod undergoes a continuous deformation, then each point moves to a new location taking the directors with it. By keeping track of the orientation of the directors relative to their orientation prior to deformation, the change in state of the rod can be completely specified. This complete specification holds for any deformation including bending, twisting, shearing, and stretching.

## 1 Special Cosserat Rod

A rod has the distinctive property that two of its dimensions are much smaller than the third. This enables to fully parameterize a rod by a single parameter, the arc length  $s \in [0, \ell]$ . The origin ( $s = 0$ ) is defined at the base of the rod and  $\ell$  is the length of the rod.

The configuration of a rod is described by a smooth curve<sup>1</sup>  $\mathcal{C}$  with points  $\mathbf{r}(s, t)$  positioned along the curve, where  $\mathbf{r}(\cdot, t)$  defines the configuration of the rod at time  $t$ , and a pair of orthonormal rod-centered unit vectors, i.e. the directors  $\mathbf{d}_1(s, t)$  and  $\mathbf{d}_2(s, t)$ , which span the cross section of the rod, see Figure 3.1. The third unit vector is defined as

$$\mathbf{d}_3 := \mathbf{d}_1 \times \mathbf{d}_2. \quad (3.1)$$

$\mathbf{d}_3$  is tangent to the curve. The vectors  $\{\mathbf{d}_1, \mathbf{d}_2, \mathbf{d}_3\}$  are a right-handed orthonormal basis located at  $\mathbf{r}(s, t)$  and called *directors*. The directors describe the deformation of material in the cross section of the rod. Thus, Cosserat theory allows for:

- (1) Normal cross-sectional extension when the magnitudes of the directors projected into the plane normal to the curve change,
- (2) Tangential shear deformation when the components of  $\mathbf{d}_i$  change in the direction of  $\mathbf{d}_3$ ,

---

<sup>1</sup>If the curve is a straight line, then the rod is called a beam.

- (3) Normal cross-sectional shear deformation when the angle between the projections of  $\mathbf{d}_1$  and  $\mathbf{d}_2$  into the plane normal to the curve changes.

Unlike  $\mathbf{r}(s, t)$ , the directors are not affected by pure translations of the rod, but may rotate independently along the curve  $\mathcal{C}$ . The length of the rod segment  $(s_1, s_2)$  in the configuration at time  $t$  is the integral  $\int_{s_1}^{s_2} \|\frac{\partial \mathbf{r}}{\partial s}\| ds$ .

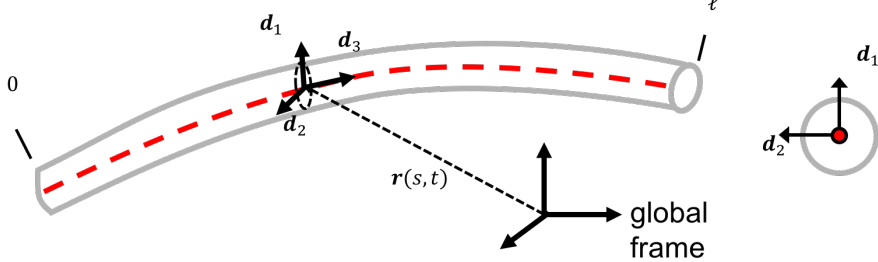


Figure 3.1: An elastic rod with its centerline described by a smooth curve  $r(s)$  in respect to a global coordinate frame and an accompanying orthonormal frame spanning its cross-section.

If the motion of a rod is regarded, we identify a reference configuration of the rod with  $\mathbf{r}^*(s)$ ,  $\mathbf{d}_1^*(s)$  and  $\mathbf{d}_2^*(s)$ .

## 2 Kinematics of the Deformation

The basis  $\{\mathbf{d}_k\}$  ( $k = 1, 2, 3$ ) is the intrinsic description of the deformation and can be decomposed into the relevant vector-valued functions

$$\mathbf{u}(s, t) = u_1 \mathbf{d}_1 + u_2 \mathbf{d}_2 + u_3 \mathbf{d}_3 \quad (3.2)$$

with the flexural (bending) strains  $u_1$ ,  $u_2$  (bending in x- and y-direction) and the torsional strain  $u_3$  (measuring the amount of twist), and

$$\partial_s \mathbf{r} = \mathbf{v}(s, t) = v_1 \mathbf{d}_1 + v_2 \mathbf{d}_2 + v_3 \mathbf{d}_3 \quad (3.3)$$

with the shear strains  $v_1$  and  $v_2$  in  $\mathbf{d}_1$  and  $\mathbf{d}_2$  directions and the dilatation  $v_3$ .  $\mathbf{v}(s, t)$  provides information in respect to the reference configuration of the rod in terms of the length ratio:

$v_3 > 0$	rod is elongated
$v_3 = 1$	rod is inextensible ( $\ell$ const.)
$v_3 < 0$	rod is compressed.

As a consequence, the strain variables  $\{u_1, u_2, u_3, v_1, v_2, v_3\}$  determine  $\mathbf{r}(s, t)$ ,  $\mathbf{d}_1(s, t)$ , and  $\mathbf{d}_2(s, t)$ , i.e. the configuration of the rod at time  $t$  and account for the change of shape.

By taking the vector product of  $\mathbf{u}$  with the directors, the following expression for the turning of the directors in space can be obtained

$$\partial_s \mathbf{d}_i = \mathbf{u} \times \mathbf{d}_i \quad (3.4)$$

with  $i = 1, 2, 3$ .

Differentiating the directors with respect to time  $t$  leads to

$$\partial_t \mathbf{d}_i = \mathbf{w} \times \mathbf{d}_i \quad (3.5)$$

with rotational velocity  $\mathbf{w}$  and  $i = 1, 2, 3$ . Since  $\partial_t \partial_s \mathbf{d}_i = \partial_s \partial_t \mathbf{d}_i$ , the following compatibility equation holds

$$\partial_t(\mathbf{u} \times \mathbf{d}_i) = \partial_s(\mathbf{w} \times \mathbf{d}_i), \quad (3.6)$$

which implies that

$$(\partial_s \mathbf{w} - \partial_t \mathbf{u}) \times \mathbf{d}_i = u_i \mathbf{w} - w_i \mathbf{u}. \quad (3.7)$$

### The Strains

$\mathbf{u}$  and  $\mathbf{v}$  are invariant under rigid body motion and thus only give information about the change of shape.

## 3 Mechanics

Adjacent material points exert a resultant contact force and contact moment on each other. Thus, for  $s \in (0, \ell)$ ,  $\mathbf{n}(s, t)$  and  $\mathbf{m}(s, t)$  are the contact force and contact moment respectively exerted by the material of  $(s, \ell]$  on that of  $[0, s)$  at time  $t$ . The force  $\mathbf{n}(s, t)$  is given by

$$\mathbf{n}(s, t) = n_1 \mathbf{d}_1 + n_2 \mathbf{d}_2 + n_3 \mathbf{d}_3, \quad (3.8)$$

where  $n_1$  and  $n_2$  are the shear forces in the directions  $\mathbf{d}_1$  and  $\mathbf{d}_2$  respectively, and  $n_3$  is the axial force in the direction  $\mathbf{d}_3$  (tension is positive and compression is negative).

The moment  $\mathbf{m}(s, t)$  is given by

$$\mathbf{m}(s, t) = m_1 \mathbf{d}_1 + m_2 \mathbf{d}_2 + m_3 \mathbf{d}_3, \quad (3.9)$$

where  $m_1$  and  $m_2$  are the bending moments about  $\mathbf{d}_1$  and  $\mathbf{d}_2$  respectively, and  $m_3$  is the twisting moment about  $\mathbf{d}_3$ .

Figure 3.2 illustrates the components of  $\mathbf{n}(s, t)$  and  $\mathbf{m}(s, t)$  acting on an element of the rod schematically. In the configuration at time  $t$ , the material of  $(b, \ell]$  exerts a resultant contact force  $\mathbf{n}^+(b, t)$  and a contact torque  $\mathbf{r}(b, t) \times \mathbf{n}^+(b, t) + \mathbf{m}^+(b, t)$  on the material of  $[a, b]$ .  $\mathbf{m}^+(b, t)$  is the resultant contact moment.  $\mathbf{n}^+(., t)$  and  $\mathbf{m}^+(., t)$  depend only on the element separating the two body parts of the rod and are independent of any other property of the rod. The resultant contact force and contact torque exerted on  $[a, b]$  by  $[0, a)$  are denoted by  $-\mathbf{n}^-(a, t)$  and  $-\mathbf{r}(a, t) \times \mathbf{n}^-(a, t) - \mathbf{m}^-(a, t)$ . The resultant of all other forces acting on the element  $[a, b]$  of the rod in this configuration at time  $t$  has the form

$$\int_a^b \mathbf{f}(s, t) ds \quad (3.10)$$

and the resultant of all other torques has the form

$$\int_a^b [\mathbf{r}(s, t) \times \mathbf{f}(s, t) + \mathbf{l}(s, t)] ds, \quad (3.11)$$

where  $\mathbf{f}(s, t)$  and  $\mathbf{l}(s, t)$  are the body force and the body moment per unit reference length at  $(s, t)$ .

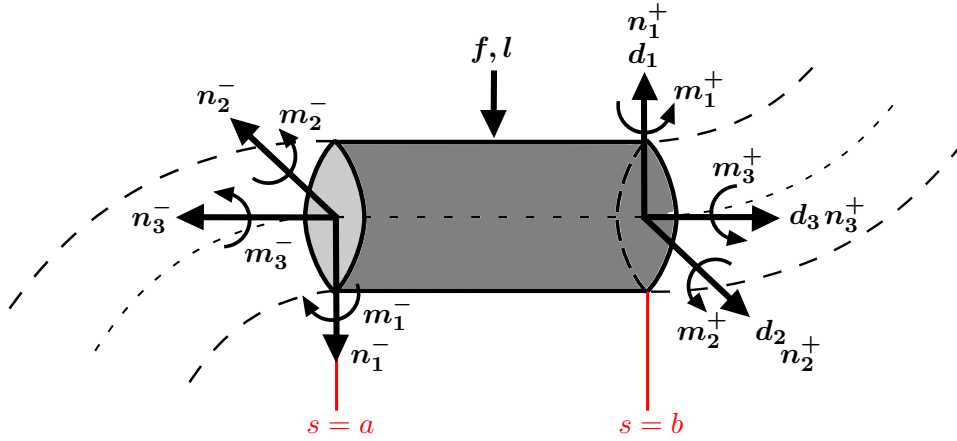


Figure 3.2: The equilibrium of an element  $ds$  of a rod involves contact forces  $\mathbf{n}_i$  and contact moments  $\mathbf{m}_i$ , body forces  $\mathbf{f}$  and body moments  $\mathbf{l}$ .

For any static equilibrium configuration, the resultant of the contact forces and contact moments acting on a rod must be zero. With the inclusion of the body force  $\mathbf{f}$  and body moment  $\mathbf{l}$ , the equilibrium of forces and moments can be written coordinate-free as

$$\partial_s \mathbf{n} + \mathbf{f} = \mathbf{0} \quad (3.12)$$

$$\partial_s \mathbf{m} + \partial_s \mathbf{r} \times \mathbf{n} + \mathbf{l} = \mathbf{0}. \quad (3.13)$$

## 4 Constitutive Relations

The constitutive relations govern how the rod responds to the bending moments  $m_1$  and  $m_2$ , to the twisting moment  $m_3$ , to the shear forces  $n_1$  and  $n_2$ , and to the axial force  $n_3$ . Thus, the constitutive relations link the forces and moments to the kinematics, i.e. they connect Eq. (3.12) and Eq. (3.13) to Eq. (3.2) and Eq. (3.3) respectively.

In the case of elastic rods, there are constitutive functions<sup>2</sup>  $\hat{\mathbf{m}}$  and  $\hat{\mathbf{n}}$  which relate the strain variables to the forces and moments:

$$\mathbf{m}(s, t) = \hat{\mathbf{m}}(\mathbf{u}(s, t), \mathbf{v}(s, t), s) \quad (3.14)$$

$$\mathbf{n}(s, t) = \hat{\mathbf{n}}(\mathbf{u}(s, t), \mathbf{v}(s, t), s) \quad (3.15)$$

with  $\mathbf{m} := (m_1, m_2, m_3)$ ,  $\mathbf{n} := (n_1, n_2, n_3)$ . Please note that  $\mathbf{u} := (u_1, u_2, u_3)$  and  $\mathbf{v} := (v_1, v_2, v_3)$  are triples of the strain variables. For each fixed  $s$  these constitutive functions describe deformations that preserve orientations.

**Linear Elastic Constitutive Relations** In the case of a linear relationship between the loads and the strains, the constitutive relations may be written in the following form

$$\begin{aligned} m_1 &= B_1(u_1 - u_1^*) & n_1 &= \bar{B}_1(v_1 - v_1^*) \\ m_2 &= B_2(u_2 - u_2^*) & n_2 &= \bar{B}_2(v_2 - v_2^*) \\ m_3 &= C(u_3 - u_3^*) & n_3 &= \bar{C}(v_3 - v_3^*) \end{aligned} \quad (3.16)$$

<sup>2</sup>Note that  $\mathbf{m}$  and  $\mathbf{n}$  are triples of the moments and forces respectively and should not be mixed up with  $\mathbf{m}$  and  $\mathbf{n}$

where  $B_i, C, \bar{B}_i, \bar{C}$  are the rigidities and  $B_1 \leq B_2$  and  $\bar{B}_1 \leq \bar{B}_2$ . In the case that  $B_1 = B_2 =: B$ , i.e. if the rod is isotropic, a useful non-dimensional characterization of a particular rod is Poisson's ratio

$$\nu = \frac{B}{C} - 1. \quad (3.17)$$

Note, that the rigidities are the product of two components, one material and one geometric:

$B_1 = EI_1$	Flexural rigidity about $\mathbf{d}_1$	[Nm <sup>2</sup> ]
$B_2 = EI_2$	Flexural rigidity about $\mathbf{d}_2$	[Nm <sup>2</sup> ]
$C = GJ$	Torsional rigidity about $\mathbf{d}_3$	[Nm <sup>2</sup> ]
$\bar{B}_1 = GA\alpha_1$	Shearing rigidity along $\mathbf{d}_1$	[N]
$\bar{B}_2 = GA\alpha_2$	Shearing rigidity along $\mathbf{d}_2$	[N]
$\bar{C} = EA$	Axial rigidity along $\mathbf{d}_3$	[N]

where  $E$  is Young's modulus and  $G$  is the shear modulus, which are both material properties.  $A$  is the area of the cross section, and  $I_1$  and  $I_2$  are the second moments of area about  $\mathbf{d}_{1/2}$ , and  $J$  is the second polar moment of area about  $\mathbf{d}_3$ . These quantities are geometric properties of the cross section.  $\alpha_1$  and  $\alpha_2$  are numerical factors (shear coefficients) which depend on the geometry of the cross section. For instance, for a circular cross section  $\alpha_1 = \alpha_2 = 4/3$ .

### Note

It is important to emphasize the distinction between constitutive equations for a material in the three-dimensional theory (Cosserat shells) and constitutive equations for a Cosserat rod. Within the context of the three-dimensional theory, constitutive equations characterize the response of a material at each material point and are independent of the shape of the three-dimensional body composed of the material. In contrast, within the context of the Cosserat rod theory, the constitutive equations necessarily couple influences of the geometry of the rod-like structure with those of the response of the three-dimensional material from which the rod is constructed. In general, the coupling of material and geometrical properties of the rod must be modeled by the Cosserat constitutive equations.

## 5 Governing Differential Equations

So far we described the deformable rod with the vector  $\mathbf{r}(s, t)$ , which points towards the centerline of the rod, and the directors  $\mathbf{d}_1(s, t)$ ,  $\mathbf{d}_2(s, t)$ ,  $\mathbf{d}_3(s, t)$ , which describe the coordinate frame at the centerline of the rod. For convenience, we now express the shape of the rod using a transformation matrix as presented in Eq. (2.5) with  $\mathbf{R}(s, t) = [\mathbf{d}_1(s, t), \mathbf{d}_2(s, t), \mathbf{d}_3(s, t)]$ .

We can rewrite the rod kinematics Eqs. (3.3) and (3.4) as (see [3])

$$\partial_s \mathbf{r} = \mathbf{R} \mathbf{v} \quad (3.18)$$

$$\partial_s \mathbf{R} = \mathbf{R} \hat{\mathbf{u}}. \quad (3.19)$$

For the remainder of the script, we assume the rod to be constituted of a linear elastic material, such that the relationship stated in Eq. (3.16) apply. These can be expressed in matrix form and lead to

$$\mathbf{n} = \mathbf{R} \mathbf{K}_{\text{SE}} (\mathbf{v} - \mathbf{v}^*) \quad (3.20)$$

$$\mathbf{m} = \mathbf{R} \mathbf{K}_{\text{BE}} (\mathbf{u} - \mathbf{u}^*), \quad (3.21)$$

with

$$\mathbf{K}_{\text{SE}}(s) = \begin{bmatrix} GA(s) & 0 & 0 \\ 0 & GA(s) & 0 \\ 0 & 0 & EA(s) \end{bmatrix} \quad \text{and}$$

$$\mathbf{K}_{\text{BT}}(s) = \begin{bmatrix} EI_1(s) & 0 & 0 \\ 0 & EI_2(s) & 0 \\ 0 & 0 & GJ \end{bmatrix}.$$

The full set of explicit differential equations governing the deformation of the Cosserat rod are then given by:

$$\begin{aligned} \partial_s \mathbf{r} &= \mathbf{R} \mathbf{v} \\ \partial_s \mathbf{R} &= \mathbf{R} \hat{\mathbf{u}} \\ \partial_s \mathbf{v} &= \partial_s \mathbf{v}^* - \mathbf{K}_{\text{SE}}^{-1} ((\hat{\mathbf{u}} \mathbf{K}_{\text{SE}} + \partial_s \mathbf{K}_{\text{SE}})(\mathbf{v} - \mathbf{v}^*) + \mathbf{R}^T \mathbf{f}) \\ \partial_s \mathbf{u} &= \partial_s \mathbf{u}^* - \mathbf{K}_{\text{BT}}^{-1} ((\hat{\mathbf{u}} \mathbf{K}_{\text{BT}} + \partial_s \mathbf{K}_{\text{BT}})(\mathbf{u} - \mathbf{u}^*) + \hat{\mathbf{v}} \mathbf{K}_{\text{SE}} (\mathbf{v} - \mathbf{v}^*) + \mathbf{R}^T \mathbf{l}) \end{aligned} \quad (3.22)$$

**Simplification** For long slender rods the effects of bending and torsion are dominant and responsible for the changes in the shape. [3] Therefore in comparison the effects of shear and extension are negligible, whereby the model can be simplified by setting  $\mathbf{v} = \mathbf{v}^*$ . With respect to Eq. (3.22), using  $\mathbf{v} = \mathbf{v}^* = \mathbf{e}_3$  (no shear and elongation), this results in the Kirchhoff Rod Equations:

$$\begin{aligned} \partial_s \mathbf{r} &= \mathbf{R} \mathbf{e}_3 \\ \partial_s \mathbf{R} &= \mathbf{R} \hat{\mathbf{u}} \\ \partial_s \mathbf{n} &= -\mathbf{f} \\ \partial_s \mathbf{u} &= \partial_s \mathbf{u}^* - \mathbf{K}_{\text{BT}}^{-1} ((\hat{\mathbf{u}} \mathbf{K}_{\text{BT}} + \partial_s \mathbf{K}_{\text{BT}})(\mathbf{u} - \mathbf{u}^*) + \mathbf{R}^T \mathbf{l}) \end{aligned} \quad (3.23)$$

**Example: Derivation of explicit cosserat rod model equations [3]**

To obtain a set of final explicit model equations that can be solved for the rod's shape, we now combine all the rod kinematics with the equilibrium equations and constitutive laws. Therefore, we first derive the first equation from the constitutive laws (3.20) with respect to the arc length  $s$ .

$$\partial_s \mathbf{n} = \partial_s \mathbf{R} \mathbf{K}_{\text{SE}}(\mathbf{v} - \mathbf{v}^*) + \mathbf{R} \partial_s \mathbf{K}_{\text{SE}}(\mathbf{v} - \mathbf{v}^*) + \mathbf{R} \mathbf{K}_{\text{SE}}(\partial_s \mathbf{v} - \partial_s \mathbf{v}^*)$$

Substituting Eqs. (3.12) and (3.18) yields

$$0 = \mathbf{R} \hat{\mathbf{u}} \mathbf{K}_{\text{SE}}(\mathbf{v} - \mathbf{v}^*) + \mathbf{R} \partial_s \mathbf{K}_{\text{SE}}(\mathbf{v} - \mathbf{v}^*) + \mathbf{R} \mathbf{K}_{\text{SE}}(\partial_s \mathbf{v} - \partial_s \mathbf{v}^*) + \mathbf{f}.$$

We can now multiply the expression by  $\mathbf{R}^T$  and solve for  $\partial_s \mathbf{v}$ :

$$\partial_s \mathbf{v} = \partial_s \mathbf{v}^* - \mathbf{K}_{\text{SE}}^{-1}((\hat{\mathbf{u}} \mathbf{K}_{\text{SE}} + \partial_s \mathbf{K}_{\text{SE}})(\mathbf{v} - \mathbf{v}^*) + \mathbf{R}^T \mathbf{f}).$$

Furthermore, deriving the second equation of the constitutive laws (3.21) results in

$$\partial_s \mathbf{m} = \partial_s \mathbf{R} \mathbf{K}_{\text{BT}}(\mathbf{u} - \mathbf{u}^*) + \mathbf{R} \partial_s \mathbf{K}_{\text{BT}}(\mathbf{u} - \mathbf{u}^*) + \mathbf{R} \mathbf{K}_{\text{BT}}(\partial_s \mathbf{u} - \partial_s \mathbf{u}^*).$$

Substituting Eqs. (3.18), (3.20) and (3.19) yields

$$\begin{aligned} (-\mathbf{R} \mathbf{v}) \times (\mathbf{R} \mathbf{K}_{\text{SE}}(\mathbf{v} - \mathbf{v}^*)) &= \mathbf{R} \hat{\mathbf{u}} \mathbf{K}_{\text{BT}}(\mathbf{u} - \mathbf{u}^*) + \mathbf{R} \partial_s \mathbf{K}_{\text{BT}}(\mathbf{u} - \mathbf{u}^*) \\ &\quad + \mathbf{R} \mathbf{K}_{\text{BT}}(\partial_s \mathbf{u} - \partial_s \mathbf{u}^*) + \mathbf{l}. \end{aligned}$$

Multiplying with  $\mathbf{R}^T$  again, using the relation  $\mathbf{a} \times \mathbf{b} = \hat{\mathbf{a}} \mathbf{b}$  and solving for  $\partial_s \mathbf{u}$  finally results in:

$$\partial_s \mathbf{u} = \partial_s \mathbf{u}^* - \mathbf{K}_{\text{BT}}^{-1}((\hat{\mathbf{u}} \mathbf{K}_{\text{BT}} + \partial_s \mathbf{K}_{\text{BT}})(\mathbf{u} - \mathbf{u}^*) + \hat{\mathbf{v}} \mathbf{K}_{\text{SE}}(\mathbf{v} - \mathbf{v}^*) + \mathbf{R}^T \mathbf{l}).$$

## Summary

The Cosserat theory describes an elastic rod under deformation as a set of coupled differential equations complemented by a set of boundary conditions.

1. **Equations of Rod Kinematics** provide description of how elastic deformations about the centerline are coded into rate of change of the centerline curve and the material frame  $\mathbf{d}_i$  at arc length  $s$  at time  $t$ .
2. **Equilibrium Equations** provide relations for force and moment equilibrium of the rod.
3. **Constitutive Equations** relate the moments and forces experienced by the cross-section to the linear and angular strains of each cross-section.

## References

- [1] Stuart S Antman. *Nonlinear Problems of Elasticity*. 2nd. Springer New York, 2005.
- [2] V.G.A. Goss. “Snap buckling, writhing and loop formation in twisted rods”. PhD thesis. University College London, 2003.
- [3] D. Caleb Rucker, Bryan A. Jones, and Robert J. Webster III. “A Geometrically Exact Model for Externally Loaded Concentric-Tube Continuum Robots”. In: *IEEE Transactions on Robotics* 26.5 (2010), pp. 769–780.

# 4 Forward Kinematic Modeling

<b>1</b>	<b>General Idea</b>	<b>32</b>
1.1	Kinematics Frameworks	32
1.1.1	Rigid Link Frameworks	32
1.1.2	Constant Curvature Frameworks	33
1.1.3	Non-constant Curvature Frameworks	34
1.2	Mechanics Frameworks	34
1.2.1	Lumped Parameter Frameworks	34
1.2.2	Energy Methods	34
1.2.3	Elasticity Theory	35
<b>2</b>	<b>Constant Curvature Kinematics Framework</b>	<b>35</b>
2.1	Robot Dependent Mapping	36
2.1.1	Tubular Continuum Robots	36
2.1.2	Tendon Actuated Continuum Robots	40
2.2	Robot Independent Mapping	44
2.2.1	Geometry of Circular Arcs	44
2.3	Using Frenet-Serret Frames	45
2.3.1	Exponential Coordinates	47
2.4	Accuracy	48
2.4.1	Accuracy for Tubular Continuum Robots	48
2.4.2	Accuracy for Tendon-actuated Continuum Robots	48
<b>3</b>	<b>Mechanics Framework using Elasticity Theory</b>	<b>50</b>
3.1	Tubular Continuum Robots	50
3.1.1	Kinematics	51
3.1.2	Kinematic Combination of Multiple Tubes	52
3.1.3	Constitutive Equations	53
3.1.4	Equilibrium Equations	53
3.1.5	Differential Kirchhoff Rod Equations	54
3.1.6	Boundary and Initial Conditions	55
3.2	Coupled Rod/Tendon Model for Tendon-actuated Continuum Robots	57
3.2.1	General Idea	57
3.2.2	Assumptions and Simplifications	57
3.2.3	Kinematics of the Tendons	58
3.2.4	Distributed Forces on Tendons	58
3.2.5	Tendon Loads on Backbone	60
3.2.6	Coupled Rod/Tendon Model Equations	60
3.2.7	Boundary Conditions	61
3.3	Solving the Explicit Model Equations	62
3.4	Accuracy	63
3.4.1	Accuracy for Tubular Continuum Robots	63

3.4.2	Accuracy for Tendon-actuated Continuum Robots . . .	64
<b>References</b>	.	<b>66</b>

Kinematic modeling is concerned with deriving a mapping between a robot's configuration space (or joint space) and the robot's task space (see Figure 4.1). The forward kinematics relates any configuration of the robot  $\mathbf{q}$  to task space  $\mathbf{x}$ . The inverse kinematics relates the robot's task space to the configuration space. The kinematic mapping may also involve the relationship between velocities  $\dot{\mathbf{x}} \Leftarrow \dot{\mathbf{q}}$  and accelerations  $\ddot{\mathbf{x}} \Leftarrow \ddot{\mathbf{q}}$ . Note that the operator  $\cdot$  denotes the derivation with respect to time.

Unlike the kinematics of rigid-link serial robots, where the pose of any joint can be determined in closed-form by relating link lengths and joint angles geometrically, the absence of joints and rigid links and the inherent compliance of continuum robots requires a continuous representation in task space and consideration of elasticity.

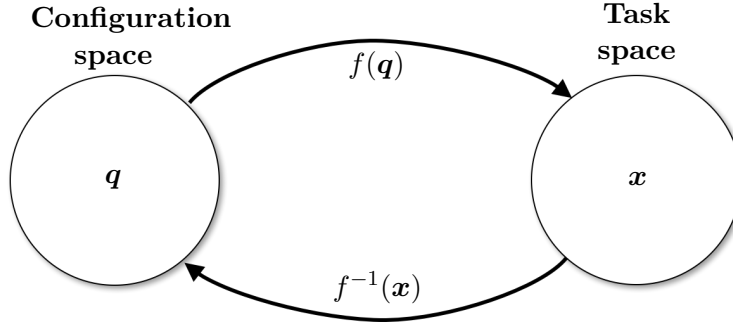


Figure 4.1: Kinematic mapping between a robot's configuration space and task space.

## 1 General Idea

Continuum robots have a fundamentally different structure than conventional robots which are composed of discrete rigid links connected by joints. When a robot has more degrees of freedom (DOF) than are necessary to execute a task (e.g. a 7 DOF robot arm with a 6 DOF task space), it is referred to as a redundant robot, or in extreme cases a hyperredundant robot. In the limit, as the number of joints tends to infinity (and the link lengths tend to zero), the robot approaches what is called a *continuum robot*. The shape and structure of a continuum robot are defined by an infinite-DOF elastic member. Usually, the configuration space is discrete, i.e. a finite number of DOF is used to determine the shape in task space.

There exist various approaches to establish the kinematic mapping between configuration and task space of continuum robots. Figure 4.2 provides an overview of the different categories of modeling approaches, which are summarized in the following.

### 1.1 Kinematics Frameworks

#### 1.1.1 Rigid Link Frameworks

Perhaps the most familiar kinematic framework for roboticists is the discrete approach employed in conventional rigid-link manipulator models. In this approach, a series of rigid links connected by conventional revolute, universal, or spherical joints is described using a series of homogeneous transformations, for example generated from classic Denavit-Hartenberg (D-H) parameter tables. These models are entirely appropriate in the case of hyperredundant or quasi-continuous robots, which are characterized by a discrete structure in Fig. 4.2, but discrete models can also provide good approximate representations of continuous elastic structures.

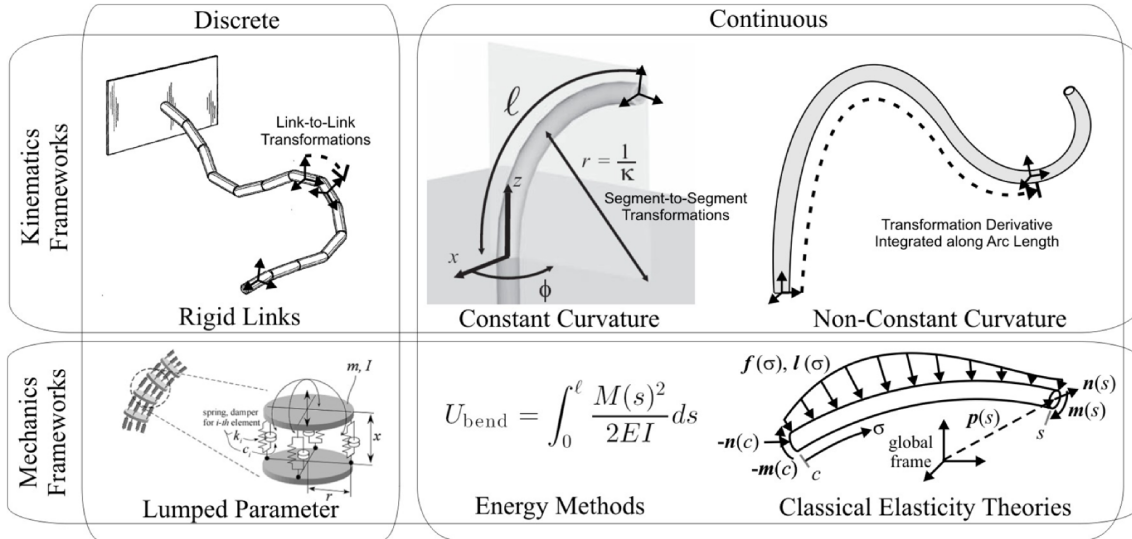


Figure 4.2: Modeling frameworks of discrete and continuous types of robots.

### 1.1.2 Constant Curvature Frameworks

In contrast with rigid-link models, constant curvature kinematic frameworks represent the continuum robot geometry with a finite number of mutually tangent curved segments each having a constant curvature along its length. Note that “constant” here refers to invariance with respect to arc length, not time. In this framework, the curvature, length, and angle of the curve’s bending plane (known as the “arc parameters”) of each segment form a set of configuration coordinates that completely describes the shape of the robot, i.e. the position and orientation at any point on the robot, can be written as a function of the arc parameters and the arc length along the backbone to that point. Similar to D-H parameters, each arc parameter could be a constant or vary with actuation, depending on the robot design. Usually, a single constant-curvature segment is employed for each actuatable segment of the robot.

Constant curvature is perhaps the most well-known and widely used kinematic framework for continuum robots, and the homogeneous transformation along a constant curvature robot backbone has been derived from a variety of perspectives, such as D-H parameters [1], Frenet-Serret frames [2], integral representation [3], and exponential coordinates [4]. Webster and Jones have devoted a large portion of their review paper [5] to showing equivalency between these formulations. Constant curvature modeling is described in detail in Section 2.

Constant curvature is often referred to as “the constant curvature assumption”, but care must be taken when using this phrase because it may not always accurately describe the methodology used in developing a constant curvature model. One can indeed make an *a priori* assumption of piecewise constant curvatures and subsequently formulate mechanics relationships and robot models under that assumption. However, constant curvature robot shape also arises as a natural result from mechanical principles when certain robot designs and assumptions are considered within a more general, variable-curvature framework (see e.g. [6]).

### 1.1.3 Non-constant Curvature Frameworks

The earliest continuum robot modeling approaches actually employed variable curvature kinematic frameworks as tools to resolve redundancy and control the shape of hyper-redundant serial manipulators [3]. Advanced kinematic models have adopted similar approaches for continuum robots which do not conform accurately to a constant curvature shape [7, 8, 9]. Variable-curvature frameworks typically describe a material-attached homogeneous reference frame comprising a position vector and a rotation matrix expressing the shape of the robot as a function of arc length. As depicted in Figure 4.2, the rotation matrix evolves along the arc length according to the differential kinematic relationship with a curvature vector  $\mathbf{u}$  containing angular rates of change about the current axes of the frame using the Lie algebra of  $SO(3)$ . The curvature vector is directly analogous to the angular velocity vector of a rigid body expressed in body-frame coordinates, except the derivative is with respect to arc length instead of time. Similarly, the position of the frame evolves along the arc length according to the differential kinematic relationship which uses the linear velocity vector of a rigid body  $\mathbf{v}$  expressed in body-frame coordinates. If the functions  $\mathbf{u}(s)$  and  $\mathbf{v}(s)$  are known, then the continuum robot backbone shape can be subsequently calculated by solving differential kinematic equations and an initial value problem from base to tip. Closed-form solutions to these differential equations are usually unknown, so general methods must employ a numerical integration scheme along the length from base to tip.

## 1.2 Mechanics Frameworks

The mechanics frameworks depicted in the second row of Figure 4.2 are not necessarily mutually exclusive. Each framework can be combined with various kinematic frameworks to arrive at a mechanics-based representation of the governing equations for the continuum robot shape.

### 1.2.1 Lumped Parameter Frameworks

Lumped parameter mechanics models arise almost automatically as an extension of discrete-link kinematic frameworks, but lumped-parameter approaches can also be imposed on top of constant-curvature kinematics frameworks. The approach involves attaching discrete mechanical elements such as point masses, springs, and dampers, to the kinematic framework in order to approximate the mechanical behavior of a continuous elastic and/or viscous medium. The governing equations for lumped-parameter models can be obtained by energy methods or classical Newton-Euler equations describing how forces and moments propagate from link to link.

### 1.2.2 Energy Methods

Energy methods are a powerful class of tools that have been used for a variety of purposes in continuum robot research. Elastic energy minimization was used in efforts to control hyper-redundant robots using a continuous modal framework [3] (by applying the Euler-Lagrange equations to an elastic energy function). Energy minimization was also used to derive both constant and variable curvature models for concentric-tube robots and to analyze their unstable torsional behavior [4, 8]. For multi-backbone robots, energy-based analysis (using the principle of virtual work) under a constant curvature framework has led to intrinsic wrench sensing capabilities [10]. Continuum manipulator dynamics have been approached by the principle of virtual power in a lumped-parameter, constant-curvature model [11], and by a Lagrangian approach [12, 13].

### 1.2.3 Elasticity Theory

There are various classical elasticity theories for long slender objects such as rods and strings that have been successfully adapted to describe continuum robots. The widely used constitutive law that internal moment is proportional to change in curvature (i.e.  $M = EI\Delta\kappa$ ) originates from classical Bernoulli-Euler beam theory. The use of Cosserat theory for elastic rods and its special case of a Kirchhoff rod, which neglects shear and axial strain, have become an effective method for obtaining general models of continuum robots. This approach is described in detail in Section 4.3.

## 2 Constant Curvature Kinematics Framework

The constant curvature kinematics framework assumes that a continuum robot's shape is composed of a finite number of curved links. These curved links are constant in curvature. This piecewise constant curvature assumption has the advantage that the kinematics can be decomposed into two mappings: a robot dependent mapping and a robot independent mapping. Figure 4.3 illustrates the decomposition.

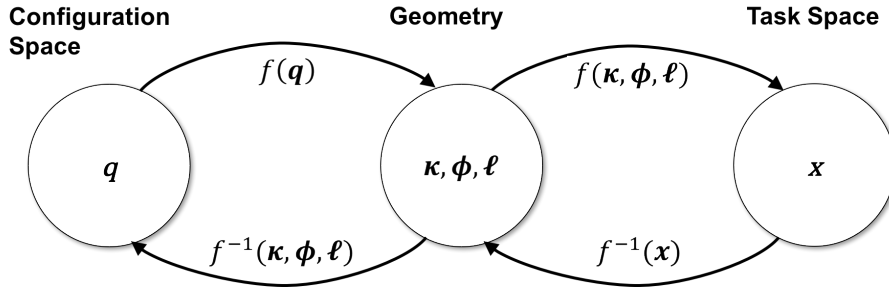


Figure 4.3: The constant curvature kinematic framework differentiates two mappings. The robot dependent mapping from configuration space  $\mathbf{q}$  to arc parameters  $\kappa, \phi, \ell$  and the robot independent mapping from arc parameters  $\kappa, \phi, \ell$  to task space  $\mathbf{x}$ .

The robot dependent mapping  $(\kappa_j, \phi_j, \ell_j) = f(\mathbf{q})$  relates the robot's configuration space  $\mathbf{q}$  to the geometry in terms of circular arc parameters  $(\kappa_j, \phi_j, \ell_j)$ , where  $j$  is the number of links. Arc parameters, which define the geometry of the robot, consist of triplets of curvature  $(\kappa(\mathbf{q}))$ , the angle of the plane containing the arc  $(\phi(\mathbf{q}))$ , and arc length  $(\ell(\mathbf{q}))$ , or sometimes  $s \in [0, \ell]$  (see Figure 4.4). Alternatively, the relationship  $\theta = \kappa s$  allows parameterization based on the angle  $\theta$  through which the arc bends.

The robot independent mapping  $\mathbf{x} = f(\kappa, \phi, \ell)$  relates the geometrical parameters to the task space. In task space, a continuum robot is either represented discretely by the position and orientation of the end point of each curved link or continuously by a 3D curve composed of the concatenated circular arcs describing each link.

Consequently, the inverse kinematics is also decomposed into two mappings. The robot independent inverse mapping from task space to geometrical parameters relates the desired

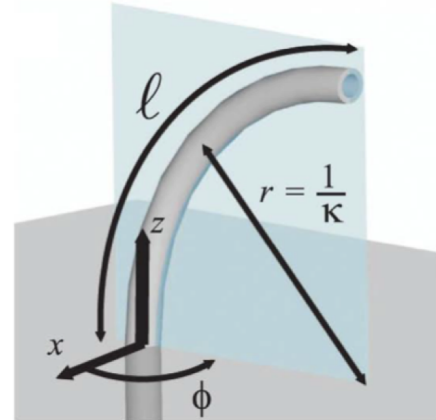


Figure 4.4: A circular arc is described by its curvature  $\kappa$ , the angle  $\phi$  of the plane containing the arc, and length  $\ell$  [4].

position or pose of the robot's tip to arc parameters. The robot dependent inverse mappings then determines the respective configuration parameters in order to achieve the arc parameters for each segment. In general, the inverse kinematics of robots is challenging as the number of solutions is not definite and a close-form solution does not necessarily exist. This is in particular challenging for hyperredundant and continuum robots. Closed-form solutions to the robot dependent inverse kinematics mapping do only exist for simplistic continuum robots, such as single section continuum robots (e.g. [14]) or two tube continuum robots of which only one is precurved (e.g. [15]). This version of the script is primarily concerned with forward kinematics.

## 2.1 Robot Dependent Mapping

The mapping from the configuration space of a continuum robot to arc parameters is robot-specific, since the actuators and unique robot design influence arc parameters in different ways. In particular, consideration of the forces and moments applied by actuators coupled with suitable approximations yields this mapping from actuator variables (pressure, length, rotation angles etc.) to curved links described by arc parameters. The following sections describe the robot dependent mapping for two examples of continuum robots: Tubular continuum robots and tendon actuated continuum robots.

### 2.1.1 Tubular Continuum Robots

Tubular continuum robots are composed of at least two ( $n \geq 2$ ) precurved elastic tubes. Those tubes are concentrically nested inside of each other (see Figure 4.5). The index  $i = \{1, \dots, n\}$  denotes each tube, starting with the innermost tube. In the following, we will consider tubes composed of a straight section with length  $L_i^s$  and a curved section with length  $L_i^c$  and constant curvature  $\kappa_i$  in only one direction. The total length of each tube then results in  $L_i = L_i^s + L_i^c$ . The precurvature of a tube is defined in the xz-plane, where the z axis is tangential to the constrained outlet at  $s = 0$ .

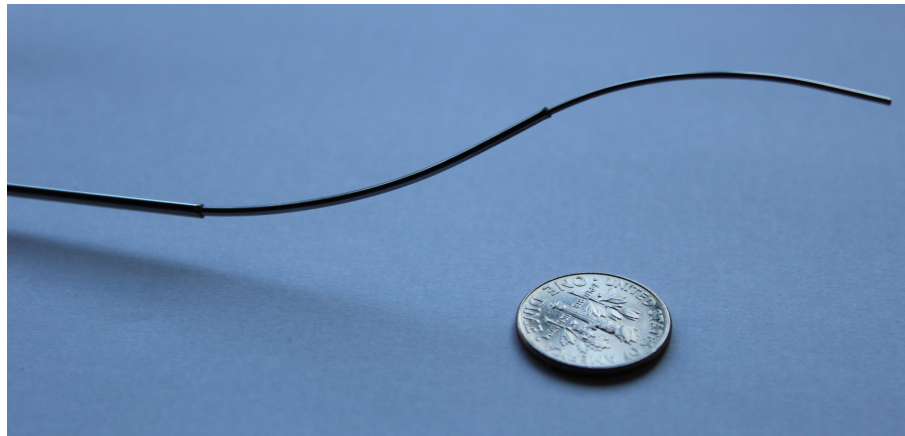


Figure 4.5: A Tubular Continuum Robot of three precurved tubes composed of superelastic NiTi. Each tube can be translated and axially rotated.

**Configuration Space** The motion of the robot results from the elastic interactions between all of its tubes. The independent translation and rotation of each tube represent the actuation of the robot and lead to different space curves of the backbone. Thus, there are two degrees of freedom per tube. Any configuration of the robot can be described by

a vector

$$\mathbf{q} = [\alpha_1, \dots, \alpha_n, \beta_1, \dots, \beta_n]^T,$$

where  $\alpha_i$  describe the rotation and  $\beta_i$  the translation of each tube with respect to the robots base. For each robot configuration, the following constraints apply:

$$\begin{aligned}\alpha_i &\in [-\pi, \pi) \\ \beta_i &\in [-L_i, 0] \\ \beta_1 &\leq \dots \leq \beta_n \leq 0 \\ L_n + \beta_n &\leq \dots \leq L_1 + \beta_1 \leq 0\end{aligned}$$

These constraints arise from the possible ranges of the rotational and the translational values (each tube can be retracted at maximum by its length). Furthermore, no tube can be fully retracted into any outer one.

**Number of Segments** Under the assumption that the robot's shape is composed of constant curvature segments, its shape can be expressed as a concatenation of multiple circular arcs. Each circular arc corresponds to one segment  $j$  and each segment is described by its length  $\ell_j$ , curvature  $\kappa_j$  and bending plane angle  $\phi_j$ .

### Modelling Assumptions

- Pure bending,
- no torsion,
- no friction,
- neglection of gravitational effects and
- neglection of external forces.

The first step is to find the transitions points along the robot where the curvature changes. This happens at the end of the straight section of any tube ( $\beta_i + L_i^s$ ) or when any tube ends along the robot's backbone ( $\beta_i + L_i^s + L_i^c$ ). Thus, all possible transition points along the robot can be expressed as the set  $T$ :

$$T = \{0, \beta_1 + L_1^s, \beta_1 + L_1^s + L_1^c, \beta_2 + L_2^s, \beta_2 + L_2^s + L_2^c, \dots, \beta_n + L_n^s, \beta_n + L_n^s + L_n^c\}. \quad (4.1)$$

From the resulting values of the set  $T$ , all elements are omitted which are  $< 0$ , i.e. the segment or respective tube section is located within the actuation unit. The robot's backbone is defined for  $s \geq 0$ .

**Note**

It is important for the correctness of the kinematic modeling, that the order of the transition points of equation (4.1) is always sorted **ascending**:

$$T = \text{sort}_{\text{asc}}\{0, \beta_1 + L_1^s, \dots, \beta_n + L_n^s + L_n^c\}$$

Hence,  $T$  represents all transition points along the robot's backbone starting from its base ( $s = 0$ ).

Using these transition points  $T$  the constant curvature segments of the robot can be defined. Tubular continuum robots can have a maximum number of  $2n$  segments. The number of actual segments is dependent on the current configuration  $\mathbf{q}$  as some segments might be located within the actuation unit. An example for segments of a tubular continuum robot with  $n = 3$  tubes is shown in Figure 4.6. Note that the outermost tube is straight in this example, resulting in  $2n - 1$  maximal links in this particular case.

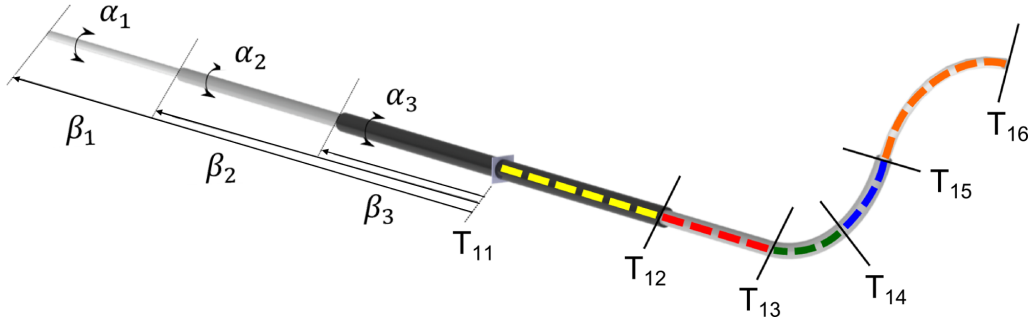


Figure 4.6: A tubular continuum robot with configuration parameters  $\alpha_i$  and  $\beta_i$  and the resulting segments (dotted lines) of the robot's backbone defined by the transition points  $[T_{11}, \dots, T_{16}]$ .

The arc lengths  $\ell_j$  for the segments are defined as follows:

$$\begin{aligned} \ell_1 &= T_{12} - T_{11} = T_{12} - 0 \\ \ell_2 &= T_{13} - T_{12} \\ &\vdots \\ \ell_j &= T_{1j+1} - T_{1j}, \end{aligned} \tag{4.2}$$

with  $j \in 1, \dots, m$  and  $m$  is the number of segments (number of elements in  $T$  minus one).

**Curvature and Bending Plane per Segment** The curvatures  $\kappa_j$  of each individual segment can be determined by considering each segment as a beam and using the Euler-Bernoulli beam theorem:

$$\kappa_j = \frac{d\theta_j}{ds_j} = \frac{M_j}{E_j I_j}, \tag{4.3}$$

where  $\theta$  is the angle measured from the tangent vector,  $s$  is the arc-length,  $M$  is the moment applied to a differential element,  $E$  is the modulus of elasticity (Young's modulus), which is determined by the tube's material, and  $I$  is the cross-sectional moment of inertia which results from  $I_i = \frac{\pi}{4}((R_{o_i})^4 - (R_{i_i})^4)$  with  $R_{o_i}$  and  $R_{i_i}$  being the inner and outer radius of a tube.

When considering two precurved tubes nested inside of each other, the tubes mechanically interact. If the two precurvatures of both tubes lie within the same plane, resulting

shape of the two tubes is determined by the equilibrium curvature (see Figure 4.7 (a)). Since the curvatures of the tubes are constant, they apply a constant resulting moment and the curvature of the two overlapping tubes arises from

$$\kappa_j = \frac{E_1 I_1 \kappa_1 + E_2 I_2 \kappa_2}{E_1 I_1 + E_2 I_2}.$$

For a general collection of  $n$  tubes with constant precurvature, where all curvatures are within the same plane, the equilibrium curvature is given as

$$\kappa_j = \frac{\sum_{i=1}^n E_i I_i \kappa_i}{\sum_{i=1}^n E_i I_i} \quad (4.4)$$

for  $n$  tubes where  $\kappa_i$  is the preformed curvature of each individual tubes.

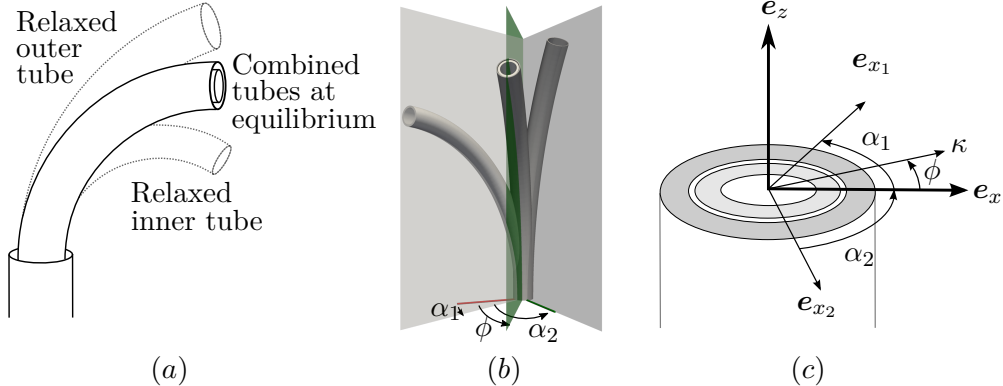


Figure 4.7: (a) Combined tubes with precurvature aligned in a plane with a resultant equilibrium curvature. (b) Tubes with an initial base rotation whose combination results in a equilibrium bending plane. (c) Cross-sectional view of the two combined tubes. The initial rotations are  $\alpha_1$  and  $\alpha_2$ . The resulting equilibrium plane of the tubes deviates from the initial xz-plane by  $\phi_j$ .

As each tube can be axially rotated, tubes with bending planes that are not aligned in a plane have to be considered as well. Therefore, Equation (4.4) has to be extended. Figure 4.7 (b) shows the equilibrium plane of two interacting tubes which are rotated in opposite directions from the initial position by the same rotation angle. The equilibrium plane is defined by the rotational angle  $\phi_j$  (see Figure 4.7(c)). The initial bending plane axis  $e_{x_1}$  and  $e_{x_2}$  of the two tubes are defined by their rotational actuator values  $\alpha_1$  and  $\alpha_2$ .

Since the equilibrium plane of the tubes is rotated from the xz-plane by  $\phi_j$ , an y-component of the moment occurs. Summing the moments of the component projections of  $x$  and  $y$  results in:

$$\kappa_{j_x} = \frac{\sum_{i=1}^n E_i I_i \kappa_i \cos(\alpha_i)}{\sum_{i=1}^n E_i I_i} \quad \text{and} \quad \kappa_{j_y} = \frac{\sum_{i=1}^n E_i I_i \kappa_i \sin(\alpha_i)}{\sum_{i=1}^n E_i I_i}. \quad (4.5)$$

The final mapping from configuration space  $\mathbf{q}$  to arc parameters of each segment is completed by the relationship between the curvature components and arc parameters:

$$\kappa_j = \sqrt{\kappa_{j_x}^2 + \kappa_{j_y}^2} \quad \text{and} \quad \phi_j = \tan^{-1} \frac{\kappa_{j_y}}{\kappa_{j_x}}. \quad (4.6)$$

The geometrical parameter of the tubular continuum robot are now completely described by  $m$  constant curvature segments with their lengths  $\ell_j$ , curvatures  $\kappa_j$  and bending plane angles  $\phi_j$ .

### 2.1.2 Tendon Actuated Continuum Robots

Tendon actuated continuum robots are composed of several spacer disks, equally distributed along a continuous central backbone. Tendons or wires are routed through channels within these spacer disks, such that they can be actuated and bend by pulling or pushing a tendon/wire. Figure 4.8 illustrates a tendon actuated continuum robot composed of two segments, where each segment contains three tendons.

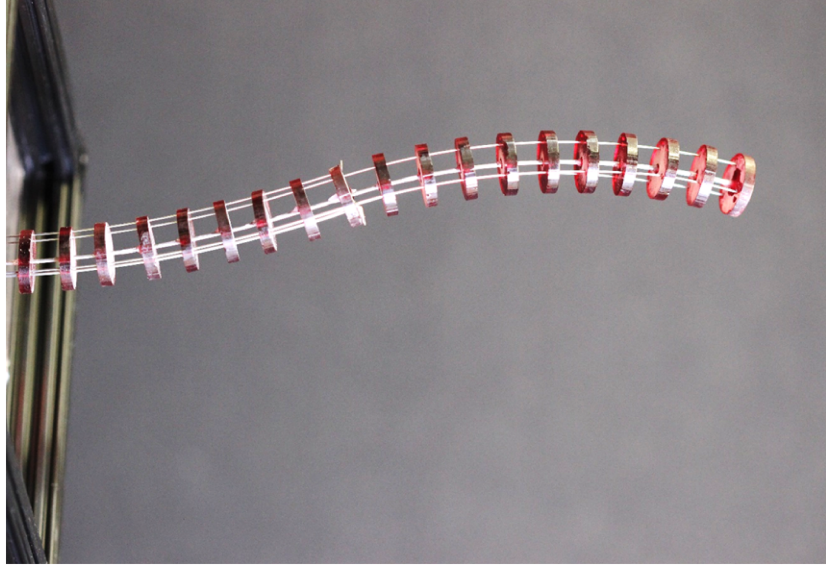


Figure 4.8: Tendon actuated robot composed of two segments and three wires per segment.

The constant curvature kinematic framework can be used to model tendon actuated continuum robots under the following assumptions:

#### Assumptions

- Pure bending,
- infinite torsional rigidity,
- no transverse shear,
- neglection of friction,
- neglection of gravitational effects
- neglection of forces.

To determine the robot dependent parameters for a tendon actuated continuum robot, the structure is divided into  $j$  segments of constant curvature. Each segment has a fixed length which is given by the length of the backbone  $\ell_j$ . For the two segment example robot in Figure 4.8, each segment  $j \in 2$  can be actuated independently by  $i = 3$  wires. The central curve of each continuously bending segment  $j$  is parameterized in respect to arc length  $s_j$  and is defined by the constant curvature  $\kappa_j(s)$ . Under the assumptions mentioned above, the actuated segment  $j$  bends in a plane, perpendicular to the segment's base disk. The constant curvature arc of the robot's  $j^{\text{th}}$  segment is then defined by the rotational angle  $\phi_j$ , the curvature  $\kappa_j$  and segment length  $\ell_j$ .

**Configuration Space** The motion of the robot results from pulling or releasing the tendons. The configuration of the robot is determined by the change in tendon length per segment

$$\mathbf{q} = [\Delta\ell_{1_1}, \dots, \Delta\ell_{1_i}, \dots, \Delta\ell_{j_1}, \dots, \Delta\ell_{j_i}],$$

where  $\Delta\ell_{j_i} = \ell_{j_i} - \ell_j$ . In the initial configuration, the tendon actuated continuum robot is straight and the length of each tendon  $\ell_{j_i}$  equals the length of the segment  $\ell_j$ , i.e.  $\mathbf{q} = \mathbf{0}$ .

The following constraints hold:

$$\sum_{i=1}^{i_{\max}} q_{j_i} = 0,$$

which implies, that it is impossible to either pull or push all tendons/wires simultaneously.

**Geometry of a Single Segment** To model a tendon actuated continuum robot with multiple segments using the constant curvature approach, each segment is regarded separately. In the following, the central backbone of the robot is referred to as the primary backbone and the tendons are referred to as secondary backbones, with  $i \in [1, 3]$ . A single segment is described by three coordinate frames, as illustrated in Figure 4.9. The base disk coordinate frame  $\mathbf{B}_j$  is centered onto the base disk and functions as the reference coordinate frame. Its origin lies in the centerpoint of the base disk at  $s = 0$ , where the  $x$ -axis points from the centerpoint towards the first secondary backbone  $i_j = 1$ . The tendons are numbered counter-clockwise, see Figure 4.9 (right).

The bending plane coordinate frame  $\mathbf{P}_j$  also lies at  $s = 0$ , where the  $x$ -axis points into the bending direction of the  $j^{\text{th}}$  segment. Hence, it differs from  $\mathbf{B}_j$  by a rotation about  $e_{z_B}$  with the rotation angle  $\phi_j$ . The end disk coordinate frame  $\mathbf{E}_j$  defines the position and orientation of the last disk of the  $j^{\text{th}}$  segment. It is rotated about  $e_{y_{P_j}}$  by the rotation angle  $\tilde{\theta}$ , as illustrated in Figure 4.10, and its origin lies at the tip of the robot's primary backbone at  $s_j = \ell_j$ .

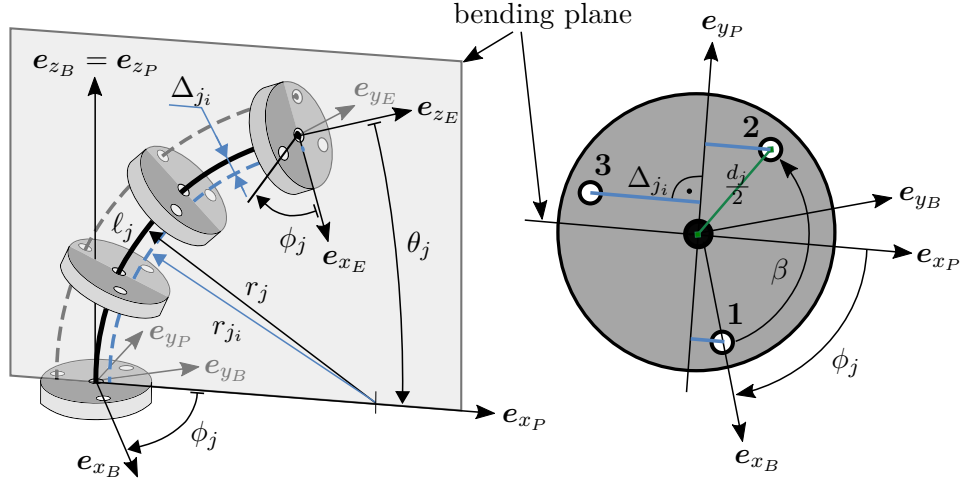


Figure 4.9: A single segment of the tendon actuated continuum robot (left). The blue dashed line shows the projection of the first tendon to the segment bending plane. Cross-sectional view of the base disk (right).

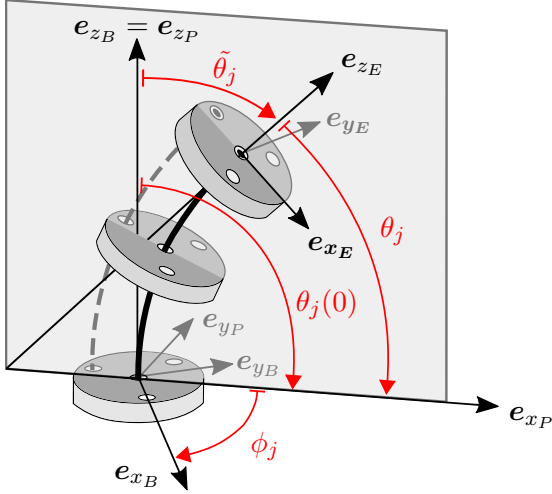


Figure 4.10: Rotational bending angles  $\phi_j$  and  $\theta_j$  (or  $\tilde{\theta}_j$ ).

To describe the position and orientation of the secondary backbones with respect to the primary backbone, an offset  $\Delta_{j_i}$  is defined as the orthogonal distance of each tendon to the  $e_{y_{P_j}}$ -axis (see Figure 4.9 (right))

$$\Delta_{j_i} = \frac{d_j}{2} \cdot \cos(\sigma_{j_i}), \quad (4.7)$$

where  $d_j$  is the pitch circle diameter of the wires/tendons and  $\sigma_i$  defines the rotation of each secondary backbone about  $e_{z_{B_j}}$  and is described by

$$\sigma_{j_i} = \phi_j + (i - 1) \cdot \beta, \quad (4.8)$$

$$\text{with } i = 1, 2, 3 \text{ and } \beta = \frac{2\pi}{\max(i)}.$$

To obtain a relation between the radius of curvature of the primary backbone  $r_j$  and the secondary backbone  $r_{j_i}$ , tendons are projected onto the segment bending plane. The projection of the first tendon is exemplary shown in Figure 4.9 (left) by the blue dashed line. The radius of curvature of the primary backbone and the secondary backbone are thereby related according to

$$r_j = r_{j_i} + \Delta_{j_i}. \quad (4.9)$$

**Arc Parameters** Based on these geometric relations for a single segment of a tendon actuated continuum robots, the determination of the bending radii  $\phi_j$  and  $\theta_j$  (see Figure 4.10) and the curvatures  $\kappa_j$  for each segment can be determined. Note, that  $\phi_j$  remains constant for a single segment, while  $\theta_j$  and  $\tilde{\theta}_j$  respectively vary from disk to disk. The arc length per segment  $j$  corresponds to the segment length  $\ell_j$ , which is fixed (note that the length could vary in tendon actuated continuum robots with variable segment lengths).

The bending angle  $\theta_j$  of the  $j^{\text{th}}$  segment results from the relation between the length of the central backbone and the length of the  $i^{\text{th}}$  tendon of the robot. Applying Equation (4.9) yields:

$$\begin{aligned} \ell_{j_i} &= \int ds_{j_i} = \int ds_{j_i} - \int ds_j + \int ds_j \\ &= \int_{\theta_j(\ell_j)}^{\theta_j(0)} (r_{j_i} - r_j) d\theta + \ell_j \\ &= \ell_j - \Delta_{j_i} (\theta_j(0) - \theta_j(\ell_j)). \end{aligned} \quad (4.10)$$

Rearranging Equation (4.10) results in an expression describing the rotation angle  $\theta_{\ell_j}$ , which characterizes the degree of curvature of the robot's  $j^{\text{th}}$  segment:

$$\theta_j(\ell_j) = \theta_j(0) - \frac{\ell_j - \ell_{j_i}}{\Delta_{j_i}}. \quad (4.11)$$

Equation (4.11) enables the determination of the bending angle  $\theta_j$  for every position  $s_j$  along the segment's backbone. The central angle of the sector of the circle  $\tilde{\theta}_j$  arises from

$$\tilde{\theta}_j(s_j) = \theta_j(0) - \theta_j(s_j). \quad (4.12)$$

Hence, the curvature  $\kappa_j$  of a single segment dependent on arc length  $s_j$  is

$$\kappa_j(s_j) = \frac{\tilde{\theta}_j(s_j)}{s_j}. \quad (4.13)$$

Assuming that the local tangents of all backbones remain parallel to one another, a kinematic compatibility condition can be defined, as the rotational parameter  $\theta_j(\ell_j)$  remains constant

$$\theta_j(0) - \frac{\ell_j - \ell_{j_1}}{\Delta_{j_1}} = \theta_j(0) - \frac{\ell_j - \ell_{j_2}}{\Delta_{j_2}}. \quad (4.14)$$

Note, that this kinematic compatibility condition remains valid for any other combination of secondary backbones. Equation (4.14) then yields a description for the rotation angle  $\phi_j$  by using Equations (4.8) and (4.7),  $q_{j_i} = \ell_{j_i} - \ell_j$  and trigonometric relations

$$\tan(\phi_j) = \frac{-q_{j_1} \cdot \cos(\beta) + q_{j_2}}{-q_{j_1} \cdot \sin(\beta)}. \quad (4.15)$$

As the arctan function has the deficit that its argument can only assign a function value in two quadrants, the atan2 function is applied

$$\phi_j = \text{atan2}(-q_{j_1} \cdot \cos(\beta) + q_{j_2}, -q_{j_1} \cdot \sin(\beta)). \quad (4.16)$$

The interval  $[0, 2\pi]$  for all bending directions is therefore clearly defined.

### Definition of atan2

One possible definition for the multi-valued inverse tangent (atan2) is dividing it into six cases as

$$\text{atan2}(y, x) = \begin{cases} \arctan\left(\frac{y}{x}\right) & , \text{ if } x > 0 \\ \arctan\left(\frac{y}{x}\right) + \pi & , \text{ if } x < 0, y \geq 0 \\ \arctan\left(\frac{y}{x}\right) - \pi & , \text{ if } x < 0, y < 0 \\ \frac{\pi}{2} & , \text{ if } x = 0, y > 0 \\ -\frac{\pi}{2} & , \text{ if } x = 0, y < 0 \\ \text{undefined} & , \text{ if } x = 0, y = 0 \end{cases}$$

## 2.2 Robot Independent Mapping

The mapping from arc parameters to task space, i.e. the pose  $\mathbf{x}$  along the continuum robot's backbone is robot independent, because it is applicable to all robots which can be approximated by piecewise constant curvature arcs. This is a purely kinematic mapping, transforming from arc parameters for each link  $(\phi_j, s_j, \kappa_j)$  to a space curve in task space.

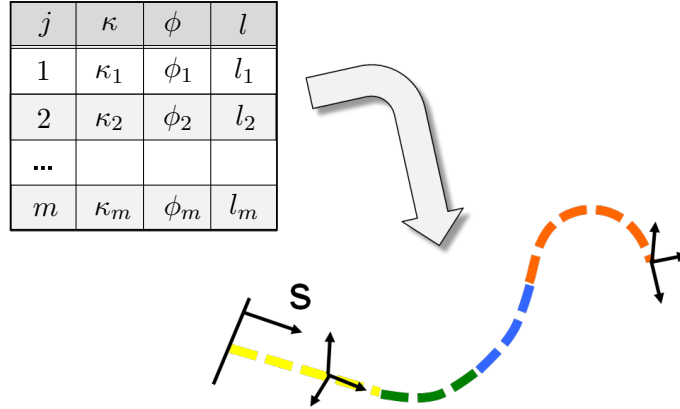


Figure 4.11: Sketch of the Robot Independent Mapping process.

A wide variety of conventions, formalism, and coordinate frame choices exist in the literature to accomplish the robot independent mapping. In this script, we show that the various methods all fundamentally produce the same result for piecewise constant-curvature continuum robots. To illustrate this, we choose a coordinate frame convention. The positive z-axis of the base coordinate frame is tangent to the continuum robot. When  $\phi = 0$ , positive curvature ( $\kappa > 0$ ) produces bending about the y-axis such that when the continuum robot backbone has traced out an angle of  $\pi$  radians it will touch the x-axis.

### 2.2.1 Geometry of Circular Arcs

The geometry of a circular arc provides means of determining the pose of points along it. In Figure 4.12, when  $\phi = 0$  the coordinates of the end point of a circular arc with curvature  $\kappa$  ( $\kappa = 1/r$  where  $r$  is the radius of curvature) in the x-z-plane centered at  $[\kappa^{-1} 0 0]^T$  are given by

$$\mathbf{p} = \begin{bmatrix} \frac{1}{\kappa} \cdot (1 - \cos(\kappa s)) \\ 0 \\ \frac{1}{\kappa} \cdot \sin(\kappa s) \end{bmatrix}. \quad (4.17)$$

Note that this motion includes a rotation  $\mathbf{R}_y(\theta)$  about the positive y-axis, where  $\mathbf{R}_y(\theta) \in SO(3)$  indicates a rotation about the y-axis by the angle  $\theta$

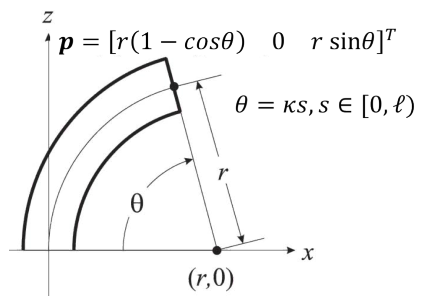


Figure 4.12: The inplane position of the tip of a circular arc is determined by the arc's radius  $r$  and opening angle  $\theta$ .

$$\mathbf{R}_y(\theta) = \begin{bmatrix} \cos(\theta) & 0 & \sin(\theta) \\ 0 & 1 & 0 \\ -\sin(\theta) & 0 & \cos(\theta) \end{bmatrix} \quad (4.18)$$

where  $\theta = \kappa \cdot \ell$  is the opening angle of the circular arc. Rotating the entire arc about the z-axis by  $\phi$  moves the robot's curved link out of the x-z-plane. The rotation about the z-axis is described by  $\mathbf{R}_z(\phi) \in SO(3)$

$$\mathbf{R}_z(\phi) = \begin{bmatrix} \cos(\phi) & -\sin(\phi) & 0 \\ \sin(\phi) & \cos(\phi) & 0 \\ 0 & 0 & 1 \end{bmatrix}. \quad (4.19)$$

As a result, the pose of one curved link of a continuum robot can be completely determined by  $\mathbf{R}_y(\theta_j)$ ,  $\mathbf{R}_z(\phi_j)$ , and  $\mathbf{p}_j$ . The relationship  $\theta_j = \kappa_j \ell_j$  allows to formulate the transformation in respect to

$$s = \begin{cases} [0, \sum_j \ell_j) & \text{for } j < N \\ [0, \sum_j \ell_j] & \text{for } j = N \end{cases} \quad (4.20)$$

which is the arc length parameter of the curve representing the continuum robot's entire backbone and  $N$  is the overall number of links

$${}^{j-1}\mathbf{T}_j(s) = \begin{bmatrix} \mathbf{R}_z(\phi_j) & 0 \\ 0 & 1 \end{bmatrix} \begin{bmatrix} \mathbf{R}_y(\kappa_j s_j) & \mathbf{p}_j(s_j) \\ 0 & 1 \end{bmatrix}. \quad (4.21)$$

As a result, the transformation Equation (4.21) of the  $j^{th}$  link is

$$\begin{aligned} {}^{j-1}\mathbf{T}_j(s) &= \begin{bmatrix} \mathbf{R}_z(\phi_j) & 0 \\ 0 & 1 \end{bmatrix} \begin{bmatrix} \mathbf{R}_y(\kappa_j s) & \mathbf{p}_j(s) \\ 0 & 1 \end{bmatrix} \\ &= \begin{pmatrix} \cos(\phi_j) \cdot \cos(\kappa_j s) & -\sin(\phi_j) & \cos(\phi_j) \cdot \sin(\kappa_j s) & \cos(\phi_j) \cdot (1 - \cos(\kappa_j s)) / \kappa_j \\ \sin(\phi_j) \cdot \cos(\kappa_j s) & \cos(\phi_j) & \sin(\phi_j) \cdot \sin(\kappa_j s) & \sin(\phi_j) \cdot (1 - \cos(\kappa_j s)) / \kappa_j \\ -\sin(\kappa_j s) & 0 & \cos(\kappa_j s) & \sin(\kappa_j s) / \kappa_j \\ 0 & 0 & 0 & 1 \end{pmatrix}. \end{aligned}$$

A concatenation of these transformation matrices yields to the pose of the tip of the continuum robot at  $s = \ell$ , i.e. the pose of the last curved link  $m$

$${}^0\mathbf{T}_j(\ell) = {}^0\mathbf{T}_1 \dots {}^{j-1}\mathbf{T}_j \quad (4.22)$$

for  $j = 1 \dots m$ .

### 2.3 Using Frenet-Serret Frames

Another approach to calculate the end effector pose of a robot's segment is applying Frenet-Serret Frames presented in Section 3 of Chapter 2. Let us assume that the robot's first segment is bent and rotated about the  $e_z$ -axis by  $\phi_1$  (see Figure 4.13 where  $\phi_1 = 0$ ). The convention that the initial tangent vector  $\mathbf{e}_t(0)$  is tangent to the continuum robot at its base and the initial normal vector  $\mathbf{e}_n(0)$  depends on the bending direction, defined by the angle  $\phi$ , yields

$$\begin{aligned} \mathbf{e}_{t_1}(0) &= [0 \ 0 \ 1]^T, \\ \mathbf{e}_{n_1}(0) &= [\cos(\phi_1) \ \sin(\phi_1) \ 0]^T. \end{aligned} \quad (4.23)$$

The points along the centerline of the robot's backbone  $\mathbf{r}(s)$  are defined by integrating the tangent vector  $\mathbf{e}_t$  over the interval of each individual segment. Therefore a point on the  $j^{th}$  segments's arc at  $s$  is defined as:

$$\mathbf{r}_j(s) = \int_0^s \mathbf{e}_{t_j}(s) ds. \quad (4.24)$$

Using the Frenet-Serret Relations  $\mathbf{e}'_t(s) - \kappa(s)\mathbf{e}_n(s) = 0$  and  $\mathbf{e}'_n(s) = -\kappa(s)\mathbf{e}_t(s)$  of Section 3 in Chapter 2 under constant curvature assumption ( $\kappa(s) \equiv \kappa$ ) and neglection of torsion ( $\tau(s) \equiv 0$ ), yields after differentiating and substituting to  $\mathbf{e}''_t(s) + \kappa^2\mathbf{e}_t(s) = 0$ . Solving this results in the tangent vector:

$$\mathbf{e}_{t_j}(s) = \mathbf{e}_{t_j}(0) \cdot \cos(\kappa_j s) + \mathbf{e}_{n_j}(0) \cdot \sin(\kappa_j s). \quad (4.25)$$

Therefore we obtain the 3D space curve of the robot's first segment in respect to arc-length  $s$  by inserting Equation (4.25) into (4.24) as:

$$\begin{aligned} \mathbf{r}_1(\ell_1) &= \int_0^{\ell_1} \mathbf{e}_{t_1}(\ell_1) ds \\ &= \mathbf{e}_{t_1}(0) \cdot \frac{1}{\kappa_1} \cdot \sin(\kappa_1 \ell_1) + \mathbf{e}_{n_1}(0) \cdot \frac{1}{\kappa_1} \cdot (1 - \cos(\kappa_1 \ell_1)). \end{aligned} \quad (4.26)$$

The following segments are calculated by the similar equations with new initial vectors. While the initial tangent vector of the next segment is equal to the tangent vector of the tip of the previous segment ( $\mathbf{e}_{t_{j+1}}(0) = \mathbf{e}_{t_j}(\ell_j)$ ), the normal vector differs (see Figure 4.13). Due to the different orientation in 3D space of the next segment's curvature, its initial normal vector is rotated around the tangent vector. The difference in the orientation is expressed by  $\gamma = \phi_j - \phi_{j+1}$  (see Figure 4.13). Therefore the new initial normal vector results from

$$\mathbf{e}_{n_{j+1}}(0) = \mathbf{R}_{e_t \gamma} \cdot \mathbf{e}_{n_j}(\ell_j), \quad (4.27)$$

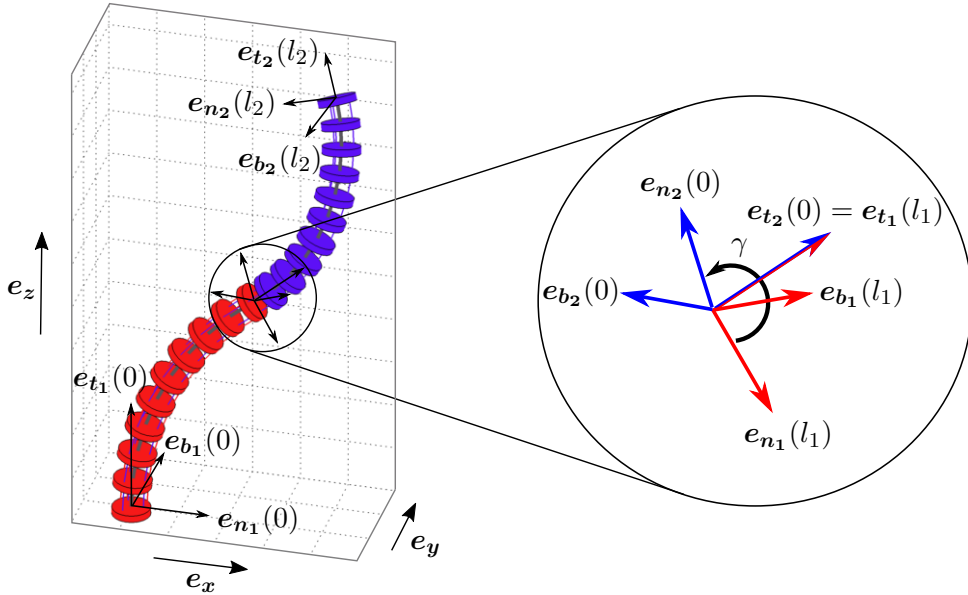


Figure 4.13: Example configuration of a TACR consisting of two segments and the segment based individual unit tangent, normal and binormal vectors  $\mathbf{e}_t$ ,  $\mathbf{e}_n$  and  $\mathbf{e}_b$ . Note that the second segment is twisted to the first one by the angle  $\gamma = \phi_1 - \phi_2$

where  $\mathbf{R}_{\mathbf{e}_t \gamma}$  describes the rotation about  $\mathbf{e}_{t_{j+1}}(0)$  by  $\gamma$ . Substituting  $\mathbf{e}_{t_{j+1}}(0)$  and  $\mathbf{e}_{n_{j+1}}(0)$  in Equation 4.25 and integrating the term as in Equation (4.24) results in the arc-length of the second link in 3D space. Note that  $\mathbf{e}_{n_j}(\ell_j)$  arises from the Frenet-Serret Relation  $\mathbf{e}'_n(s) = -\kappa(s) \cdot \mathbf{e}_t(s)$  (under neglection of torsion). Substituting and integrating yields:

$$\mathbf{e}_{n_j}(s) = \mathbf{e}_{t_j}(0) \cdot -\sin(\kappa_j s) + \mathbf{e}_{n_j}(0) \cdot \cos(\kappa_j s) \quad (4.28)$$

Subsequently the segments are connected by translating each segments to the tip of its previous segment to yield the 3D space curve of the robot in the basic coordinate system.

### Analogy of Results

The result is the same as presented above using the geometry of circular arcs by applying the transformation matrices (Equation (4.22)). The difference lies in the fact that the orientation is already defined by calculating a new unit normal vector using Equation (4.27). Therefore its only necessary to translate the points along the segment to the tip of the previous segment. Due to this, the end effector coordinates  $\mathbf{x}$  are calculated and the Forward Kinematic Modeling is completed.

### 2.3.1 Exponential Coordinates

Exponential coordinates are based on Lie group theory (see Chapter 2 Section 1) and the following equations refer to the notation and convention outlined in [16], where a more detailed description can be found. Using exponential coordinates, the circular arc is defined by the arc parameters and the product of exponential formulas. Following Equation (4.21), a homogeneous transformation for a circular arc can be defined by a rotation and an inplane transformation, which is the same using exponential coordinates. The joint twists associated with the arc parameters are described by:

$$\boldsymbol{\xi}_{rot} = \begin{bmatrix} \mathbf{v}_{rot} \\ \boldsymbol{\omega}_{rot} \end{bmatrix} = [0 \ 0 \ 0 \ 0 \ 1]^T, \quad (4.29)$$

$$\boldsymbol{\xi}_{inp} = \begin{bmatrix} \mathbf{v}_{inp} \\ \boldsymbol{\omega}_{inp} \end{bmatrix} = [0 \ 0 \ 1 \ 0 \ \kappa \ 0]^T. \quad (4.30)$$

Here,  $\mathbf{v}$  and  $\boldsymbol{\omega}$  are linear and angular differential motions, where  $\boldsymbol{\xi}_{inp}$  corresponds to the translation along a link and  $\boldsymbol{\xi}_{rot}$  corresponds to the rotation of a link. Then, referring to Chapter 2 Section 1.4, the twist coordinates are transferred into twists

$$\hat{\boldsymbol{\xi}}_{rot} = \begin{bmatrix} \hat{\boldsymbol{\omega}}_{rot} & \mathbf{v}_{rot} \\ 0 & 0 \end{bmatrix} = \begin{bmatrix} 0 & -1 & 0 & 0 \\ 1 & 0 & 0 & 0 \\ 0 & 0 & 0 & 0 \\ 0 & 0 & 0 & 0 \end{bmatrix}, \quad (4.31)$$

$$\hat{\boldsymbol{\xi}}_{inp} = \begin{bmatrix} \hat{\boldsymbol{\omega}}_{inp} & \mathbf{v}_{inp} \\ 0 & 0 \end{bmatrix} = \begin{bmatrix} 0 & 0 & \kappa & 0 \\ 0 & 0 & 0 & 0 \\ -\kappa & 0 & 0 & 1 \\ 0 & 0 & 0 & 0 \end{bmatrix}^T. \quad (4.32)$$

Using the product of exponentials formula yields:

$$T = e^{(\hat{\boldsymbol{\xi}}_{rot}\phi)} e^{(\hat{\boldsymbol{\xi}}_{inp}\ell)}, \quad (4.33)$$

which is identical to the transformation matrix of Eq. (4.21). Hence, recalling from Eq. (4.22) applying Eq. (4.33) for segment  $j$  results in

$$T\left(\sum_j (\ell_j)\right) = T_1 \dots T_j, \quad \text{for } j = 1 \dots m. \quad (4.34)$$

## 2.4 Accuracy

As long as effects such as torsion, friction, the interaction between two adjacent curved sections or any other external loads are negligible for a continuum robot, the constant curvature kinematics framework provides good modeling accuracy at relatively low modeling complexity. The closed-form solution leads to efficient computation times and straightforward application.

The accuracy of constant curvature kinematic frameworks is depending on the actual continuum robot and how well it suits the modeling assumption. There is no general statement on how well the model performs in terms accuracy. In the following, we present some representative results on the accuracy obtained with real continuum robots, in particular for tubular continuum robots and tendon-actuated continuum robots.

### 2.4.1 Accuracy for Tubular Continuum Robots

Results on the accuracy of constant curvature kinematic frameworks for a tubular continuum robots composed of two tubes were reported by Webster et al. [4] (outer tube: OD 2.39 mm, ID 2.01 mm, straight length 93.5 mm, curved length 92.3 mm with curvature of  $0.0099 \text{ mm}^{-1}$ ; inner tube: OD=ID 1.6 mm (wire), straight length 218.5 mm, curved length 85 mm with curvature of  $0.0138 \text{ mm}^{-1}$ ). Overall 26 robot configurations were evaluated in terms of the error at the robot's tip compared to the predicted tip position using the constant curvature kinematics framework described above. Measurements of the shape are obtained contact-free using a stereo-camera setup.

The mean tip error over all 26 experiments is 24.8 mm with a maximum error of 54.3 mm [4]. The mean tip error corresponds to 12 % of the overall arc length. Figure 4.14 illustrates two robot configurations with the corresponding measured shape and the predicted model shape of the robot. More details on the experimental setup and further results are available in [4].

### 2.4.2 Accuracy for Tendon-actuated Continuum Robots

In the course of the continuum robotics lecture in the winter term 2016/2017, the accuracy of the constant curvature kinematics model was assessed for the tendon-actuated continuum robot depicted in Figure 4.8. The robot with an overall length of 194 mm consists of 2 segments with 10 tendon routing disks per segment. 10 different robot configurations were measured with 10 repetitions for each. The positions of the tendon routing disks and the robot's tip are experimentally determined using a tactile measurement with a point

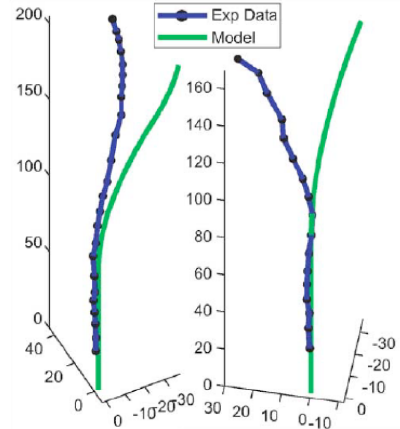


Figure 4.14: Experimental data and model predictions (values in mm)[4].

probe. The Euclidean distances between the measured positions and the model predicted points by the model are determined.

Example robot configurations and the measured and model calculated shape are depicted in Figure 4.15. Overall, the mean tip error is 24.4 mm and the maximum tip error observed was 34.2 mm. The mean tip error corresponds to 12.5 % of the overall arc length of the robot.

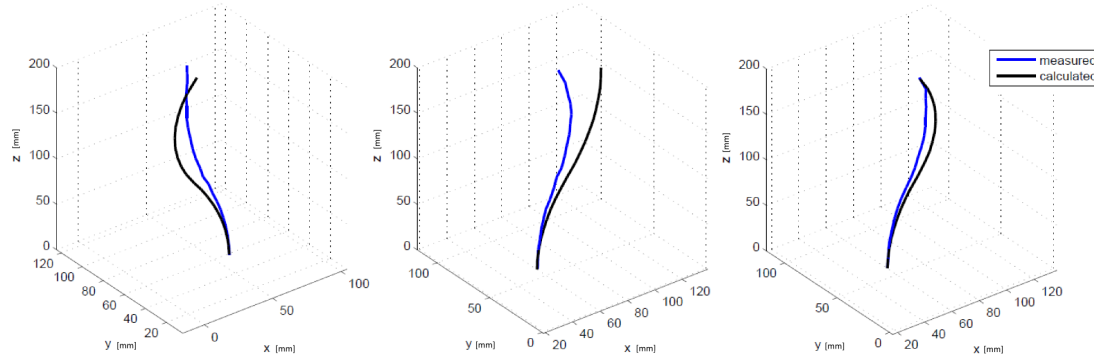


Figure 4.15: Example tendon-actuated robot configurations with the measured shape (blue) and calculated shape by the constant curvature kinematics model (black).

### 3 Mechanics Framework using Elasticity Theory

The assumption which underlies the constant curvature kinematic frameworks introduced in the previous section, i.e. a continuum robot conforms to a shape which is composed of mutually tangent curved segments with constant curvature, is restrictive. While the assumption might hold for some continuum robots under specific conditions, there exist continuum robots which cannot be modeled under the constant curvature assumption due to their design and continuum robots which operate under conditions which cause non-constant curvature, e.g. as external forces and moments act on the robot or the robot conforms to its environment as it is inherently elastic.

A general and powerful modeling framework involves utilization of Cosserat theory for elastic rods (see Chapter 3). The idea is to represent the deformation of a continuum robot in respect to its reference state by six strain variables, namely  $\mathbf{u}(s, t)$  and  $\mathbf{v}(s, t)$  parameterized by arc length  $s$  at time  $t$ . Cosserat theory of elastic rods accounts for bending and torsion as well as shear deformation. As summarized in Chapter 3 Section 5, the model leads to coupled set of differential equations governing the **rod kinematics**, the **equilibrium equations**, and the **constitutive equations**. Those are accompanied by a set of boundary conditions.

In the following, we describe how the mechanics framework using elasticity theory can be derived for two types of continuum robots: tubular continuum robots and tendon-actuated continuum robots.

#### 3.1 Tubular Continuum Robots

Tubular continuum robots consist of multiple tubes and as such can be modeled as multiple rods applying Cosserat theory of elastic rods. Each component tube is described as a Kirchhoff rod undergoing bending and torsion to derive a forward kinematic model for tubular continuum robots in order to describe the position and orientation of the robot's backbone curve in free-space. The described model was originally published by Rucker et al. [9].

##### Modeling Assumptions

- inextensible tubes,
- no transverse shear of the tubes,
- neglection of torsion,
- absence of friction between tubes,
- linear constitutive equations for bending and torsion.

Extension and transverse shear can be neglected for thin rods and also the gravitation has only little effect on the scales and stiffnesses of the tubes, such that it is neglected.

To further describe the model, we consider a tubular continuum robot composed of  $n = 3$  precurved tubes, as illustrated in Figure 4.16, where the precurved sections of the tubes are straightened for clarity (refer to Figure 4.6). The tubular continuum robot is defined by 6 DoF, which are the translation  $\beta_i$  and rotation  $\alpha_i$  for each tube  $i$ . The forward kinematic mapping can be described as the mapping from actuator values  $\mathbf{q} = [\alpha_i, \beta_i]$  and a given set of tubes to the position and orientation of the robot's space curve.

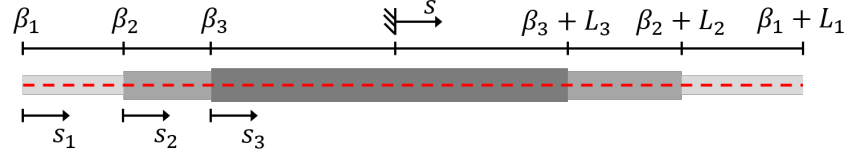


Figure 4.16: Depiction of a concentric tube robot (straightened tubes for clarity), with length  $\beta_i$  and  $\beta_i + \ell_i$  located at the proximal and distal ends of the tubes.

### 3.1.1 Kinematics

The shape of a single tube  $i$  can be defined by an arc-length  $s$  parameterized curve  $\mathbf{r}_i^*(s)$  in its reference state (denoted by  $*$ ), where  $L_i$  denotes the length of the tube. At each point along the space curve of the centerline of the curve an accompanying orthonormal frame is defined  $\{\mathbf{d}_{x_i}^*, \mathbf{d}_{y_i}^*, \mathbf{d}_{z_i}^*\}$ . The local  $\mathbf{d}_{z_i}^*$  axis is defined such that it is tangent to the curve and the  $\mathbf{d}_{x_i}^*$  and  $\mathbf{d}_{y_i}^*$  axes are established such that they span the cross-section of the tube in a canonical way (Bishop's frames).

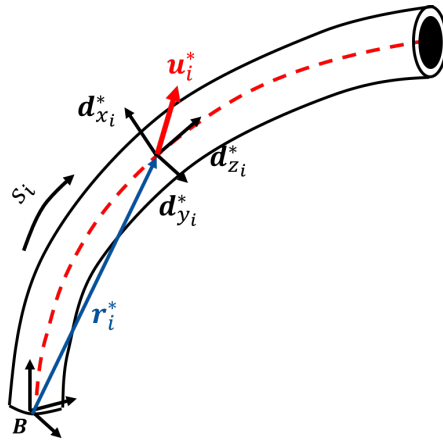


Figure 4.17: The reference shape of the  $i$ th tube is described by the position  $\mathbf{r}_i^*$  as a function of arc length  $s$ . At each point along the centerline curve, a coordinate frame is attached  $\{\mathbf{d}_{x_i}^*, \mathbf{d}_{y_i}^*, \mathbf{d}_{z_i}^*\}$ .

The combination of position and rotation matrices forms an element of the special Euclidean group  $SE(3)$  and is denoted with  $\mathbf{g}_i^*(s)$ .

$$\mathbf{g}_i^*(s) = \begin{bmatrix} \mathbf{R}_i^*(s) & \mathbf{r}_i^*(s) \\ \mathbf{0}^T & 1 \end{bmatrix},$$

where  $\mathbf{R}_i^*(s) \in SO(3)$  describes the orientation at arc length  $s$  with respect to a fixed base frame  $\mathbf{B}$ , where  $\mathbf{R}_i^* = [\mathbf{d}_{x_i}^*, \mathbf{d}_{y_i}^*, \mathbf{d}_{z_i}^*]$  and  $\partial_s \mathbf{r} = \mathbf{d}_{z_i}^* = \mathbf{R}_i^* \mathbf{e}_3$  (see equation 3.18). The local curvature vector can then be obtained by using the relationship

$$\mathbf{u}_i^*(s) = (\mathbf{R}_i^{*T}(s) \partial_s \mathbf{R}_i^*)(s)^\vee, \quad (4.35)$$

where  $^\vee$  denotes a mapping from  $\mathfrak{se}(3)$  to  $\mathbb{R}^6$  and the operator  $^\wedge$  denotes its inverse. When considering the effects of bending and torsion between tubes, the curve of tube  $i$  undergoes a shape change denoted as  $\mathbf{g}_i(s)$ .

To describe the rate of change of the initial state  $\mathbf{g}_i^*(s)$  to a deformed backbone state  $\mathbf{g}_i(s)$  (see Figure 4.18), we define a twist vector  $\boldsymbol{\xi}_i^*(s_i) = [\mathbf{v}_i^{*T} \ \mathbf{u}_i^{*T}]^T$  (where  $\mathbf{v}_i^{*T} = \mathbf{e}_3^T$  in Kirchhoff rod theory), such that the change in  $\partial_s \mathbf{g}_i^*(s_i)$  is influenced by this twist

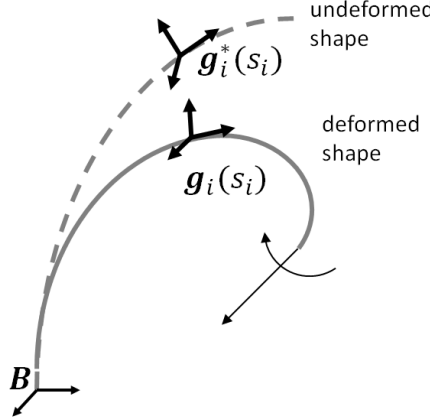


Figure 4.18: Undeformed reference shape  $\mathbf{g}_i^*(s)$  and deformed shape  $\mathbf{g}_i(s)$  with common base frame  $\mathbf{B}$ .

$$\partial_s \mathbf{g}_i^*(s) = \mathbf{g}_i^*(s) \hat{\boldsymbol{\xi}}_i^*(s).$$

Any deformation of a tube from its initial state  $\mathbf{g}_i^*(s)$  to a new state  $\mathbf{g}_i(s)$  can thereby be described by a corresponding change from  $\hat{\boldsymbol{\xi}}_i^*(s)$  to  $\hat{\boldsymbol{\xi}}_i(s)$ , which is denoted by  $\Delta\hat{\boldsymbol{\xi}}_i(s) = \hat{\boldsymbol{\xi}}_i(s) - \hat{\boldsymbol{\xi}}_i^*(s)$ . The components of  $\Delta\mathbf{u}_i$  are the bending strains about  $\mathbf{d}_{x_i}^*$  and  $\mathbf{d}_{y_i}^*$  and the torsion (material twist) about  $\mathbf{d}_{z_i}^*$ , such that the change in  $\mathbf{g}_i(s)$  can be described as

$$\partial_s \mathbf{g}_i(s) = \mathbf{g}_i(s) \hat{\boldsymbol{\xi}}_i(s),$$

or equivalently

$$\partial_s \mathbf{r}_i(s) = \mathbf{R}_i(s) \mathbf{e}_3, \quad \partial_s \mathbf{R}_i(s) = \mathbf{R}_i(s) \hat{\mathbf{u}}_i(s),$$

where  $\mathbf{u}_i(s) = \mathbf{u}_i^*(s) + \Delta\mathbf{u}_i(s)$ .

### 3.1.2 Kinematic Combination of Multiple Tubes

We consider now multiple overlapping tubes and introduce an angle  $\theta_i(s)$  to describe the difference in rotation about the  $\mathbf{d}_z$ -axis of tube 1 to the outer tube  $i$ , such that  $\theta_i(s)$  relates  $\mathbf{g}_1(s)$  to  $\mathbf{g}_i(s)$ . One can parameterize this difference as

$$\mathbf{R}_i(s) = \mathbf{R}_1(s) \mathbf{R}_{\theta_i}, \quad (4.36)$$

with  $\mathbf{R}_{\theta_i} = \begin{bmatrix} \cos(\theta_i) & -\sin(\theta_i) & 0 \\ \sin(\theta_i) & \cos(\theta_i) & 0 \\ 0 & 0 & 1 \end{bmatrix}$ . Substituting  $\mathbf{R}_i$  into the definition for  $\mathbf{u}_i$  (equation 4.35) leaves

$$\mathbf{u}_i(s) = (\mathbf{R}_i^T(s) \partial_s \mathbf{R}_i(s))^\vee = \mathbf{R}_{\theta_i}^T \mathbf{u}_1 + \partial_s \theta_i \mathbf{e}_3. \quad (4.37)$$

Interpreted geometrically, this equation says that the local x and y curvatures of each deformed tube are equal when expressed in a common reference frame. The torsional z components are free to vary independently for each tube. The variable  $\theta_i$  provides a parameterization of this variation, see Figure 4.19 as

$$\partial_s \theta_i = \mathbf{u}_{i,z} - \mathbf{u}_{1,z}.$$

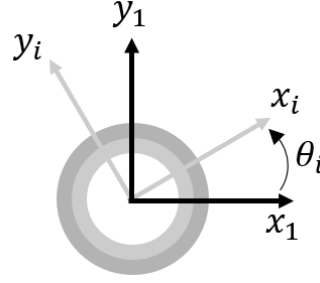


Figure 4.19: Internal moments  $m$  and forces  $n$  and external forces  $f(s)$  and  $l(s)$  acting on a section of the rod from 0 to  $l$ .

### 3.1.3 Constitutive Equations

To describe the relationship between  $\Delta\mathbf{u}$  and the internal moments  $\mathbf{m}_i$ , as illustrated in Figure 4.20, linear constitutive equations (see Equations (3.16) for general cosserat rod theory) are utilized, which consider material properties and the tube's cross section for each tube  $i$

$$\sum_{i=1}^n \mathbf{m}_i(s) = \sum_{i=1}^n \mathbf{R}_i(s) \mathbf{K}_i(s) (\mathbf{u}_i(s) - \mathbf{u}_i^*(s)), \quad (4.38)$$

where

$$\mathbf{K}_i(s) = \begin{bmatrix} E_i(s) I_i(s) & 0 & 0 \\ 0 & E_i(s) I_i(s) & 0 \\ 0 & 0 & G_i(s) J_i(s) \end{bmatrix}.$$

$E_i(s)$  is Young's modulus,  $I_i(s)$  is the second moment of area of the tube cross section,  $G_i(s)$  is the shear modulus, and  $J_i(s)$  is the polar moment of inertia of the tube cross section.

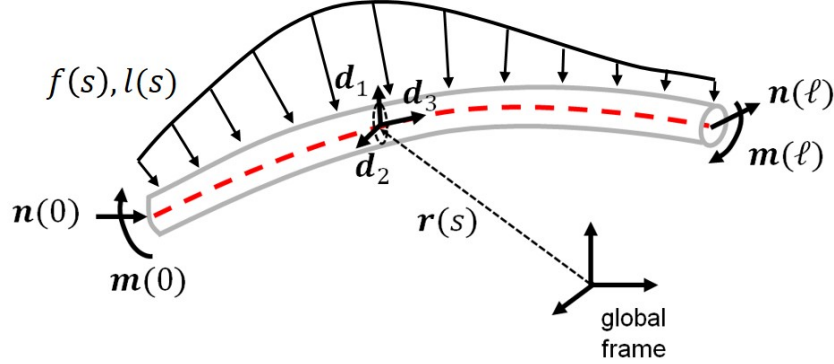


Figure 4.20: Internal moments  $m$  and forces  $n$  and external forces  $f(s)$  and  $l(s)$  acting on a section of the rod from 0 to  $l$ .

### 3.1.4 Equilibrium Equations

Considering multiple precurved overlapping tubes, we derive the equilibrium equations (see equation 3.12 and 3.13 for a single Cosserat rod) by summing moments and forces over all tubes from arc length  $s$  to  $l$

$$\int_s^l \sum_{i=1}^n \mathbf{f}_i(\sigma) d\sigma - \sum_{i=1}^n \mathbf{n}_i(s) = \mathbf{0}, \quad (4.39)$$

and

$$\int_s^l \left( \mathbf{r}(\sigma) \times \sum_{i=1}^n \mathbf{f}_i(\sigma) + \sum_{i=1}^n \mathbf{l}_i(\sigma) \right) d\sigma - \sum_{i=1}^n (\mathbf{m}_i(s) - \mathbf{r}(s) \times \mathbf{n}_i(s)) = \mathbf{0}, \quad (4.40)$$

where  $f$  and  $l$  represent external forces and loads distributed on the section from  $s$  to  $l$ , as illustrated in Figure 4.20. Taking the derivative of equation (4.39) and (4.40) with respect to  $s$  leaves

$$\sum_{i=1}^n (\partial_s \mathbf{n}_i(s) + \mathbf{f}_i(s)) = \mathbf{0}, \quad (4.41)$$

$$\sum_{i=1}^n (\partial_s \mathbf{m}_i(s) + \partial_s \mathbf{r}(s) \times \mathbf{n}_i(s) + \mathbf{l}(s)) = \mathbf{0}. \quad (4.42)$$

### 3.1.5 Differential Kirchhoff Rod Equations

The following equations connect the kinematic constraints to the constitutive and equilibrium laws to obtain a set of differential equations. Deriving the constitutive law (equation (4.38)) with respect to  $s$  yields (where  $s$  is omitted in the following)

$$\sum_{i=1}^n \partial_s \mathbf{m}_i = \sum_{i=1}^n \partial_s \mathbf{R}_i \mathbf{K}_i (\mathbf{u}_i - \mathbf{u}_i^*) + \sum_{i=1}^n \mathbf{R}_i \partial_s \mathbf{K}_i (\mathbf{u}_i - \mathbf{u}_i^*) + \sum_{i=1}^n \mathbf{R}_i \mathbf{K}_i (\partial_s \mathbf{u}_i - \partial_s \mathbf{u}_i^*). \quad (4.43)$$

Substitute equation (4.43) into equation (4.42) and substitute  $\partial_s \mathbf{R}_i = \mathbf{R}_i \hat{\mathbf{u}}_i$  (see equation 3.19 for the evolution of  $\mathbf{R}_i$ )

$$\sum_{i=1}^n \mathbf{R}_i (\mathbf{K}_i (\partial_s \mathbf{u}_i - \partial_s \mathbf{u}_i^*) + (\hat{\mathbf{u}}_i \mathbf{K}_i + \partial_s \mathbf{K}_i) (\mathbf{u}_i - \mathbf{u}_i^*)) + \sum_{i=1}^n (\partial_s \mathbf{r} \times \mathbf{n} + \mathbf{l}) = \mathbf{0}.$$

Using equation (4.36) we obtain

$$\sum_{i=1}^n \mathbf{R}_1 \mathbf{R}_{\theta_i} (\mathbf{K}_i (\partial_s \mathbf{u}_i - \partial_s \mathbf{u}_i^*) + (\hat{\mathbf{u}}_i \mathbf{K}_i + \partial_s \mathbf{K}_i) (\mathbf{u}_i - \mathbf{u}_i^*)) + \sum_{i=1}^n (\partial_s \mathbf{r} \times \mathbf{n} + \mathbf{l}) = \mathbf{0}. \quad (4.44)$$

Applying  $\partial_s \mathbf{r} = \mathbf{R}_1 \mathbf{e}_3$  (see equation 3.18 for the evolution of  $\mathbf{r}_i$ ) and equation (4.41) yields

$$\sum_{i=1}^n \mathbf{R}_1 \mathbf{R}_{\theta_i} (\mathbf{K}_i (\partial_s \mathbf{u}_i - \partial_s \mathbf{u}_i^*) + (\hat{\mathbf{u}}_i \mathbf{K}_i + \partial_s \mathbf{K}_i) (\mathbf{u}_i - \mathbf{u}_i^*)) + \mathbf{R}_i \mathbf{e}_3 \times \int_s^l \mathbf{f}(\sigma) d\sigma + \mathbf{l} = \mathbf{0}, \quad (4.45)$$

where  $\mathbf{f}(s) = \sum_{i=1}^n \mathbf{f}_i(s)$  and  $\mathbf{l}(s) = \sum_{i=1}^n \mathbf{l}_i(s)$ . Multiplying then with  $\mathbf{R}_1^T(s)$  leaves

$$\sum_{i=1}^n \mathbf{R}_{\theta_i} (\mathbf{K}_i (\partial_s \mathbf{u}_i - \partial_s \mathbf{u}_i^*) + (\hat{\mathbf{u}}_i \mathbf{K}_i + \partial_s \mathbf{K}_i) (\mathbf{u}_i - \mathbf{u}_i^*)) + \mathbf{e}_3 \times \mathbf{R}_1^T \int_s^l \mathbf{f}(\sigma) d\sigma + \mathbf{R}_1^T \mathbf{l} = \mathbf{0},$$

The aim is to obtain an expression for  $\partial_s \mathbf{u}_1$  in terms of  $\mathbf{R}_1$ . Therefore, the derivative of equation (4.37) is applied as follows

$$\partial_s \mathbf{u}_i(s) = \partial_s \theta_i \frac{d \mathbf{R}_{\theta_i}^T}{d \theta_i} \mathbf{u}_1 + \mathbf{R}_{\theta_i}^T \partial_s \mathbf{u}_1 + \partial_s^2 \theta_i \mathbf{e}_3,$$

to eliminate  $\partial_s \mathbf{u}_2, \dots, \partial_s \mathbf{u}_n$  from (4.44). Now it's possible to solve equation (4.44) for the first two components  $(\partial_s \mathbf{u}_1)_x$  and  $(\partial_s \mathbf{u}_1)_y$  in terms of the state variables by using equation (4.45)

$$\begin{bmatrix} (\partial_s \mathbf{u}_1)_x \\ (\partial_s \mathbf{u}_1)_y \end{bmatrix} = -\mathbf{K}^{-1} \sum_{i=1}^n \mathbf{R}_{\theta_i} \left( \mathbf{K}_i \left( \partial_s \theta_i \frac{dR_{\theta_i}^T}{d\theta_i} \mathbf{u}_1 - \partial_s \mathbf{u}_i^* \right) + (\hat{\mathbf{u}}_i \mathbf{K}_i + \partial_s \mathbf{K}_i)(\mathbf{u}_i - \mathbf{u}_i^*) \right) \Big|_{x,y} - \mathbf{K}^{-1} \left( \hat{\mathbf{e}}_3 \mathbf{R}_1^T \int_s^l \mathbf{f}(\sigma) d\sigma + \mathbf{R}_1^T \mathbf{l} \right) \Big|_{x,y},$$

where  $\mathbf{K} = \sum_{i=1}^n \mathbf{K}_i$  and  $|_{x,y}$  denotes selection of only the first two components of a vector. To determine the third component  $\partial_s u_{i,z}$ , we consider the differential Kirchhoff rod equation for a single tube which is

$$\partial_s \mathbf{u} = \partial_s \mathbf{u}^* - \mathbf{K}^{-1} ((\hat{\mathbf{u}} \mathbf{K} + \partial_s \mathbf{K})(\mathbf{u} - \mathbf{u}^*)),$$

rewrite it for multiple tubes and solve for  $\partial_s u_{i,z}$

$$(\partial_s \mathbf{u}_i)_z = \partial_s \mathbf{u}_{i,z}^* + \frac{E_i I_i}{G_i J_i} (\mathbf{u}_{i,x} \mathbf{u}_{i,y}^* - \mathbf{u}_{i,y} \mathbf{u}_{i,x}^*) + \partial_s \frac{(G_i J_i)}{G_i J_i} (\mathbf{u}_{i,z}^* - \mathbf{u}_{i,z}) - \frac{1}{G_i J_i} \hat{\mathbf{e}}_3^T R_i^T \mathbf{l}_i.$$

### Example: Neglecting external forces

When neglecting external forces  $f, l$  the differential model equations simplify to:

$$\begin{aligned} \partial_s \mathbf{r} &= \mathbf{R} \hat{\mathbf{e}}_3 \\ \partial_s \mathbf{R} &= \mathbf{R} \hat{\mathbf{u}} \\ \begin{bmatrix} (\partial_s \mathbf{u}_1)_x \\ (\partial_s \mathbf{u}_1)_y \end{bmatrix} &= -\mathbf{K}^{-1} \sum_{i=1}^n \mathbf{R}_{\theta_i} \left( \mathbf{K}_i \left( \partial_s \theta_i \frac{dR_{\theta_i}^T}{d\theta_i} \mathbf{u}_1 - \partial_s \mathbf{u}_i^* \right) + (\hat{\mathbf{u}}_i \mathbf{K}_i + \partial_s \mathbf{K}_i)(\mathbf{u}_i - \mathbf{u}_i^*) \right) \Big|_{x,y} \\ (\partial_s \mathbf{u}_i)_z &= \partial_s \mathbf{u}_{i,z}^* + \frac{E_i I_i}{G_i J_i} (\mathbf{u}_{i,x} \mathbf{u}_{i,y}^* - \mathbf{u}_{i,y} \mathbf{u}_{i,x}^*) \end{aligned}$$

### 3.1.6 Boundary and Initial Conditions

To apply Kirchhoff rod theory to tubular continuum robots, we need to consider geometric constraints of the robot and also the boundary conditions at the transition points, as we divide the robot into links of constant curvature. These boundary conditions are that  $s = 0$  at the constrained entry point and that the tubes are straight for  $s < 0$ . Boundary conditions at each transition point also need to be enforced, such that the orientation and position are continuous

$$\mathbf{g}_i(s^-) = \mathbf{g}_i(s^+),$$

where  $s^-$  defines the condition right before the transition point and  $s^+$  the condition right after the transition point. The static equilibrium requires

$$\sum_{i=1}^n \mathbf{m}_i(s^-) = \sum_{i=1}^n \mathbf{m}_i(s^+) + \sum_{i=1}^n \mathbf{l}_{p,i}(s),$$

where  $\mathbf{l}_{p,i}(s)$  is a point moment applied to tube  $i$ . Due to vanishing moments at the distal end of the robot, the following equation is valid

$$\sum_{i=1}^n \mathbf{m}_i(s) = \sum_{i=1}^n \mathbf{l}_{p,i}(s).$$

The initial conditions for  $\mathbf{r}_1, \mathbf{R}_{\theta_1}, \theta_1$  and  $\theta_i$  are

$$\begin{aligned} \mathbf{r}_1(0) &= \mathbf{0}, \\ \mathbf{R}_{\theta_1} &= \begin{bmatrix} \cos(\alpha_1 + \beta_1 \mathbf{u}_{1,z}^*) & -\sin(\alpha_1 + \beta_1 \mathbf{u}_{1,z}^*) & 0 \\ \sin(\alpha_1 + \beta_1 \mathbf{u}_{1,z}^*) & \cos(\alpha_1 + \beta_1 \mathbf{u}_{1,z}^*) & 0 \\ 0 & 0 & 1 \end{bmatrix}, \\ \theta_1(\beta_1) &= 0, \\ \theta_i &= (\alpha_1 + \beta_i \mathbf{u}_{i,z}^*) - (\alpha_1 + \beta_1 \mathbf{u}_{1,z}^*). \end{aligned}$$

### 3.2 Coupled Rod/Tendon Model for Tendon-actuated Continuum Robots

While the previous presented constant curvature kinematic framework to model tendon actuated continuum robots is very straightforward and fast, it is also restrictive due to the assumption of piecewise bending in circular arcs. This assumption only holds for small tendon-actuated continuum robots with appropriately distributed spacer disks which are not subject to any external forces and moments.

In order to derive a more general model, Cosserat theory of elastic rods can be applied to tendon actuated continuum robots. Rucker and Webster proposed a coupled rod/tendon model [17] which will be explained in the following. Beside the consideration of external loads and non constant curvature bending, this model also accounts for more general routing paths of the tendons (e.g. helically). An example for general tendon routing is shown in Fig. 4.21. We note, that constant curvature kinematic framework models for tendon-actuated continuum robots explicitly assume that tendons are routed in parallel to the backbone, i.e. they are straight.

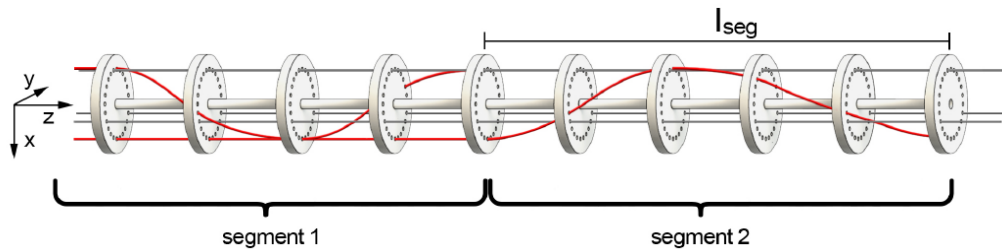


Figure 4.21: Example general tendon routing paths for tendon actuated continuum robots. The robot consists of two segments. For both, helically wrapped tendons (red) is used to enable more complex motions.

#### 3.2.1 General Idea

The coupled rod/tendon model for tendon-actuated continuum robots is decomposed into four steps:

1. The **Cosserat Rod Model** is used for the backbone of the robot expressed in terms of the kinematic variables (see Section 5). Later this implicit equations can be manipulated into a explicit, first-order, state-vector form to solve for the locations of the backbone.
2. A **Geometric Coupling** of the rod and the routing paths of the tendons is used to determine the tendon shapes.
3. The **Classic Cosserat String Model** is used to model the tendons as extensible strings and solved in order to calculate the internal forces for each tendon.
4. A **Load Coupling** determines the loads on the rod as an input to the Cosserat Rod Model. The individual loads that tendons apply on the backbone as well as external loads are considered.

An overview of the approach is shown in Fig.4.22.

#### 3.2.2 Assumptions and Simplifications

First of all it is assumed that there is frictionless interaction between the tendons and the channel or spacer disks where the tendons are routed through. Therefore, the tension of each tendon is assumed as constant along their lengths.

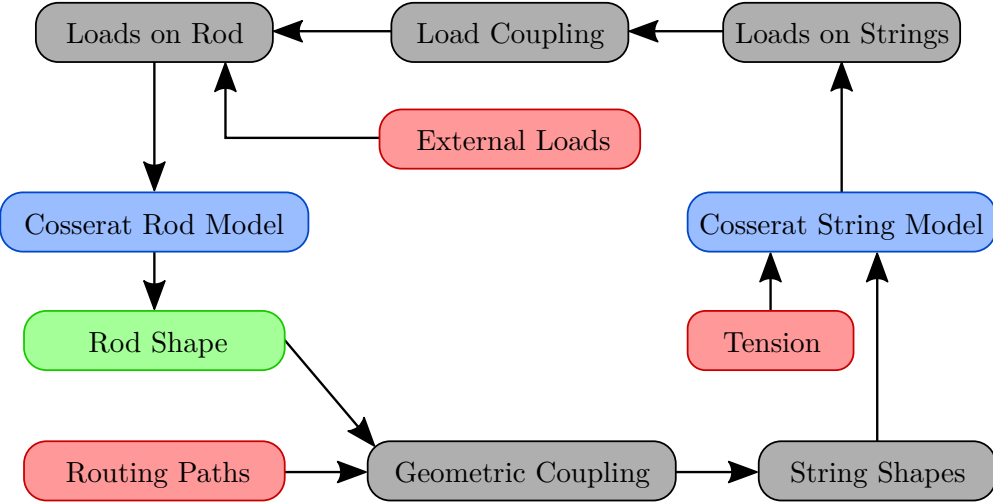


Figure 4.22: Overview of the coupled rod/tendon model. (green: model output, red: model input, blue: model type)

Furthermore, the location of the tendons are fixed within the cross-section of the robot and cannot change during the robots motion. This holds if tendons are routed within embedded sleeves, tendon routing channels with tight tolerances, and designs with closely spaced routing disks.

#### Model Assumptions

- constant tendon tension along length of tendon
- constant tendon location within cross-section

#### 3.2.3 Kinematics of the Tendons

To determine the impact of the tendons on the backbone the location of each tendon within the robots cross-section has to be mathematically described. Thus, the routing path of the  $i^{\text{th}}$  tendon is described by two functions  $x_i(s)$  and  $y_i(s)$  that describe the body-frame coordinates of the tendon at the intersection with the  $x$ - $y$  plane of the backbone at the arc length  $s$  (see Figure 4.23). We can then obtain a vector pointing from the origin of the attached frame on the robot's backbone to the tendon location with

$$\mathbf{t}_i(s) = [x_i(s) \quad y_i(s) \quad 0]^T$$

We can then easily describe the space curve of the tendon path in the undeformed and deformed (e.g. due to external loads) state as

$$\begin{aligned} \text{undeformed} \quad & \mathbf{r}_i^*(s) = \mathbf{R}^*(s)\mathbf{t}_i(s) + \mathbf{r}^*(s) \\ \text{deformed} \quad & \mathbf{r}_i(s) = \mathbf{R}(s)\mathbf{t}_i(s) + \mathbf{r}(s) \end{aligned} \quad (4.46)$$

where  $\mathbf{r}(s)$  and  $\mathbf{R}(s)$  are the position vector and Rotation matrix of the robot's backbone along the arc length  $s$ .

#### 3.2.4 Distributed Forces on Tendons

The distributed forces on the tendons can be described by first taking the derivative of the static equilibrium conditions for a finite section (see Figure 4.24). The internal force

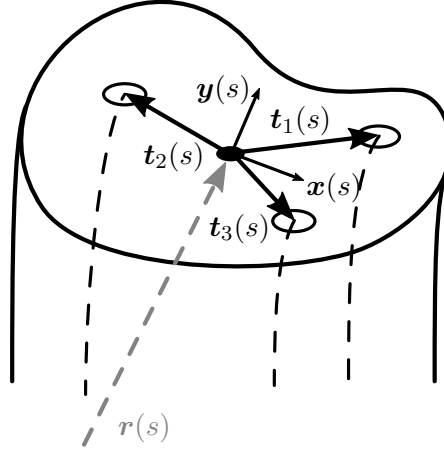


Figure 4.23: Routing paths of the tendons with respect to the robot's backbone

derivative then results in:

$$\partial_s \mathbf{n}_i(s) + \mathbf{f}_i(s) = 0 \quad (4.47)$$

where  $\mathbf{n}_i(s)$  is the internal and  $\mathbf{f}_i(s)$  the externally applied force for each tendon  $i$ . Other than a Cosserat rod, it is assumed that strings are perfectly flexible which leads to the absence of internal moments and shear forces. Therefore, only tension has to be considered, which is constant due to the neglection of friction (see model assumptions). For that reason the internal force has to be tangent to the curve  $\mathbf{r}_i(s)$  at any given point:

$$\mathbf{n}_i(s) = \tau_i \frac{\partial_s \mathbf{r}_i(s)}{\|\partial_s \mathbf{r}_i(s)\|} \quad (4.48)$$

Substituting equation (4.47) into (4.48) and solving for the distributed force on the tendon yields:

$$\mathbf{f}_i = \tau_i \frac{\hat{\partial_s} \mathbf{r}_i^2}{\|\partial_s \mathbf{r}_i\|^3} \partial_s^2 \mathbf{r}_i \quad (4.49)$$

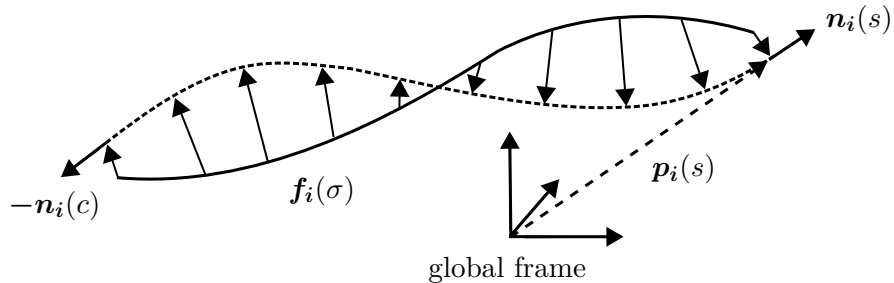


Figure 4.24: Internal forces  $\mathbf{n}_i$  and distributed external forces  $\mathbf{f}_i$  on tendon  $t_i$ .

### 3.2.5 Tendon Loads on Backbone

Using the distributive loads of each tendon  $\mathbf{f}_i$  we can now express the collective distributed loads  $\mathbf{f}_t$  and  $\mathbf{l}_t$  that the tendons apply to the robot's backbone as:

$$\mathbf{f}_t = - \sum_i \mathbf{f}_i \quad (4.50)$$

$$\mathbf{l}_t = - \sum_i (\mathbf{r}_i - \mathbf{r}) \times \mathbf{f}_i = - \sum_i (\mathbf{R}\mathbf{t}_i)^\wedge \mathbf{f}_i \quad (4.51)$$

using the lever principle for the distributed moment  $\mathbf{l}_t$  (see also Fig. 4.25). Substituting equation (4.49) for the tendons internal forces  $\mathbf{f}_i$  yields:

$$\mathbf{f}_t = - \sum_i \tau_i \frac{\partial_s^2 \mathbf{r}_i}{\|\partial_s \mathbf{r}_i\|^3} \mathbf{f}_i \quad (4.52)$$

$$\mathbf{l}_t = - \sum_i \tau_i (\mathbf{R}\mathbf{t}_i)^\wedge \frac{\partial_s^2 \mathbf{r}_i}{\|\partial_s \mathbf{r}_i\|^3} \mathbf{f}_i \quad (4.53)$$

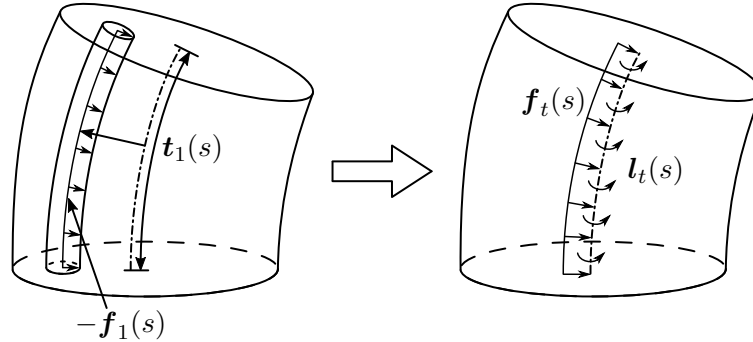


Figure 4.25: Expressing the loads of each tendon as distributed loads along the robot's backbone

### 3.2.6 Coupled Rod/Tendon Model Equations

To obtain a complete coupled model to solve for the robot's backbone location we express the force and moment distribution in terms of the kinematic variables. Therefore, we start with differentiation (4.46) twice and substituting the explicit cosserat rod equations (3.22):

$$\begin{aligned} \partial_s \mathbf{r}_i &= \mathbf{R}(\hat{\mathbf{u}}\mathbf{t}_i + \partial_s \mathbf{t}_i + \mathbf{v}) \\ \partial_s^2 \mathbf{r}_i &= \mathbf{R}(\hat{\mathbf{u}}(\hat{\mathbf{u}}\mathbf{t}_i + \partial_s \mathbf{t}_i + \mathbf{v}) + (\partial_s \mathbf{u})^\wedge \mathbf{t}_i + \hat{\mathbf{u}}\partial_s \mathbf{t}_i + \partial_s^2 \mathbf{t}_i + \partial_s \mathbf{v}) \end{aligned}$$

These can now be substituted into the force and moment equations (4.52) and (4.53):

$$\begin{aligned} \mathbf{f}_t &= \mathbf{R}(\mathbf{a} + \mathbf{A}\partial_s \mathbf{v} + \mathbf{G}\partial_s \mathbf{u}) \\ \mathbf{l}_t &= \mathbf{R}(\mathbf{b} + \mathbf{B}\partial_s \mathbf{v} + \mathbf{H}\partial_s \mathbf{u}) \end{aligned}$$

And substituting these with  $\mathbf{f} = \mathbf{f}_e + \mathbf{f}_t$  and  $\mathbf{l} = \mathbf{l}_e + \mathbf{l}_t$  into the explicit model equations of the cosserat rod theory (3.22) yields:

$$\begin{aligned} (\mathbf{K}_{se} + \mathbf{A})\partial_s \mathbf{v} + \mathbf{G}\partial_s \mathbf{u} &= \mathbf{d} \\ \mathbf{B}\partial_s \mathbf{v} + (\mathbf{K}_{bt} + \mathbf{H})\partial_s \mathbf{u} &= \mathbf{c} \end{aligned}$$

with:

$$\begin{aligned}
\mathbf{A}_i &= -\tau_i \frac{\hat{\partial_s} \mathbf{r}_i^2}{||\hat{\partial_s} \mathbf{r}_i||^3}, & \mathbf{A} &= \sum_i \mathbf{A}_i, \\
\mathbf{B}_i &= \hat{\mathbf{t}}_i \mathbf{A}_i, & \mathbf{B} &= \sum_i \mathbf{B}_i \\
\mathbf{G} &= -\sum_i \mathbf{A}_i \hat{\mathbf{t}}_i, & \mathbf{H} &= -\sum_i \mathbf{B}_i \hat{\mathbf{t}}_i, \\
\mathbf{a}_i &= \mathbf{A}_i (\hat{\mathbf{u}} \partial_s \mathbf{r}_i + \hat{\mathbf{u}} \partial_s \mathbf{t}_i + \partial_s^2 \mathbf{t}_i), & \mathbf{b}_i &= \hat{\mathbf{t}}_i \mathbf{a}_i, \\
\mathbf{a} &= \sum_{i=1}^n \mathbf{a}_i, & \mathbf{b} &= \sum_{i=1}^n \mathbf{b}_i, \\
\mathbf{c} &= \mathbf{K}_{bt} \partial_s \mathbf{u}^* - \hat{\mathbf{u}} \mathbf{K}_{bt} (\mathbf{u} - \mathbf{u}^*) & - \hat{\mathbf{v}} \mathbf{K}_{se} (\mathbf{v} - \mathbf{v}^*) - \mathbf{R}^T \mathbf{l}_e - \mathbf{b}, \\
\mathbf{d} &= \mathbf{K}_{se} \partial_s \mathbf{v}^* - \hat{\mathbf{u}} \mathbf{K}_{se} (\mathbf{v} - \mathbf{v}^*) & - \mathbf{R}^T \mathbf{f}_e - \mathbf{a}.
\end{aligned}$$

We can now simply write the final model equations as:

$$\begin{aligned}
\partial_s \mathbf{r} &= \mathbf{R} \mathbf{v} \\
\partial_s \mathbf{R} &= \mathbf{R} \hat{\mathbf{u}} \\
\begin{bmatrix} \partial_s \mathbf{v} \\ \partial_s \mathbf{u} \end{bmatrix} &= \begin{bmatrix} \mathbf{K}_{se} + \mathbf{A} & \mathbf{G} \\ \mathbf{B} & \mathbf{K}_{bt} + \mathbf{H} \end{bmatrix}^{-1} \begin{bmatrix} \mathbf{d} \\ \mathbf{c} \end{bmatrix}
\end{aligned}$$

Neglecting shear forces  $\mathbf{v} = \mathbf{v}^* = [0 \ 0 \ 1]^T$  yields us the following simplified model according to the Kirchhoff Rod Equations with:

$$\begin{aligned}
\partial_s \mathbf{r} &= \mathbf{R} \mathbf{e}_3 \\
\partial_s \mathbf{R} &= \mathbf{R} \hat{\mathbf{u}} \\
\partial_s \mathbf{u} &= (\mathbf{H} + \mathbf{K}_{bt})^{-1} (\mathbf{K}_{bt} \partial_s \mathbf{u}^* - \hat{\mathbf{u}} \mathbf{K}_{bt} (\mathbf{u} - \mathbf{u}^*) - \hat{\mathbf{v}} \mathbf{R}^T \mathbf{n} - \mathbf{R}^T \mathbf{l}_e - \mathbf{b}) \\
\partial_s \mathbf{n} &= -\mathbf{R}(\mathbf{a} + \mathbf{G} \partial_s \mathbf{u}) - \mathbf{f}_e
\end{aligned} \tag{4.54}$$

### Example: Neglecting external forces

When neglecting external forces the stated explicit model equations reduce to:

$$\begin{aligned}
\partial_s \mathbf{r} &= \mathbf{R} \mathbf{e}_3 \\
\partial_s \mathbf{R} &= \mathbf{R} \hat{\mathbf{u}} \\
\partial_s \mathbf{u} &= (\mathbf{H} + \mathbf{K}_{bt})^{-1} (\mathbf{K}_{bt} \partial_s \mathbf{u}^* - \hat{\mathbf{u}} \mathbf{K}_{bt} (\mathbf{u} - \mathbf{u}^*) - \hat{\mathbf{v}} \mathbf{R}^T \mathbf{n} - \mathbf{b}) \\
\partial_s \mathbf{n} &= -\mathbf{R}(\mathbf{a} + \mathbf{G} \partial_s \mathbf{u})
\end{aligned} \tag{4.55}$$

### 3.2.7 Boundary Conditions

When considering a real robot structure boundary conditions have to be incorporated to solve the stated explicit model equations. This boundary conditions apply when a tendon terminates along the length of the robot. The tendon then applies a point force  $\mathbf{F}_i$  to the point where it is attached ( $s = \ell_i$ ) which equals the opposite of its internal force (see Eq. (4.48)).

$$\mathbf{F}_i = -\mathbf{n}_i(\ell_i) = -\tau_i \frac{\partial_s \mathbf{r}_i(\ell_i)}{||\partial_s \mathbf{r}_i(\ell_i)||}$$

Further, this forces also creates a point moment  $\mathbf{L}_i$  at the backbone centroid with a moment arm of  $\mathbf{r}_i(\ell_i) - \mathbf{r}(\ell_i)$ .

$$\mathbf{L}_i = -\tau_i(\mathbf{R}(\ell_i)\mathbf{t}_i(\ell_i))^\wedge \frac{\partial_s \mathbf{r}_i(\ell_i)}{||\partial_s \mathbf{r}_i(\ell_i)||}$$

For every location  $s = \sigma$  along the robot's backbone where point loads (whether due to external forces, tendons terminations or both) apply we must consider the following boundary conditions for the internal force and moment:

$$\begin{aligned}\mathbf{n}(\sigma^-) &= \mathbf{n}(\sigma^+) + \mathbf{F}(\sigma) \\ \mathbf{m}(\sigma^-) &= \mathbf{m}(\sigma^+) + \mathbf{L}(\sigma)\end{aligned}$$

### 3.3 Solving the Explicit Model Equations

An analytic solution to the model equations only exist when solving the differential equations for a tubular continuum robot with  $n=2$  tubes with circular precurvatures, where an analytic solution can be acquired using elliptic integrals [7, 8]. An analytic solution to the differential Kirchhoff rod equations of a tubular continuum robot with  $n > 2$  and for the tendon actuated continuum robot does not exist, such that model equations are solved numerically. A shooting method, illustrated in Figure 4.26, can be used to solve the model equations, where the algorithm should be implemented such that it integrates along the robot (Initial Value Problem (IVP) Method using e.g. Runge-Kutta Methods) and solves the equations numerically for each consecutive section. The algorithm could either be implemented such that it integrates from base to tip or from tip to base. Integration from tip to base is implemented by guessing unknown values at the proximal end and solving for unknown initial curvatures (IC) while satisfying all mentioned boundary conditions (BC).

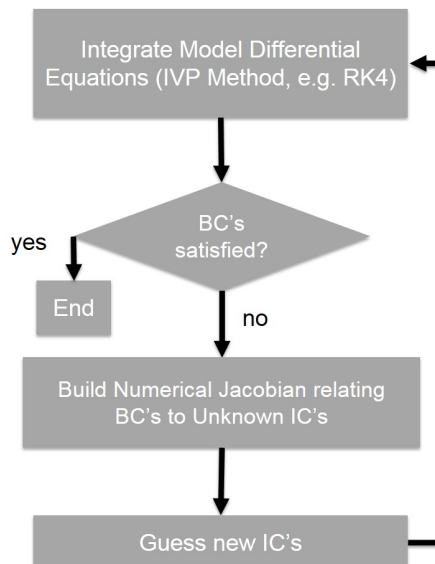


Figure 4.26: Shooting Method for numerically solving the explicit differential equations.

### 3.4 Accuracy

As mechanics frameworks using elasticity theory allow for the consideration of effects from bending, torsion, and shear deformation, the modeling accuracy, i.e. how well does the model conform to the real shape of a continuum robot, is generally increased compared to constant curvature kinematic frameworks. As the model is more complex, computation time is usually also increasing.

Please note, that the accuracy of a model is not only dependent on the theoretical framework itself, but also on how well the real robot complies with the modeling assumptions. Furthermore, the parameters of the model need to be calibrated for the specific real robot, i.e material properties, geometrical parameters, reference configuration, pre-curvatures, etc. In addition, the modeling accuracy is compromised by effects that have not been modeled, such as backlash in actuation, clearances between components, friction. Furthermore, the modeling accuracy is also depending on the experiment design (number of samples, number of robot configuration, how well do the configurations span the workspace of the robot, number of repeated measurements, etc.) and the measurement technique (tactile vs. contact-less, measurement accuracy, etc.). In the following, the accuracy of the models introduced in the previous sections are summarized for the example robots.

#### 3.4.1 Accuracy for Tubular Continuum Robots

The accuracy of the mechanics framework using elasticity theory for modeling of tubular continuum robots is generally increased compared to constant curvature kinematic frameworks as effects from torsion and external loads are considered. As the explicit modeling error depends on the geometry and composition of the tubes of a tubular continuum robot (see above), two representative evaluations of the modeling accuracy are presented in the following.

**Two Tube Continuum Robot Under External Loads** Rucker et al. reported on the tip error for a tubular continuum robot composed of two tubes [9] (outer tube: OD 2.37 mm, ID 2.0 mm, straight length 30.7 mm, curved length 102.5 mm; inner tube: OD 1.75 mm, ID 1.25 mm, straight length 122.7 mm, curved length 206.9 mm). The precurvatures of the tubes were measured experimentally and are reported in respect to arc length in [9]. Overall, 40 unloaded and 40 loaded experiments have been conducted. Measurement were obtained contact-free using a stereo-camera system.

The results are summarized in Table 4.1. Overall, 75 % of the errors  $\leq 3$  mm and 85 % of the errors  $\leq 4$  mm. The total arc length of the tubular continuum robot ranged from 105.9 mm to 197.9 mm over the experimental dataset. Thus, an average tip error of 2.91 mm is corresponding to 1.5–3 % of the arc length. A detailed description and additional results are provided in [9].

Table 4.1: Results obtained for a two tube robot in 40 unloaded and 40 loaded experiments [9].

Tip Error (mm)	Mean	Std. Dev.	Min	Max
Unloaded	2,89	2,19	0,62	8,49
Loaded	2,92	2,52	0,91	15,20
All	2,91	2,34	0,91	15,20

**Three Tube Continuum Robot in Free Space** Dupont et al. reported on the accuracy obtained experimentally using a tubular continuum robot prototype composed of three tubes [7] (outer tube: OD 2.77 mm, ID 2.55 mm, straight length 0 mm, curved length 150 mm with radii of curvature 154 mm; middle tube: OD 2.41 mm, ID 1.97 mm, straight length 18 mm, curved length 150 mm with radii of curvature 154 mm; inner tube: OD 1.85 mm., ID 1.65 mm, straight length 186 mm, curved length 57 mm with radii of curvature 35 mm). Overall 128 robot configurations were evaluated in terms of their deviation at the robot's tip in comparison to the predicted tip position. The measurements were obtained contact-free using a stereo-camera system. The results are summarized in Table 4.2. The obtained mean tip error of 4.2 mm corresponds to 1.7 % of the total arc length of the tubular continuum robot. More details on the experimental setup and additional results can be found in [7].

Table 4.2: Results obtained for a three tube continuum robot reported by Dupont et al. [7].

Tip Error	Mean (mm)	Std. Dev. (mm)	Max (mm)
Unloaded	4.2	2.0	8.3

### 3.4.2 Accuracy for Tendon-actuated Continuum Robots

The accuracy of the coupled rod/tendon model has been experimentally determined by Rucker and Webster [17]. The continuum robots was composed of a central rod backbone made of spring steel with an overall length of 242 mm and diameter of 0.8 mm, equipped with 12 tendon routing risks spaced 20 mm apart, made from Teflon with diameter 20 mm and thickness 1.57 mm. Each routing disk has 24 radially distributed channels to accommodate tendons (8 mm radius). Teflon-coated fiberglass thread with a diameter of 0.36 mm is used as tendons. As the tendon routing disks offer several channels, the tendons can be routed with variable paths. For the experiments, the conventional parallel routing was used for in-plane and out-of-plane loads. Furthermore, the tendons were routed in helical paths for experiments demonstrating the model applicability to general tendon routing

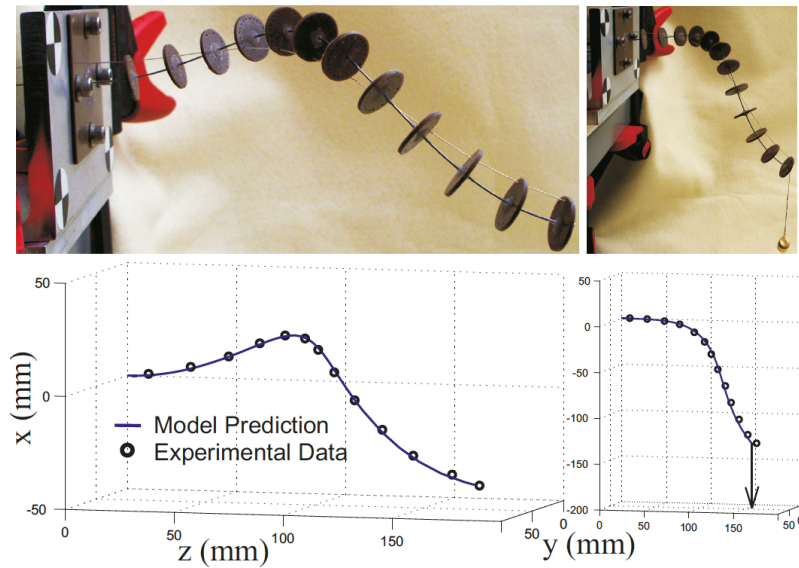


Figure 4.27: Examples of the experimental results in comparison to the coupled rod/tendon model prediction for helical tendon routing with and without applied loads [17].

(see Figure 4.27). The model prediction of the robot shape was compared to the shape of the real robot by determining tactile measurements of the robot's backbone position using a tracked pointer.

Table 4.3 summarizes the error measured at the tip of the tendon-actuated continuum robot described above for in-plane loads, out-of-plane loads as well as for helical tendon routing of two different types. The error at the tip corresponds to about 2 % of the total arc length of the continuum robot. A detailed description and additional results are provided in [17].

Table 4.3: Tip error (in mm) experimentally determined by Rucker and Webster [17] for the Coupled/Rod Tendon Model. Reported is the mean tip error and the standard deviation over the experiments as well as minimum and maximum observed tip errors.

Tip Error	mean (mm)	std. dev. (mm)	min (mm)	max (mm)
In-plane Loads	3.1	1.3	0.3	5.3
Out-of-plane Loads	4.1	2.1	0.6	7.9
Helical Tendon Routing 1	5.5	2.7	1.9	10.0
Helical Tendon Routing 2	4.6	1.9	2.7	7.2

## References

- [1] B.A. Jones and I.D. Walker. "Kinematics for multisegment continuum robots". In: *IEEE Transactions on Robotics* 22.1 (2006), pp. 43–55.
- [2] Michael W Hannan and Ian D Walker. "Kinematics and the Implementation of an Elephant's Trunk Manipulator and Other Continuum Style Robots". In: *Journal of Robotic Systems* 20.2 (2003), pp. 45–63.
- [3] G.S. Chirikjian. "Conformational Modeling of Continuum Structures in Robotics and Structural Biology: A Review". In: *Advanced Robotics* 29.13 (2015), pp. 817–829.
- [4] Robert J. Webster, Joseph M. Romano, and Noah J. Cowan. "Mechanics of Precurved-Tube Continuum Robots". In: *IEEE Transactions on Robotics* 25.1 (2009), pp. 67–78.
- [5] Robert J. Webster and Bryan A. Jones. "Design and Kinematic Modeling of Constant Curvature Continuum Robots: A Review". In: *The International Journal of Robotics Research* 29.13 (2010), pp. 1661–1683.
- [6] David B. Camarillo et al. "Mechanics Modeling of Tendon-Driven Continuum Manipulators". In: *IEEE Transactions on Robotics* 24.6 (2008), pp. 1262–1273.
- [7] Pierre E. Dupont et al. "Design and Control of Concentric-Tube Robots". In: *IEEE Transactions on Robotics* 26.2 (2010), pp. 209–225.
- [8] D. C. Rucker et al. "Equilibrium Conformations of Concentric-tube Continuum Robots". In: *The International Journal of Robotics Research* 29.10 (2010), pp. 1263–1280.
- [9] D. Caleb Rucker, Bryan A. Jones, and Robert J. Webster III. "A Geometrically Exact Model for Externally Loaded Concentric-Tube Continuum Robots". In: *IEEE Transactions on Robotics* 26.5 (2010), pp. 769–780.
- [10] Kai Xu and Nabil Simaan. "Intrinsic Wrench Estimation and Its Performance Index for Multisegment Continuum Robots". In: *IEEE Transactions on Robotics* 26.3 (2010), pp. 555–561.
- [11] William S Rone and Pinhas Ben-Tzvi. "Continuum Robot Dynamics Utilizing the Principle of Virtual Power". In: *IEEE Transactions on Robotics* 30.1 (2014), pp. 275–287.
- [12] Ilker Tunay. "Spatial Continuum Models of Rods Undergoing Large Deformation and Inflation". In: *IEEE Transactions on Robotics* 29.2 (2013), pp. 297–307.
- [13] Isuru S Godage et al. "Dynamics for variable length multisegment continuum arms". In: *The International Journal of Robotics Research* 35.6 (2016), pp. 695–722.
- [14] Srinivas Neppalli et al. "Closed-Form Inverse Kinematics for Continuum Manipulators". In: *Advanced Robotics* 23.15 (2009), pp. 2077–2091.
- [15] Josephine Granna et al. "A 3-D Volume Coverage Path Planning Algorithm With Application to Intracerebral Hemorrhage Evacuation". In: *IEEE Robotics and Automation Letters* 1.2 (2016), pp. 876–883. ISSN: 2377-3766. DOI: 10.1109/LRA.2016.2528297.
- [16] Richard M Murray, Zexiang Li, and S Shankar Sastry. *A Mathematical Introduction to Robotic Manipulation*. CRC Press, 1994.

- [17] D. Caleb Rucker and Robert J. Jones Webster III. “Statics and Dynamics of Continuum Robots With General Tendon Routing and External Loading”. In: *IEEE Transactions on Robotics* 27.6 (2011), pp. 1033–1044.